COMPARISON OF FATIGUE, CORROSION AND CORROSION FATIGUE PROPERTIES OF 3CR12, CORTEN AND MILD STEEL IN AIR AND POLYTHIONIC ACID SOLUTION

SHOOU-YIH CHEN

A dissertation submitted to the Faculty of Engineering, University of the Witwatersrand, Johannesburg in fulfilment of the requirements for the Degree of Master of Science.

Department of Metallurgy and Materials Engineering
University of the Witwatersrand
July 1991

DECLARATION

I declare that this dissertation is my own unaided work except where due acknowledgement is made to others. It is being submitted for the Degree of Master of Science to the University of the Witwatersrand, Johannesburg. It has not been submitted before for any degree or examination to any other university.

SHOU-YIN CHEN

陳守義

11th day of July 1991

SYNOPSIS

Steel 3CR12 is a 12% chromium, titanium stabilised, corrosion resisting steel which was developed in South Africa in the recent past. It is a dual-phase steel with a microstructure consisting of low-carbon martensite and ferrite obtained by carefully balancing the austenite stabilising elements.

Steel 3CR12 has found extensive industrial applications, particularly in the construction of equipment which operates under corrosive/abrasive conditions. This programme established the fatigue and corrosion fatigue properties of 3CR12 and compared them with those of Corten steel and mild steel which are sometimes used in similar applications. The influence of welding on these properties of the three steels was also examined. The results obtained were related to microstructure and other characteristics of the steel in each case.

ACKNOWLEDGEMENTS

I would like to sincere thank the following people :.

Dr, A. Koursaris, for his constant support, helpful supervision and patient throughout the duration of this work.

Prof. FPA Robinson and Dr. MN James for their helpful comment and suggestions.

Members of the Metallurgy Department at the University of the Witwatersrand, especially John Morfitt, Shadrack Moqabolane, Gill van der Heever and Karren Dow for their advice and assistance,

My friends, Yunus Turan, Serdar Ozbayraktar, Ian Schw[illegible], Andre van Bennekon and Alan Jarivs for their useful discussion, encouragement, time and help.

Mr. and Mrs. Lyle for taking care of my life in South Africa.

My family, particularly my father and my wife Li-Hsiu for all their understanding and encouragement.

Finally, to Middelburg Steel and Alloys, the CSIR and the University of the Witwatersrand for their financial support for the duration of this work.

CONTENTS

List of illustrations page

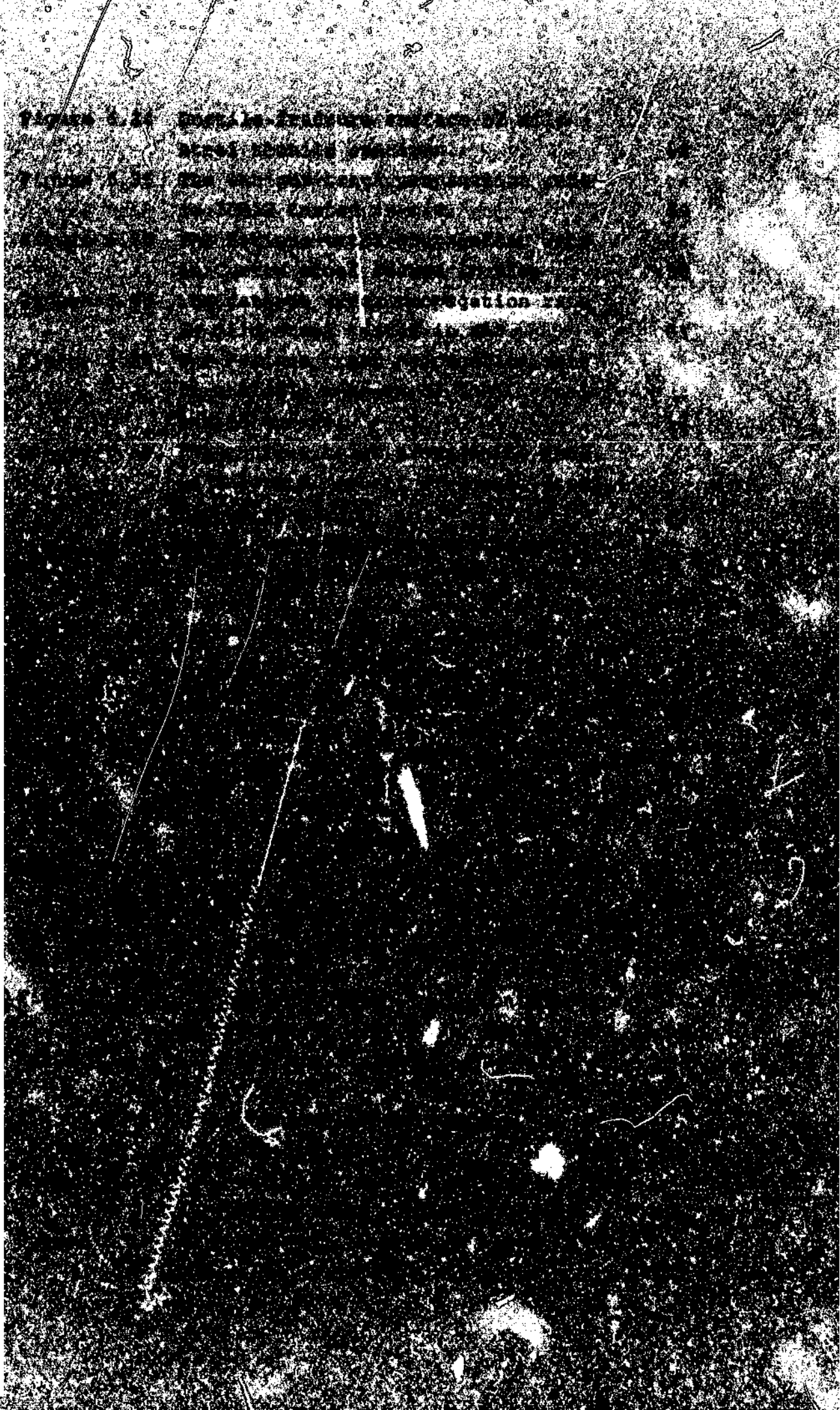

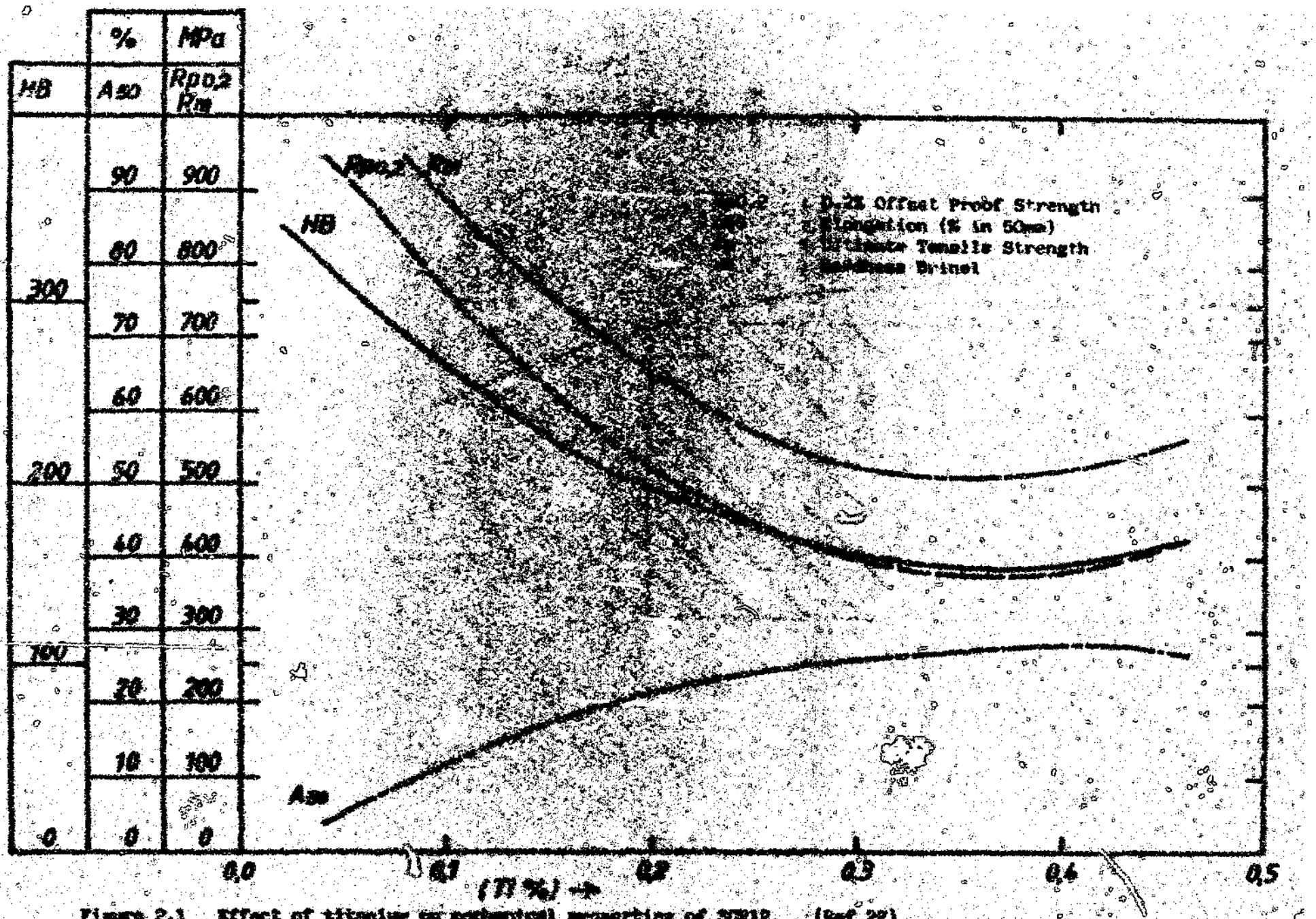

Figure 2.1 Effect of titanium on mechanical properties of 5083. (Ref 22)

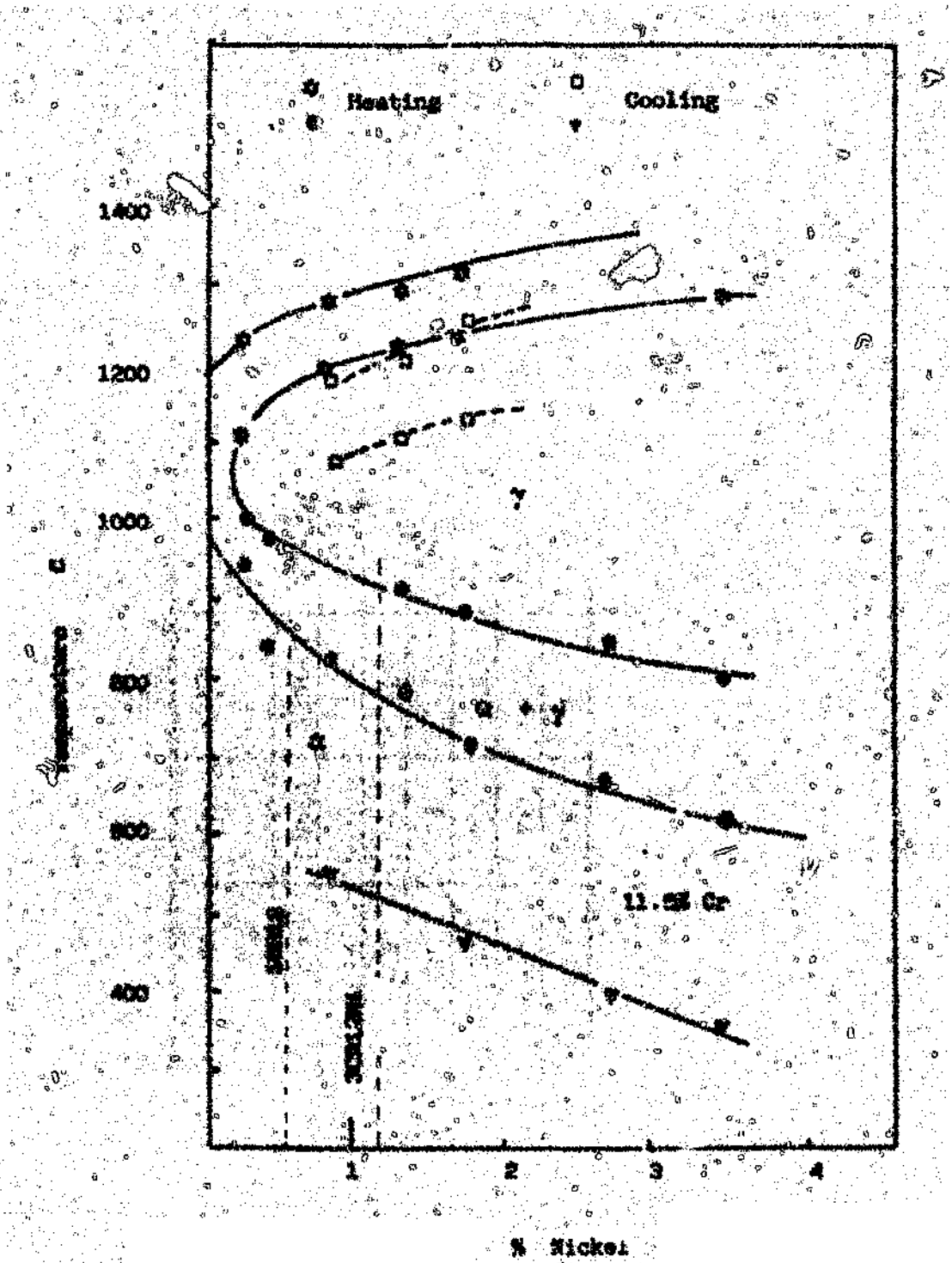

Figure 2.3 Effect of nickel on the phase diagram of duplex ferrite-martensite 12% Cr steel. (Ref 24)

Table 2.2 Average mechanical properties of hot rolled 3CR12 plate. (Ref 22)

Gauge mm	$Rp_{0,2}$	Rm	A_{50}	HB	20°C Impacts J/cm^2	Remarks
Specification	280min	460mfn	18min	220max	60min	
10 to 12	378	512	28	164	102	Full size Charpy 10 x 10mm
8 to 9,5	375	509	27	162	108	Sub size Charpy 8 x 10mm
6	400	526	24	165	108	Sub size Charpy 6 x 10mm
5	379	522	23	162	114	Sub size Charpy 5 x 10mm
4,5	388	530	24	161	-	
3,5	404	535	22	161	-	

deformation process and this is summarised in Table 2.3[22].

Smallman's explanation about these hardening stages may be summarized as follows [23]: (Figure 2.4)

a) Stage I, or the easy glide region, immediately follows the yield point and is characterized by a low rate of work hardening, up to several per cent glide; the length of this region depends on orientation, purity and size of crystals.

b) Stage II shows a rapid increase in work hardening rate. The length of the region depends on temperature, orientation or alloy content. In this stage short slip lines are formed quite suddenly during straining.

c) Stage III, the onset of which is markedly dependent on temperature, exhibits a low rate of work hardening. This stage starts at a strain which increases with increasing temperature and is probably associated with the annihilation of dislocations as a consequence of cross slip.

2.3 Weldability of 3CR12

Welding of 3CR12 using types 308L, 309Mo and 310 electrodes has been studied to produce sound joints free of cracking in either the weld deposits or HAZ. The welds produced with these consumables showed good bend test ductility and had a tensile strength equal to that of the parent material[24].

2.4 Corrosion properties of 3CR12

Table 2.4 shows the corrosion rates of 3CR12 and other common materials after 2 years exposure at different

1. INTRODUCTION

One of the most serious problems facing industry today is corrosion. The corrosion and prevention of corrosion of metallic materials constitutes a major cost to industry annually. It causes damage of billions of dollars each year[1]. This cost arises in the course of prevention of corrosion and replacement of materials. In some corrosive environments austenitic stainless steels are normally used because of their great properties of excess corrosion resistance, strength and toughness. Austenitic stainless steels are quite expensive and sometimes prone to stress-corrosion cracking (SCC)[2], so they cannot be used in all applications. SCC is a form of cracking produced by a combination of stress, environmental conditions and susceptible material. Usually [illegible] cracks [illegible] and [illegible] required [illegible] SCC [illegible]

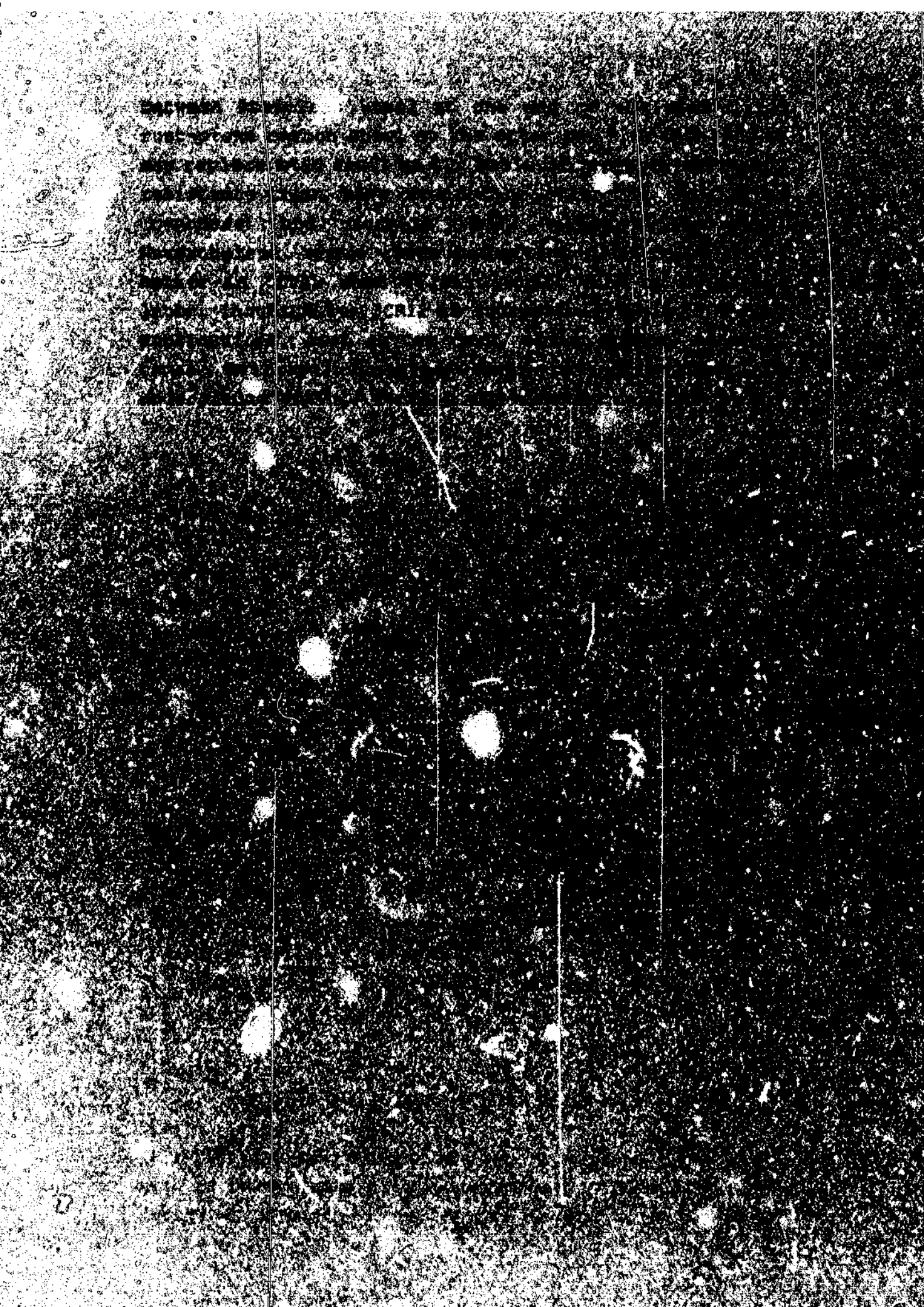

2. [illegible] OF 3CR12

3CR12 was developed from AISI 409 by carefully balancing the ferrite stabilising elements (Cr, Si, Ti) with austenite stabilising elements (C, N, Ni, Mn) using the Kaltenhauser relationship to produce a steel with a dual structure in the hot rolled condition. On tempering at [illegible] temperatures the microstructure formed consists of fine grained ferrite and low carbon martensite. [illegible] ferrite factor [illegible] martensite present is obtained [illegible] low carbon lath-type martensite [illegible]

[illegible]

[illegible]

This FF, which drops about [illegible], indicates that any steel will be ferritic at all temperatures. The mean ferrite factor of 3CR12 produced to date is [illegible], but values of

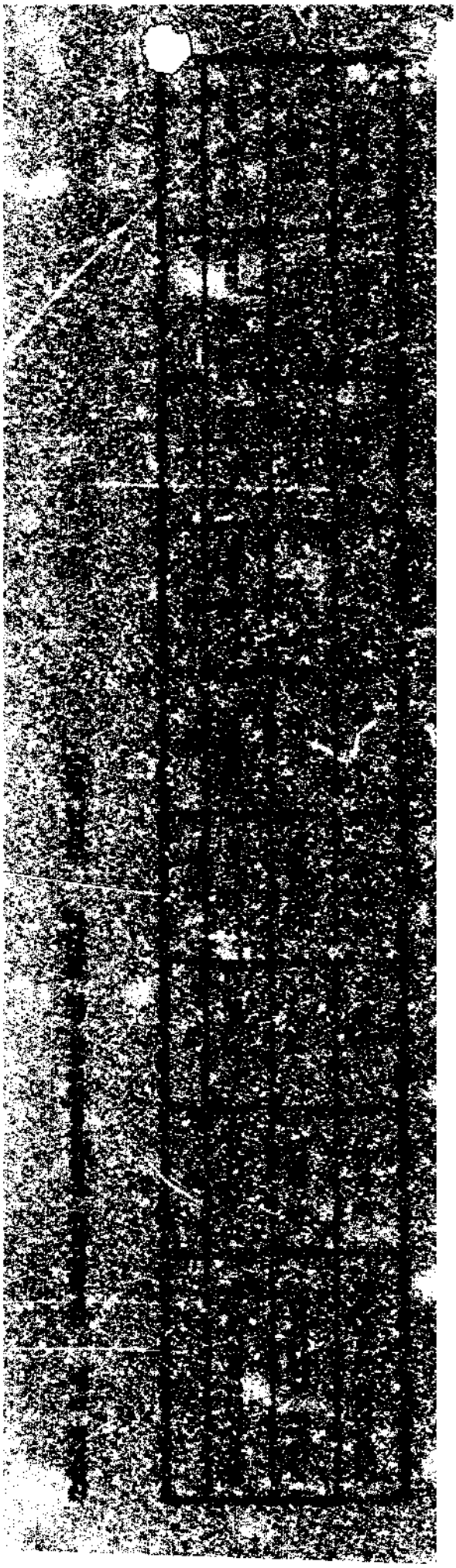

between 9.58 and 12.95 have been obtained without any deterioration of mechanical properties. It has been shown that the elements which have a very significant effect on the mechanical properties and the tempering or annealing response of 3CR12 are titanium and nickel. Figure 2.1 shows the effect of titanium on the mechanical properties of a 0.6%Ti 3CR12.

Titanium was chosen as the stabilising element in preference to niobium and vanadium since titanium carbides and nitrides are stable [22]. The titanium content must be carefully controlled to optimise properties. Excess titanium will lead to embrittlement by the formation of Laves phases or intermetallic compounds producing substantial solid solution of the ferrite.

The ratio of Ti/C+N and the ratio of Mn/S should also be controlled in order to obtain the best plate impact properties (Figure 2.2).

Nickel is an important element in 3CR12. It increases the stability of austenite and makes the steel enter the dual phase region at lower temperatures, (Figure 2.3) [22]. From Figure 2.3 it can be seen that the high nickel content 3CR12 enters the dual phase region at a temperature much lower than that of normal 3CR12.

2.2 The mechanical properties of 3CR12

Steel 3CR12 has a high yield strength to tensile strength ratio (0.73), high yield strength, high impact strength, low work hardening exponent and high elongation even after welding. Evaluation of the mechanical properties of 3CR12 for different plate thicknesses gives the average values shown in Table 2.2[22]. It is generally accepted that the phenomenon is most probably due to the presence of mobile dislocations in the ferrite phase. The work hardening behavior is the result of a three-stage

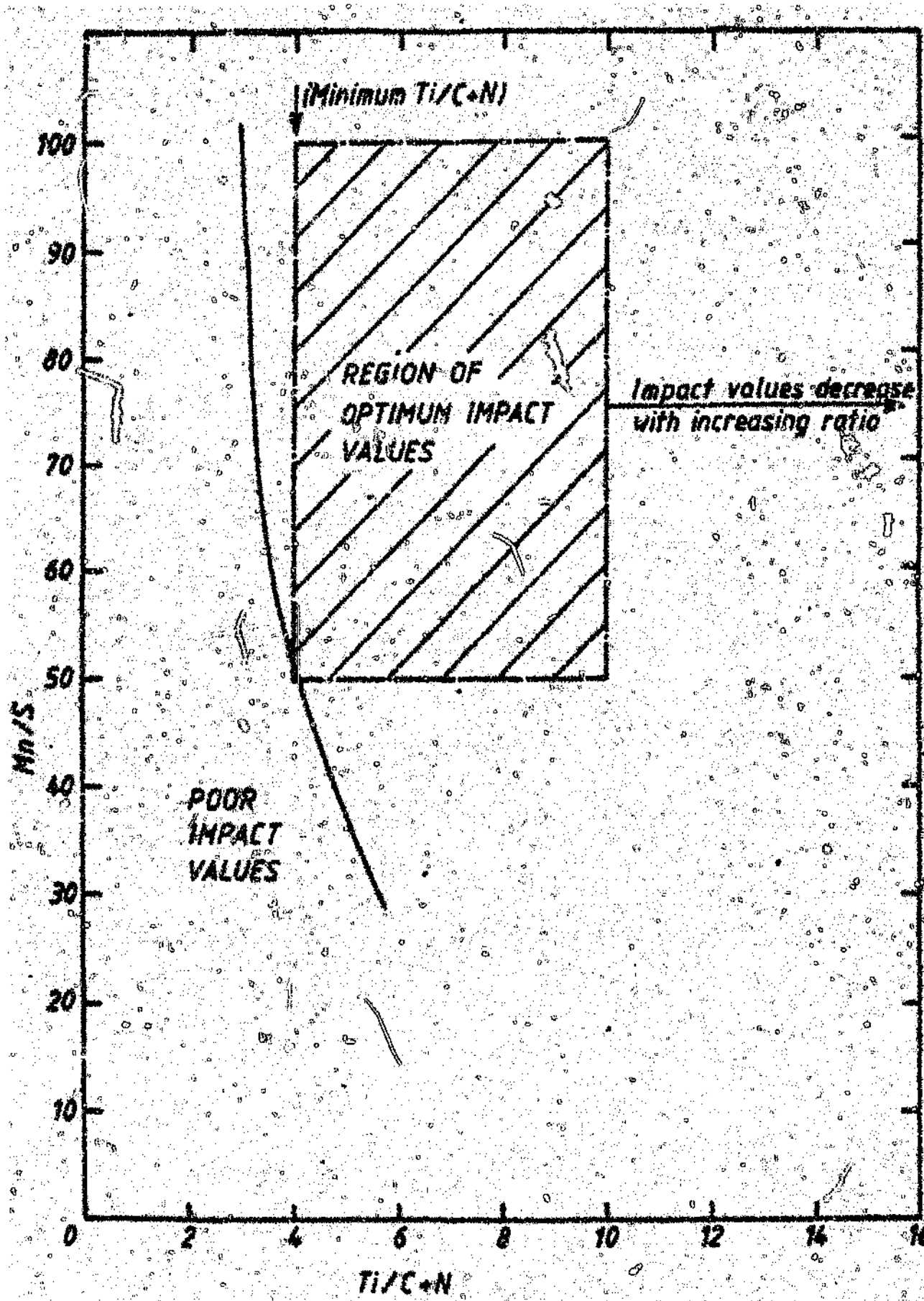

Figure 2.2 Effect of Ti/C+N and Mn/S ratio on impact properties. (Ref 22)

Table 2.3 Three-stage work hardening behaviour of 3CR12 and 3CR12Ni. (Ref 22)

	n_1	Total strain range, %	n_2	Total strain range, %	n_3	Total strain range, %	True uniform strain
3CR12 II	0,3	0,1 - 0,14	0,06	0,4 - 1,5	0,176	3,0 - 16,0	0,171
3CR12 ⊥	0,2	0,1 - 0,2	0,08	0,4 - 1,2	0,174	2,5 - 14,6	0,160
3CR12Ni II	0,2	0,2 - 0,35	0,01	0,5 - 1,0	0,080	2,5 - 7,0	0,075
3CR12Ni ⊥	0,3	0,1 - 0,3	0,02	0,5 - 1,0	0,074	2,5 - 6,0	0,070

II : longitudinal
⊥ : transverse
n_1 : stage one
n_2 : stage two
n_3 : stage three

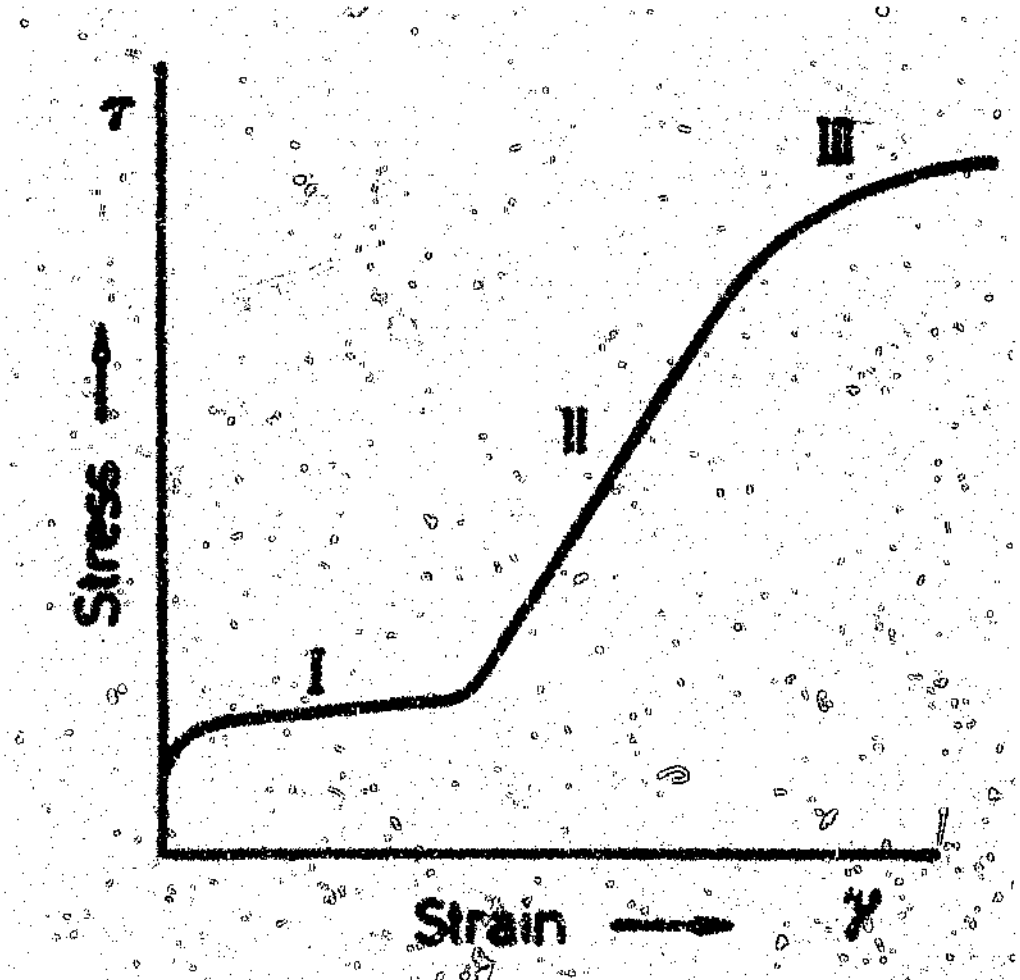

Figure 2.4 Stress-strain curve showing the three stages of work hardening. (Ref 25)

Table 2.4 Corrosion rates (in micrometres/year) after 2 years at various sites. (ref 22)

Environment	CSIR (Rural)	Durban, Harare, Island Bay, head. (Marine)	Bluff (Severe Marine)	Cape Town (Marine)	Walvis Bay (Severe Marine)	Pretoria - Iscor (Industrial)
Mild Steel	10,9	55,9	260	45,7	310	91,2
'Cor Ten' A	6,10	40,6	61,5	24,9	141	19,5
Zinc	0,203	2,39	14,5	3,20	63,1	0,279
Copper	0,838	1,45	3,25	1,40	4,34	3,48
Aluminium						
3S	0,038	0,696	3,353	0,478	0,257	0,399
M57S	0,028	0,577	2,591	0,051	0,500	
50S	0,051	0,688	2,276	0,142	0,483	
B57S	0,046	0,574	3,228	0,058	0,739	
Stainless Steel						
430	0,0025	0,0914	0,3581	0,0635	0,2210	
304	0,0025	0,0152	0,0686	0,0102	0,0330	
316	0,0025	0,0075	0,0406	0,0051	0,0229	
3CR12	0,007	0,194	1,256	0,192	1,130	0,063
(Pickled)						

sites [11]. It can be seen from this table that the corrosion rate of 3CR12 is very low compared with that of mild steel, Corten, zinc, copper and aluminium. Only in the case of Walvis Bay, which is considered to be a severe marine environment, was the corrosion rate of 3CR12 higher than that of aluminium alloys. 3CR12 has been tested in South African gold mines under abrasion/corrosion conditions against various other materials. Stainless steels showed a better wear/corrosion resistance than the other materials (Figure 2.5)[27]. From this it can be seen that corrosion is an important factor in the wear of materials in these environments. 3CR12 showed considerable potential as an abrasion-corrosion material for use in corrosive, low-stress abrasive wear environments associated with the mining and minerals processing industries.

For corrosion fatigue, 3CR12 has been tested in rotation bending with 3.5% NaCl dripping on it. The corrosion fatigue limit thus obtained showed no significa difference from the fatigue limit obtained in air [27].

The nickel content of the steel made little difference to the fatigue limit (Figure 2.6). The fatigue limit was 180 MPa and the corrosion fatigue limit was 160 MPa.

A series of static immersion tests have been undertaken in sea water and Witwatersrand and Free State mine water to compare 3CR12 (scaled and descaled) with Corten, mild steel and galvanized steel. The water analyses were as follows:

	Cl^- (ppm)	SO_4^{2-} (ppm)	pH
Sea water	18240	2980	8.05
Witwatersrand mine	400	666	7.2
Orange Free State mine	986	270	5.7

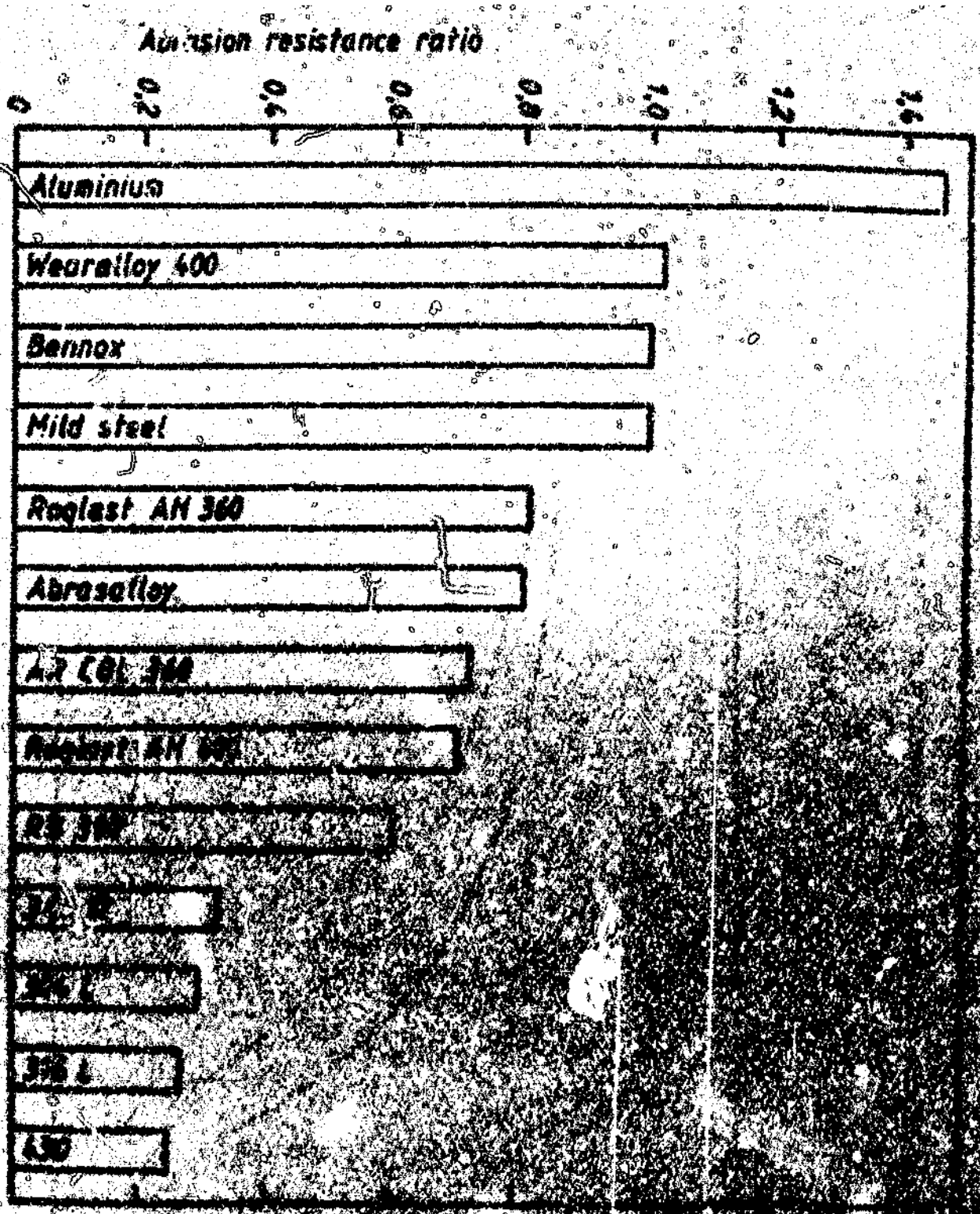

Figure 2.5 Comparative wear rates under abrasion/corrosion conditions. (Ref. 28)

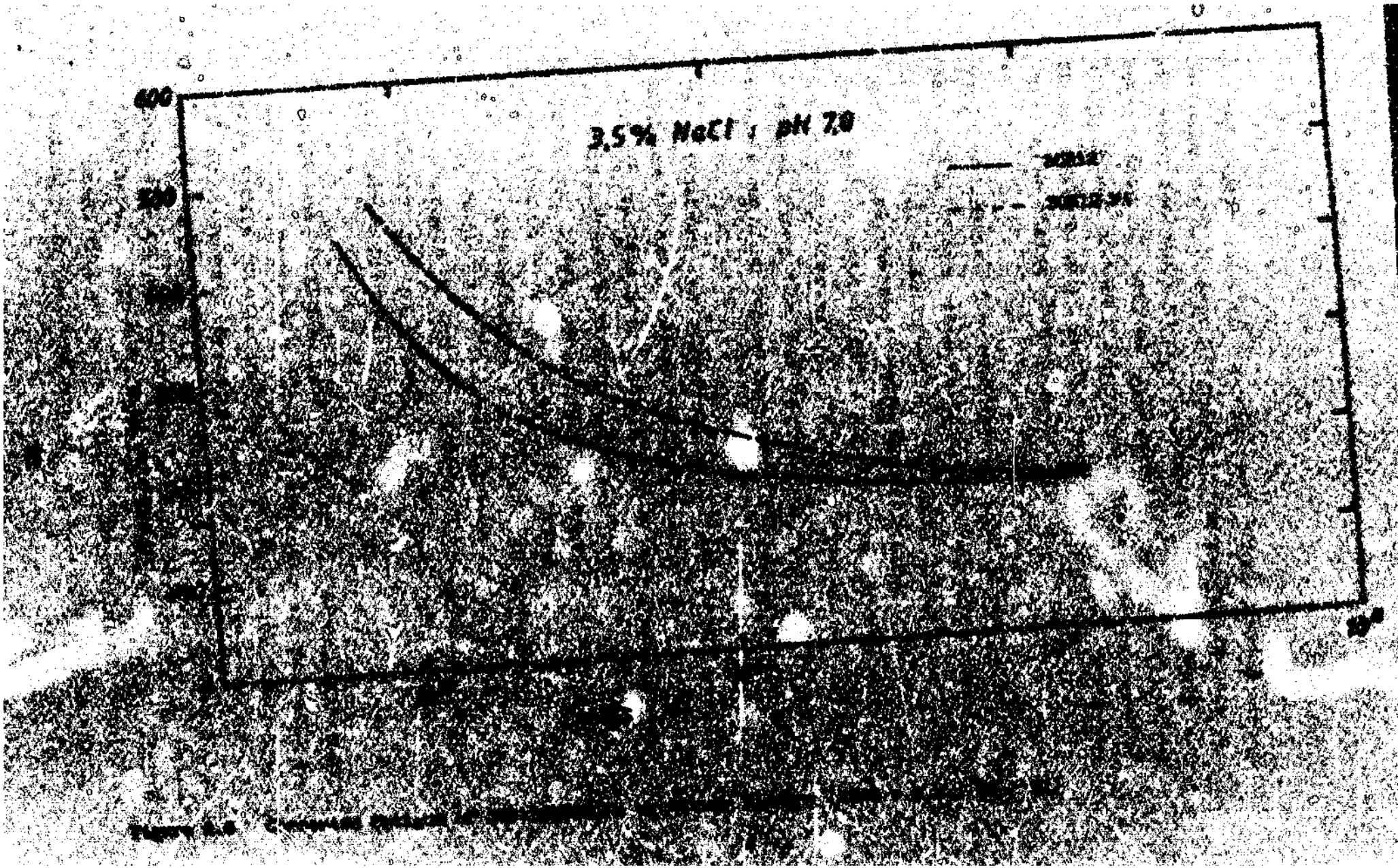
400
3,5% NaCl ; pH 7,0

In this case pickled or descaled 3CR12 showed zero corrosion rate. Figure 2.7 compares the corrosion rate of different materials in Free State mine water [7]. 3CR12 has been tested in various applications involving dilute acids, bases and salt solutions. The corrosion rate in those applications is low enough to make 3CR12 an attractive choice (Figure 2.8).

Tests according to specification ASTM A262(E), showed that 3CR12 is not prone to intergranular corrosion since the steel is stabilized. It has been shown that in certain environmental conditions crevice corrosion can occur if the weld oxide is not removed and the steel not re-passivated after welding [7]. Mild attack observed along the HAZ [8], but in most cases reasons could be traced back to the

The [illegible] corrosion [illegible] according to [illegible] boars in the exits there [illegible] at this [illegible] crevices [illegible] oxidation [illegible] [illegible] [illegible] [illegible] [illegible] oxidation [illegible]

The stress [illegible] in various [illegible] also attack [illegible] to SCC [illegible] aggressive [illegible] only [illegible] phosphoric [illegible] corrosion [illegible] sodium chloride [illegible]

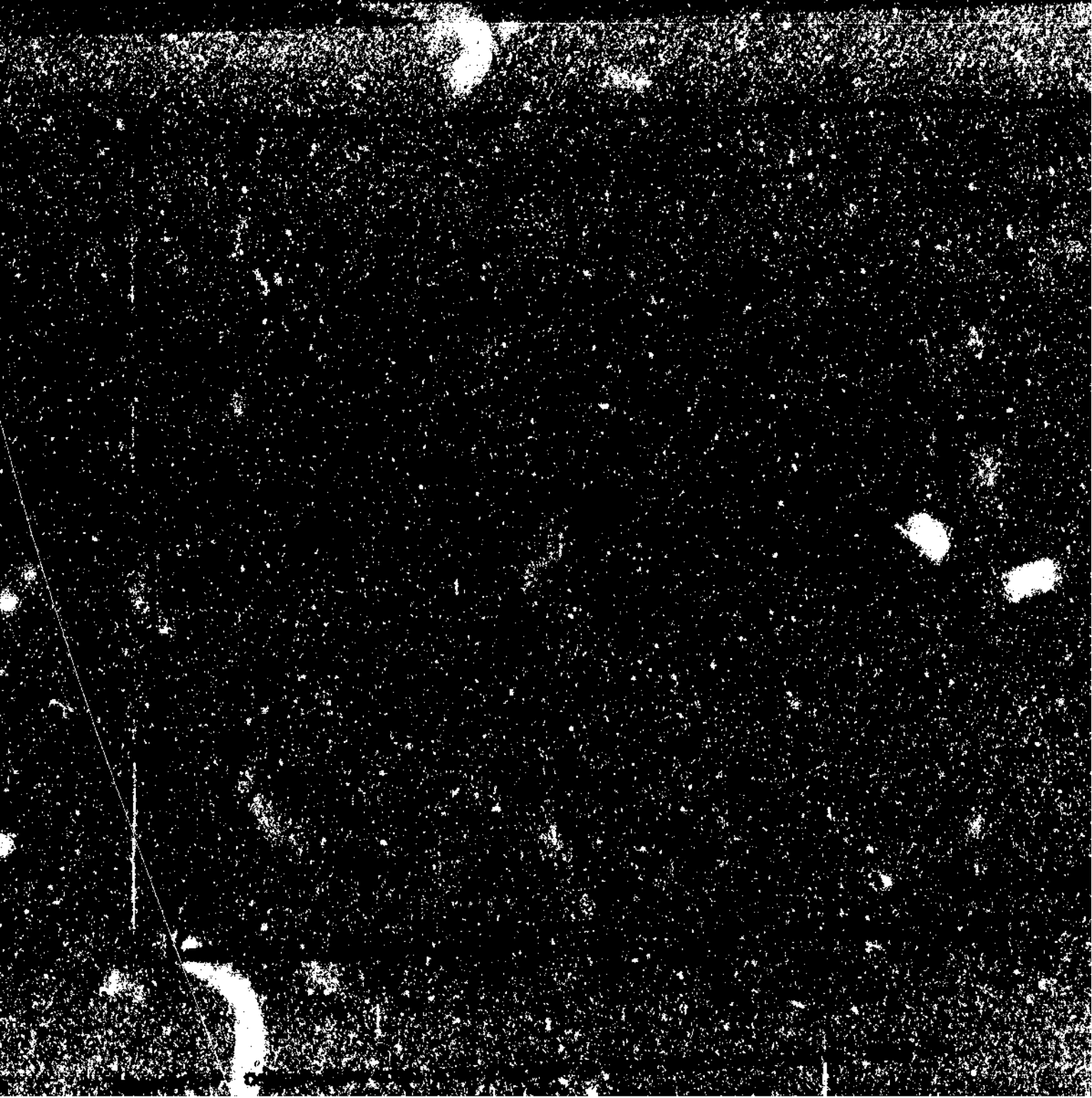

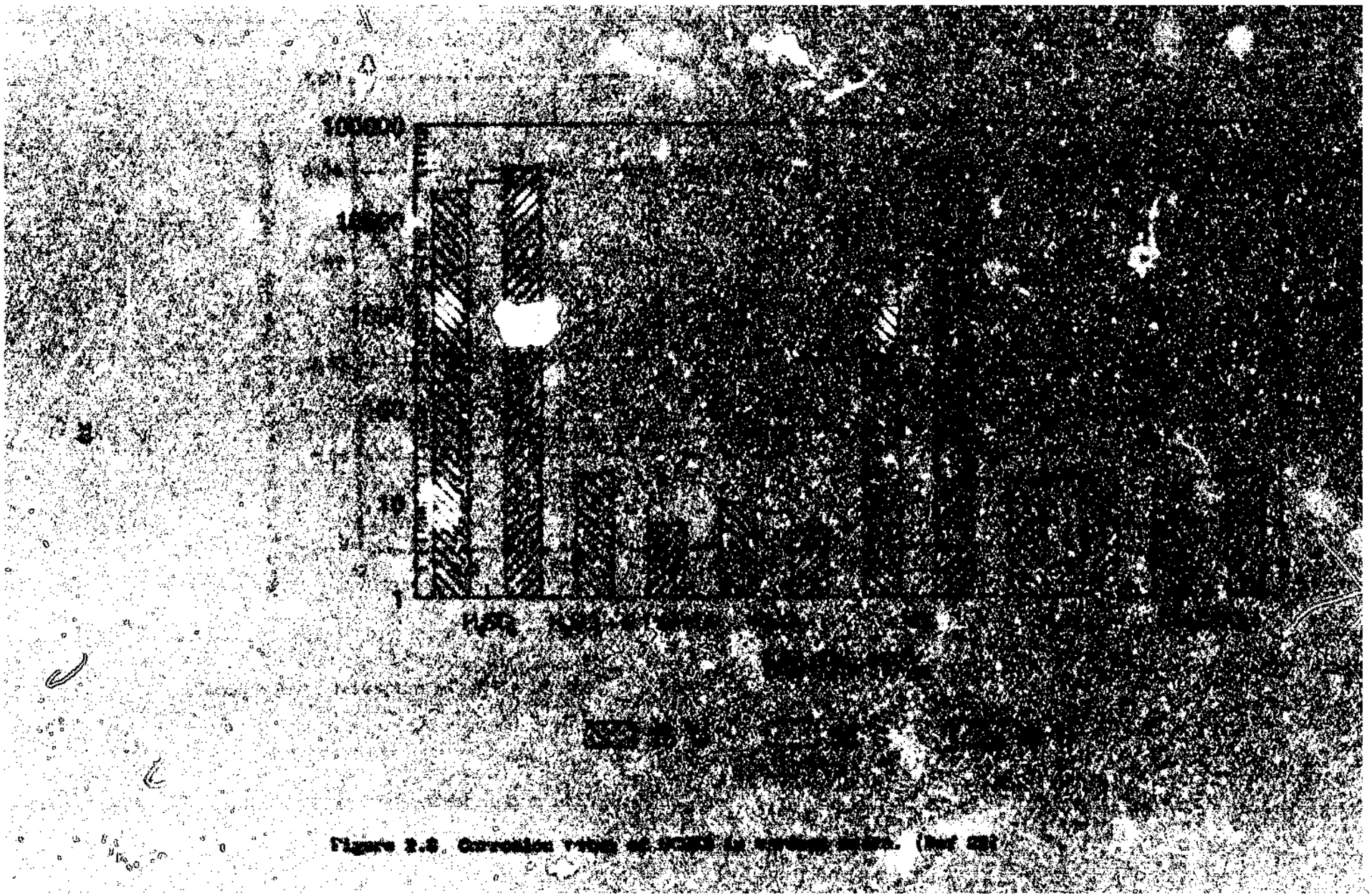

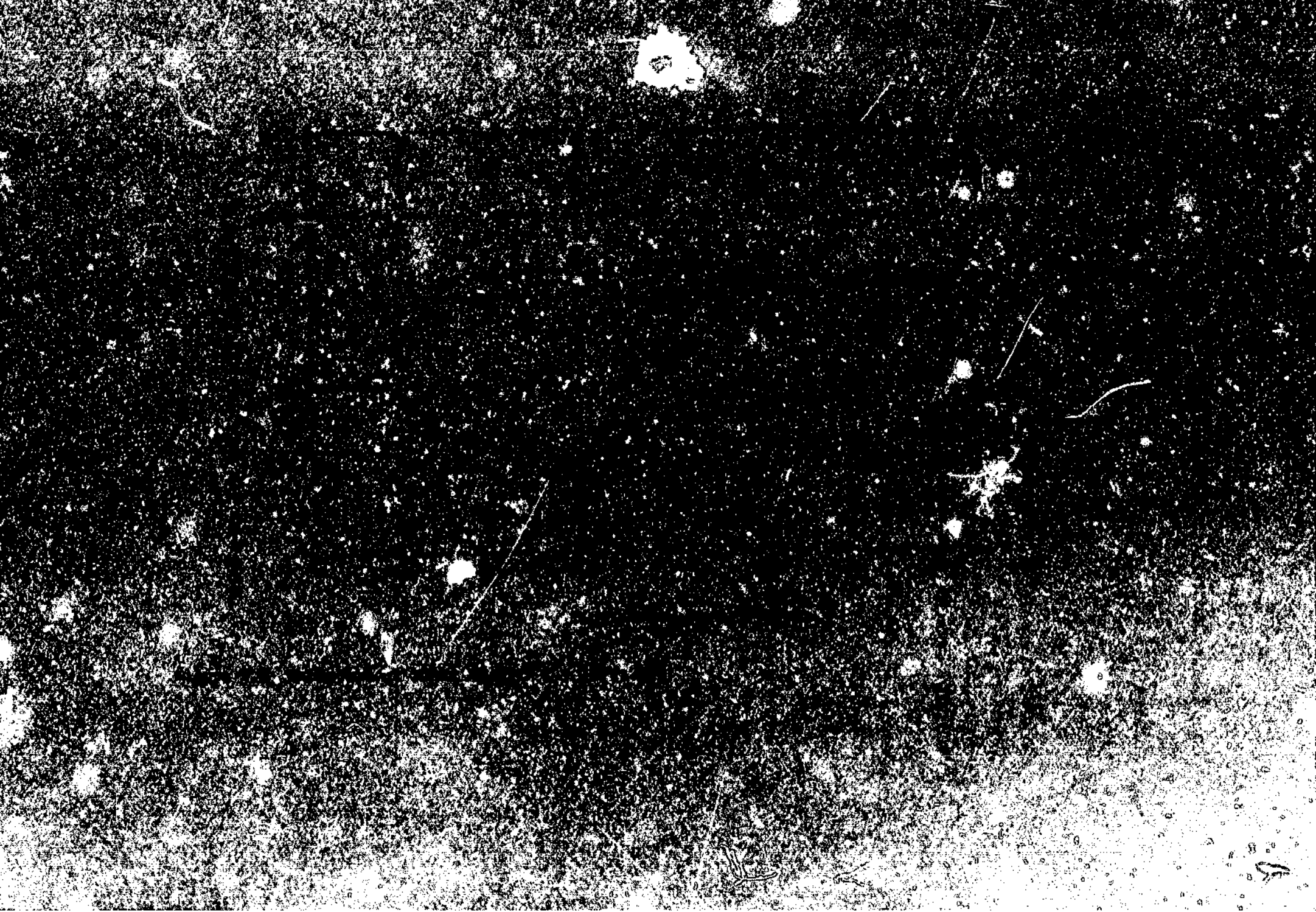

no stress corrosion occurred. Generally, 3CR12 shows good resistance to stress corrosion.

2.5 Fatigue properties of 3CR12

Fatigue failures occur as a result of a large number of load reversals at stresses well below the yield strength of the material. It has been suggested that fatigue-initiated failures may account for up to 90% of all [illegible]

3. THE METALLURGY OF CORTEN STEEL

Corten steel is a group of high-strength-low alloy (HSLA) steels, possessing excellent weathering resistance when exposed to most atmospheric conditions. To be of interest as a construction material, HSLA steels must have characteristics and properties that result in economies to the user when the steels are properly applied. They should be considerably stronger and, in many instances, tougher than structural carbon steel. They must also have sufficient ductility, formability and weldability. In addition, improved resistance to corrosion is often required so that equal service life in a thinner section or longer life in the same section is obtained in comparison to that of a structural carbon steel member.

3.1 Chemical composition of Corten steel

[redacted]

3.2 Mechanical properties of Corten steel

The mechanical properties of different types of Corten steel and structural carbon steel are shown in Table 3.2 [1]. The minimum yield point of typical structural carbon steel (ASTM A36 steel) is 350 MPa and that of Corten steel is 485 MPa. Hence, on the basis of the proportionality of their yield points, the unit working stress employed with the Corten steel may be increased by 1.4 times that used with the structural carbon steel.

Table 3.1 Chemical composition of Corten steels. (%)

	C	Mn	P	S	Si	Cu	Cr	Ni	V	Al
Corten A	0.12 max	0.20-0.5	0.07-0.15	0.05 max	0.25-0.75	0.25-0.55	0.30-1.25	0.65 max	-	-
Corten B	0.19 max	0.80-1.25	0.04 max	0.05 max	0.30-0.65	0.25-0.4	0.40-0.65	0.40 max	0.02-0.1	0.15-0.5
Corten C	0.10 max	0.90-1.35	0.04 max	0.05 max	0.30-0.65	0.25-0.4	0.40-0.7	0.20 max	0.04-0.1	0.15-0.5

Table 3.2 The mechanical properties of Corten and mild steels. (For 25 mm)

	Yield strength (MPa)	Tensile strength (MPa)	Elongation (%)
Corten A	345	485	20 (in 200 mm)
Corten B	345	490	22 (in 200 mm)
Corten C	415	550	21 (in 200 mm)
ASTM A36	250	400-550	20 (in 20 mm)

3.3 Corrosion properties of Corten steel

No material is equally resistant to all of the corrosive conditions to which it might conceivably be exposed. Its performance can only be compared to that of other materials under similar conditions. The superior atmospheric-corrosion resistance of different types of Corten steel in rack tests has been confirmed by its performance in many different kinds of service. Figure 3.1 shows the results obtained with plain carbon and Corten steels exposed to different environments [32]. The [illegible] graph are based on test results achieved [illegible] exposed. The " penetration" pertains to [illegible] of the samples, one side only, [illegible] corrosion. From the results we can [illegible] the corrosion resistance of Corten steel is [illegible] of carbon steel.

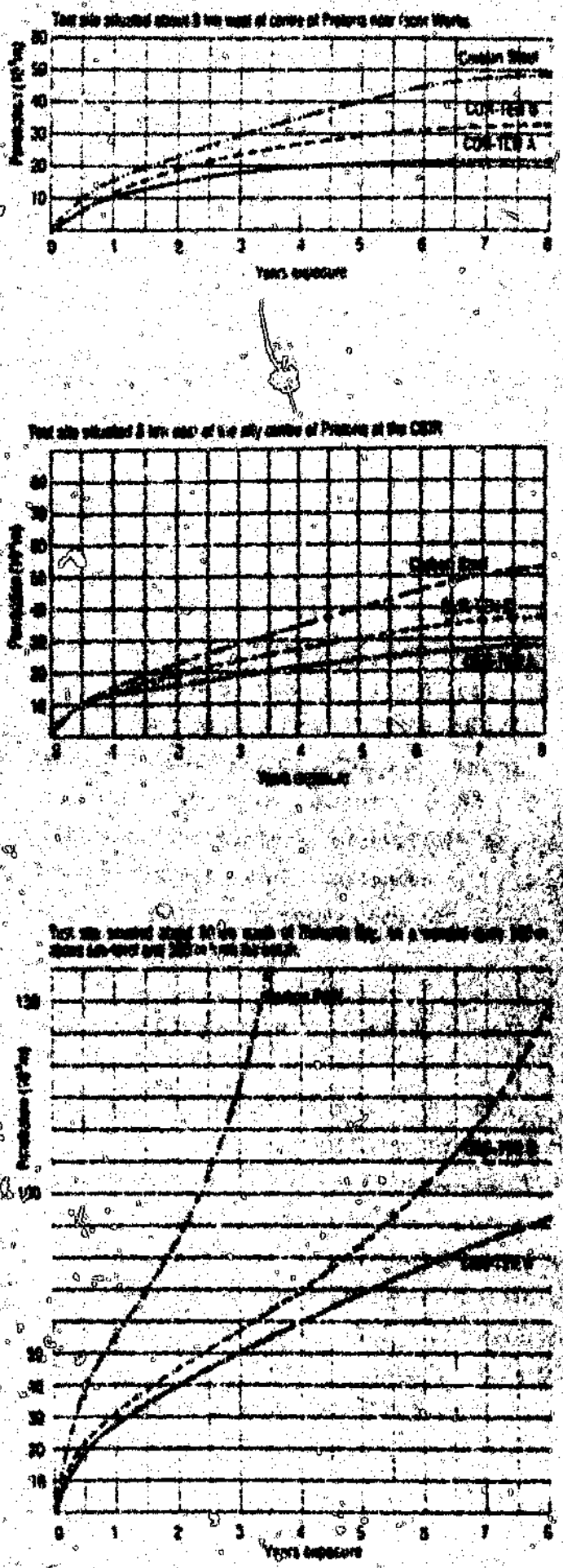

Figure 3.1 Corten and mild steels exposed in the different environments

4 THE METALLURGY OF MILD STEEL

Plain carbon steels undoubtedly represent the most important group of materials known. They represent by far the major percentage of steel production with the widest diversity of application of any of the engineering materials.

4.1 The chemical composition and microstructure of mild steel

The chemical compositions of carbon steel are shown in Table 4.1. Carbon steel with carbon content below 0.30% is normally called mild steel. The microstructure of carbon steel normally consists of ferrite and pearlite. The amount of pearlite varies from practically zero percent at very low carbon contents 0.06% to 100% for a carbon content of 0.8%. Structural carbon steel will normally contain up to about 0.3% C and its microstructure will consist of about 60% ferrite and 40% pearlite. The strength and hardness of carbon steel increase with increasing carbon content.

4.2 Mechanical properties of mild steel

The average mechanical properties of as-rolled one-inch bars of carbon steels, as a function of carbon content, are shown in Figure 4.1 [7]. This figure is illustrative of the general effect of carbon level when the microstructure and grain size are held at a reasonable level. It can be seen that the hardness, tensile strength and yield strength increase with increasing carbon content, while the elongation, reduction of area and Charpy impact values decrease sharply.

Table 4.1 The chemical composition of different types of mild steel (ref.)

AISI Number	Chemical Composition (%)			
	C	Mn	P max.	S max.
1006	0.08 max.	0.25 - 0.40	0.040	0.050
1008	0.10 max.	0.30 - 0.50	0.040	0.050
1010	0.08 - 0.13	0.30 - 0.60	0.040	0.050
1012	0.10 - 0.15	0.30 - 0.60	0.040	0.050
1015	0.13 - 0.18	0.30 - 0.60	0.040	0.050
1016	0.13 - 0.18	0.60 - 0.90	0.040	0.050
1017	0.15 - 0.20	0.30 - 0.60	0.040	0.050
1018	0.15 - 0.20	0.60 - 0.90	0.040	0.050
1019	0.15 - 0.20	0.70 - 1.00	0.040	0.050
1020	0.18 - 0.23	0.30 - 0.60	0.040	0.050
1021	0.18 - 0.23	0.60 - 0.90	0.040	0.050
1022	0.18 - 0.23	0.70 - 1.00	0.040	0.050
1023	0.20 - 0.25	0.30 - 0.60	0.040	0.050
1025	0.22 - 0.28	0.30 - 0.60	0.040	0.050
1026	0.22 - 0.28	0.60 - 0.90	0.040	0.050
1030	0.28 - 0.34	0.60 - 0.90	0.040	0.050

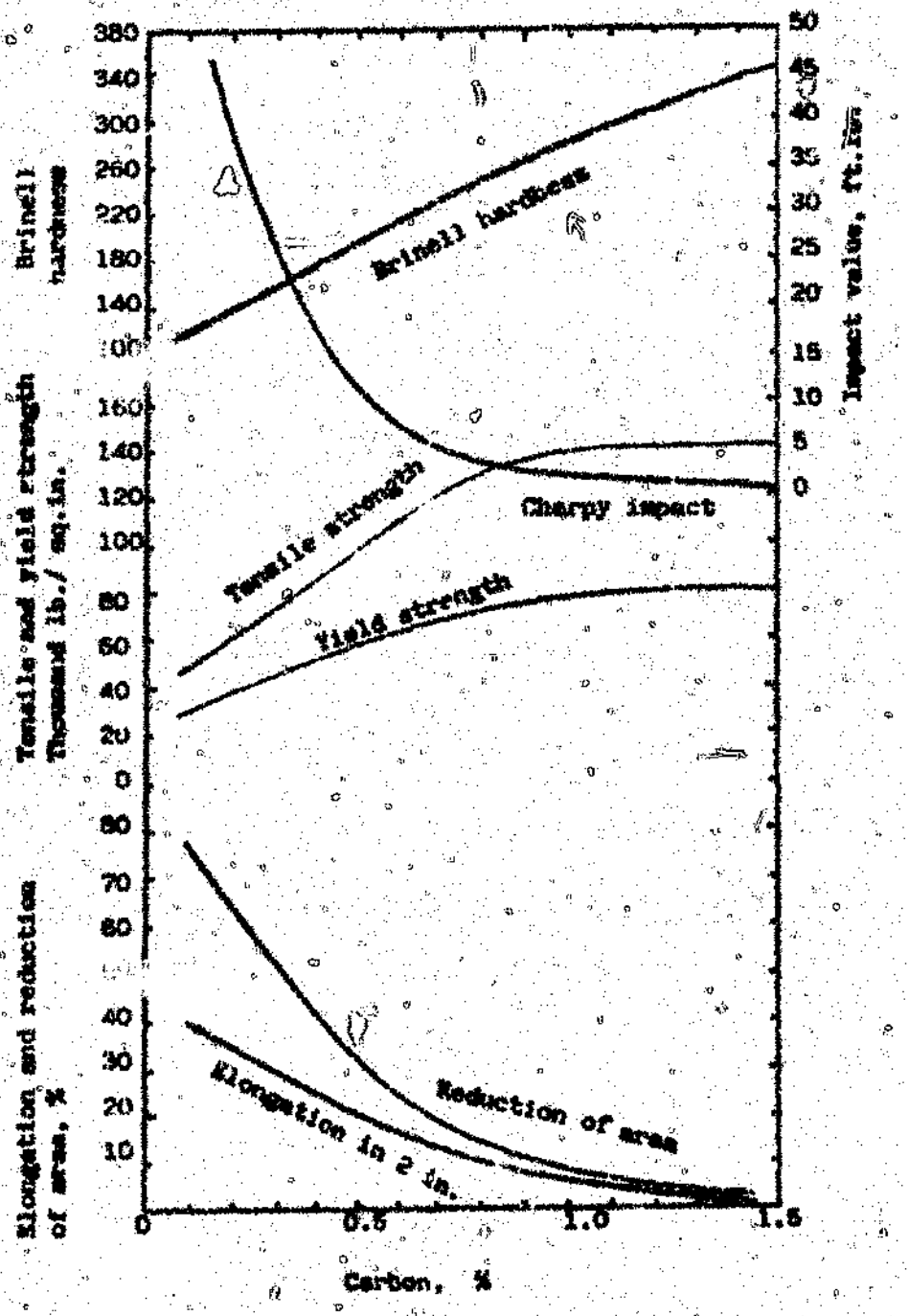

Figure 4.1 Variations in the average mechanical properties of plain carbon steels with carbon content. (Ref 33)

4.3 The corrosion fatigue properties of mild steel

The corrosion properties of carbon steel have been dealt with in previous sections from comparisons made between carbon steel and 3CR12 or Corten steels.

The corrosion fatigue crack growth rate of AISI 1018 steel has been determined at room temperature and in various selected aqueous environments. Figure 4.2.[34] shows the rate of fatigue crack growth versus stress intensity factor. The results show that polluted seawater and low alkalinity tap water promote the growth of corrosion fatigue cracks. Natural seawater appears to be a relatively milder medium for corrosion fatigue crack growth when compared to that of polluted seawater or tap water.

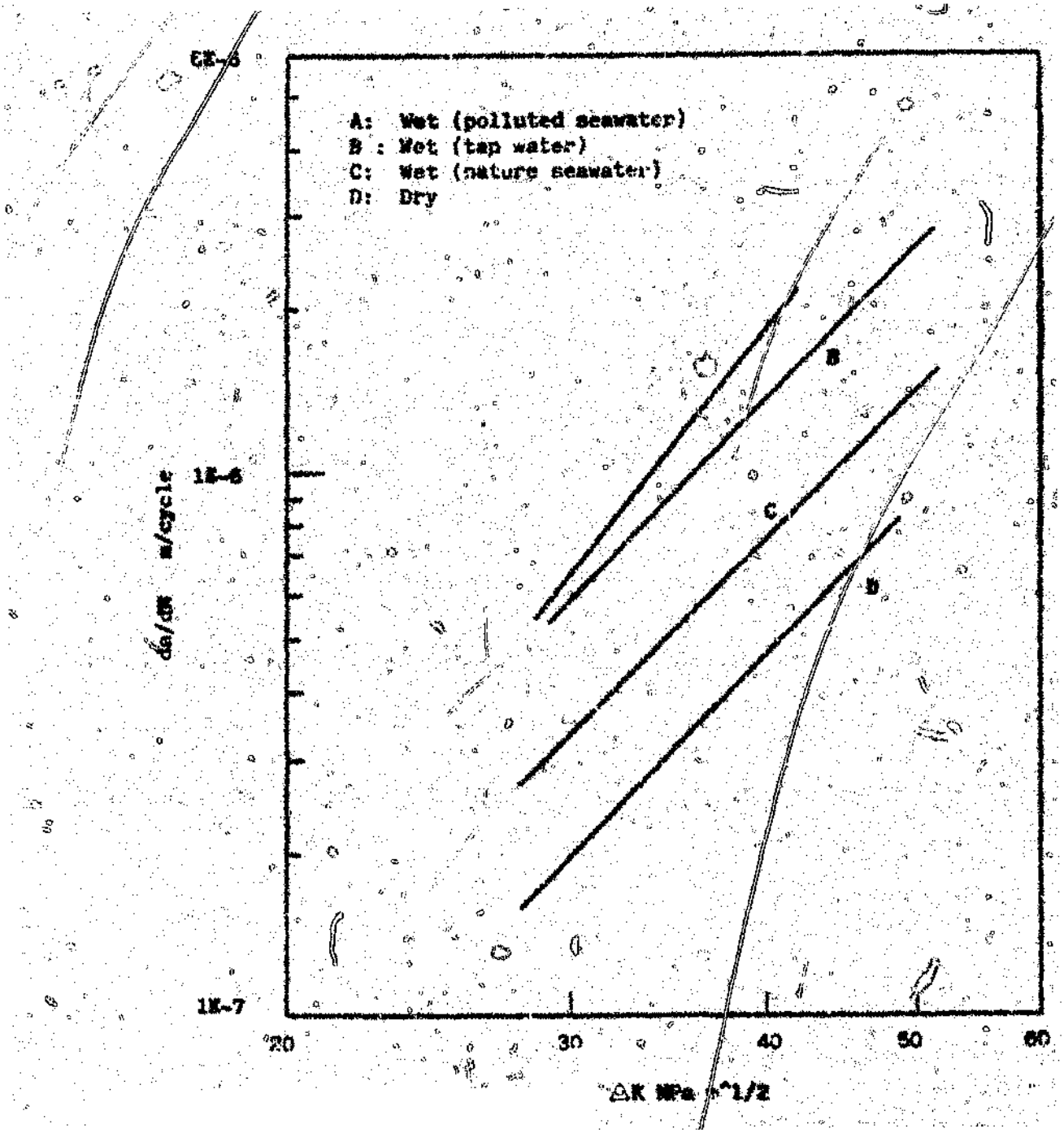

Figure 4.2 Fatigue crack growth versus ΔK for AISI 1018 in various environments. (Ref 34)

5. EXPERIMENTAL PROCEDURE

The experimental work was divided into two parts. The first part was a brief investigation into the mode of failure of coal wagons while the second part dealt with the testing of 3CR12, Corten and mild steel for fatigue, corrosion and corrosion fatigue properties.

The object of the first part of the experimental work was to gain insight into the mechanisms involved in the failure of coal wagons and to attempt to simulate in the laboratory the conditions experienced by the coal wagon materials. Then by testing the selected three steels under these simulated conditions comparative results could be obtained which might enable the best material to be chosen for the construction of such wagons.

5.1 Materials and [illegible]ermination

Coal wagons were examined at the maintenance workshop of the SATS in Cape Town and the marshalling yard in Bonnie. Serious rust problems were found on Corten wagons. Thick layers of scale were found to form on the side walls of the wagons about 1 m up from the floor. A sample of scale was taken from the side wall of a Corten wagon, which had been used as a coal carrier for about ten years.

A sample of 3CR12 plate was taken from the floor of a wagon which had been in use for about three months.

The 3CR12, Corten and mild steel used in the second part of this study were obtained from Middelburg Steel and Alloys, ISCOR and Trident respectively. The chemical composition of these three steels were determined and are shown in Table 5.1. The analysis of the Corten scale is also shown in Table 5.1.

Table .) Chemical composition of as-received 3CR12, Corten, mild steel and Corten scale.

0	C	Si	S	P	Mn	V	Ni	Cr	Mo	Cu	Al
3CR12 steel	0.023	0.302	0.021	0.024	1.209	-	0.66	11.56	0.66	0.079	0.016
Corten steel	0.10	0.30	0.005	0.062	0.35	0.005	0.31	0.51	0.001	0.30	0.006
Mild steel	0.16	0.20	0.028	0.013	0.054	-	-	-	-	-	-
Corten scale	-	0.05	0.134	-	0.03	0.01	0.04	0.59	0.04	0.26	-

5.1.1 Microstructural examination of 3CR12, Corten and mild steel

Specimens were prepared metallographically and examined by optical microscopy. The specimens were mounted separately in plastic and prepared by grinding to 1200 grit finish on silicon carbide paper and polishing to a 3 μm finish with diamond. Specimens were examined in the polished and in the etched conditions. Nital etching (2ml HNO_3, 98ml methanol) was used for Corten and mild steels. Nital revealed the grain boundaries and constituents in these steels. Vilella's reagent (100 ml ethanol, 5ml HCl, 1g picric acid) was used for steel 3CR12. Vilella's reagent is good for ferrite-carbide structures and enabled the martensite to be identified by its darker colour. Etching time was about 10-25 s.

5.1.2 Hardness tests of 3CR12, Corten and mild steel

Hardness tests were carried out with a Vickers hardness tester using a load of 10 kg. At least 10 hardness measurements were performed on each specimen.

5.1.3 Tensile tests of 3CR12, Corten and mild steel

Hounsfield tensile specimens, Figure 5.1, were machined in the longitudinal and transverse directions with respect to the rolling direction of the steels. All tests were carried out at room temperature. The tensile tests were performed on an Instron servo-hydraulic testing machine of 100 kN capacity at a cross-head speed of 1 mm/min. The ultimate tensile strength, 0.2% proof stress and elongation of all the specimens were measured. The results tested for the mean value at 95% confidence limit.

5.1.4 Impact tests on 3CR12, Corten and mild steel

Sub-size Charpy-V-Notch (CVN) specimens were used to evaluate the impact properties of 3CR12, Corten and mild steels in the as received condition . Specimens were machined in the longitudinal and transverse directions for all steels. The dimensions of the CVN specimen are shown in Figure 5.2. At least three tests were performed on each steel.

5.2 [illegible]

[illegible]

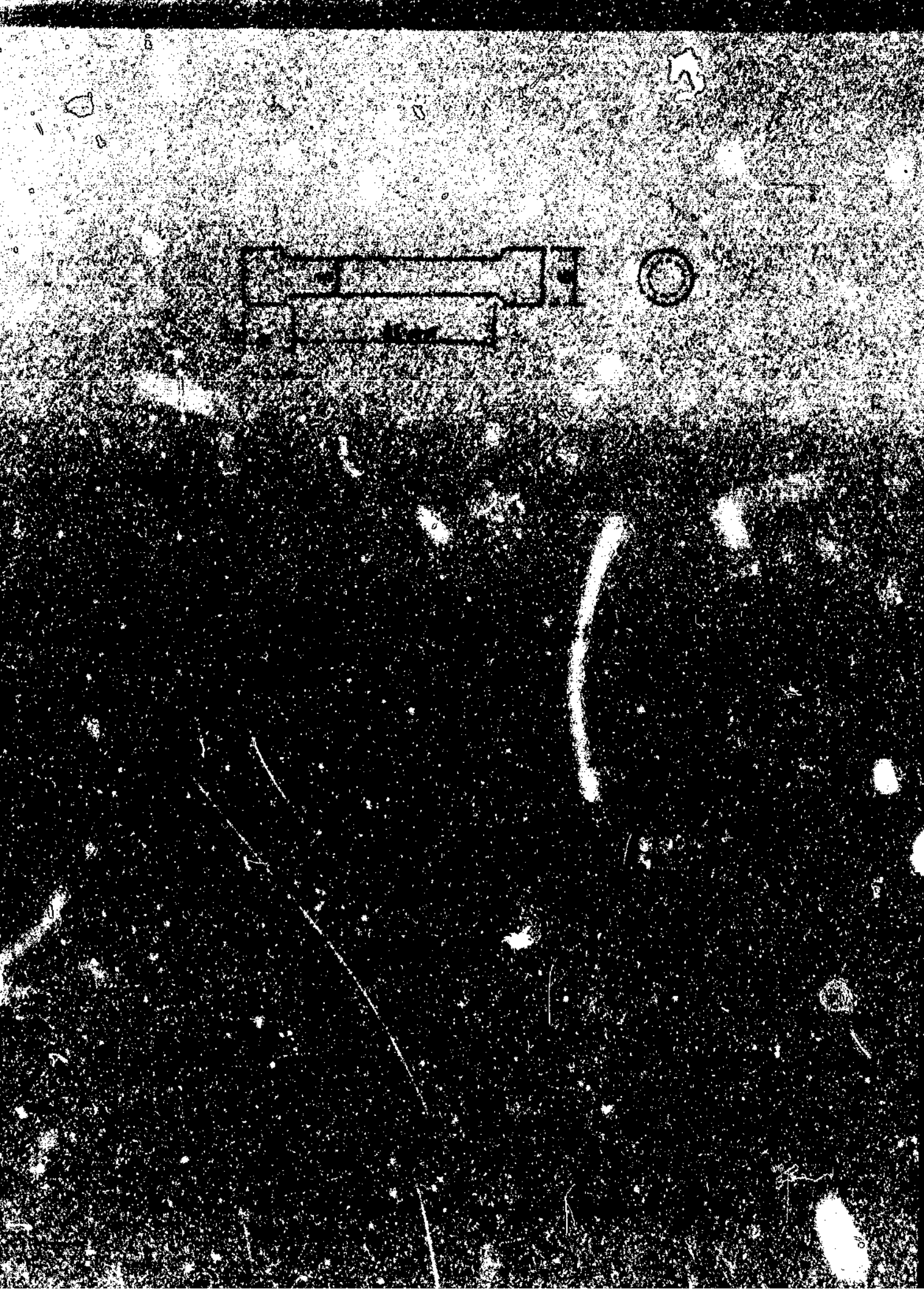

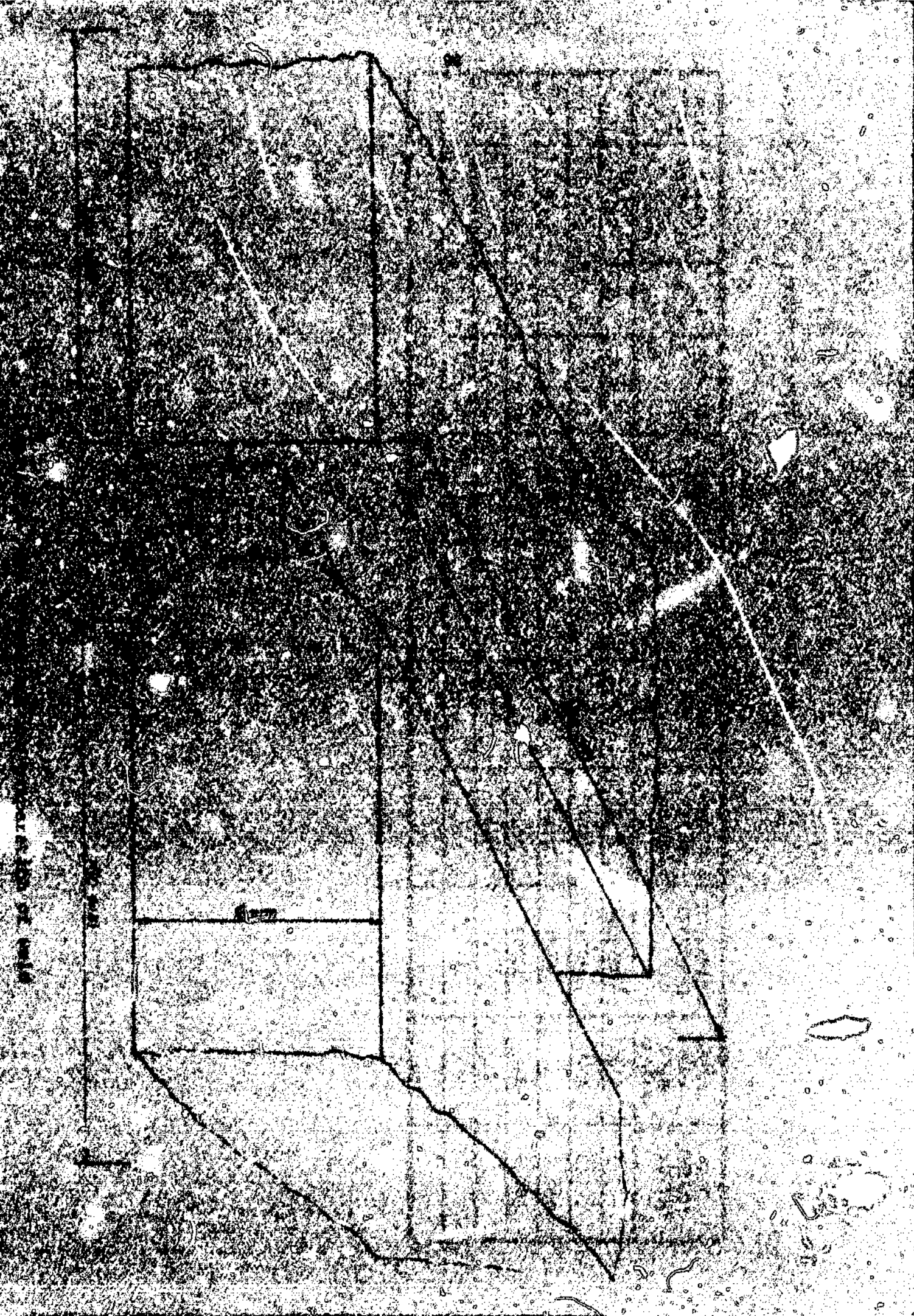

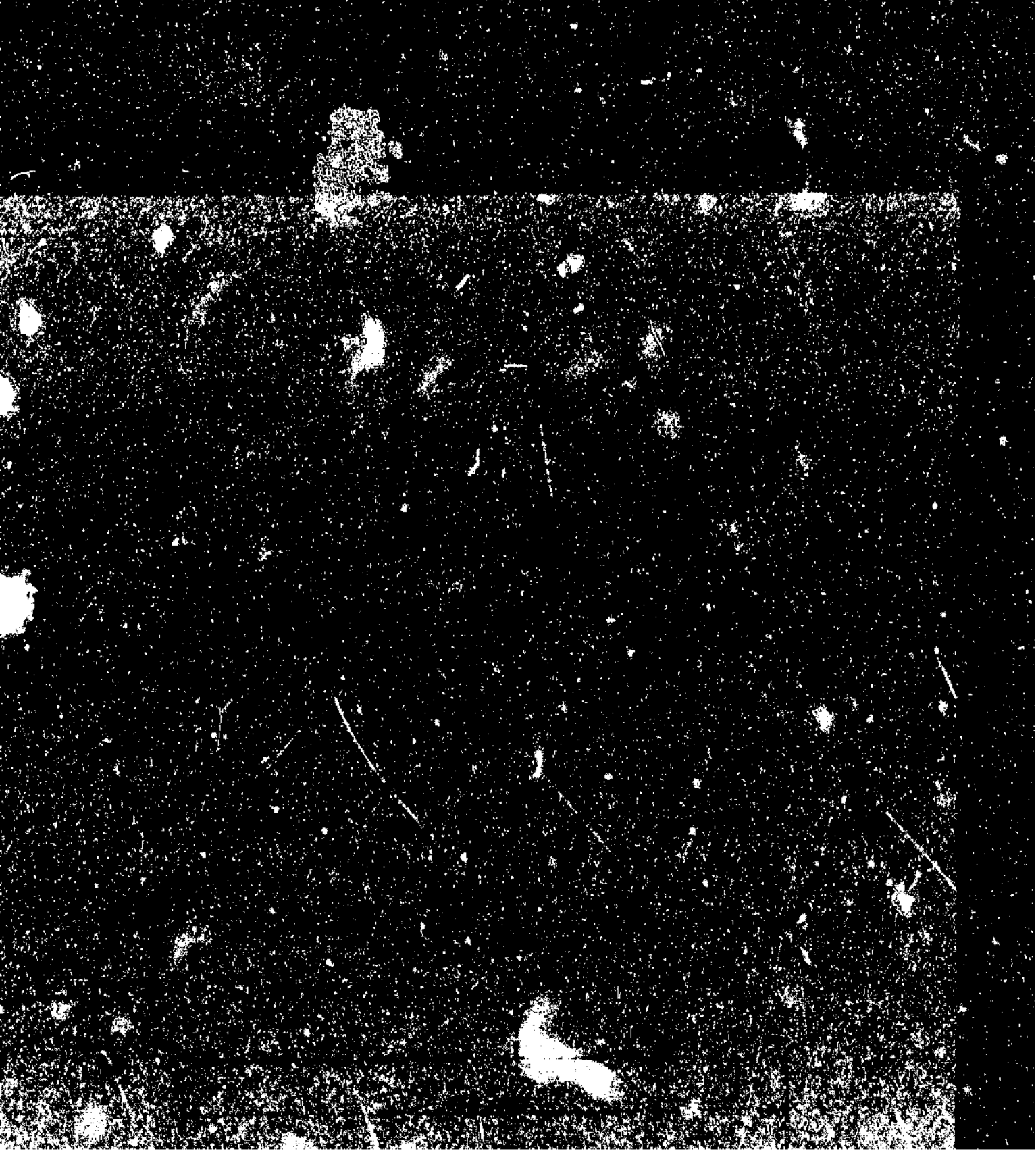

Table 5.4 The record of Welding parameters of mild steel

WELD TYPE	FILLER MATERIAL	DIA (MM)	RUN NO	CURRENT TYPE & POL	AMPERAGE	VOLTAGE	TRAVEL SPEED (MM/SEC)	[illegible]	[illegible]
[illegible]	[illegible]	3.15	[illegible]	[illegible]	150	[illegible]	[illegible]	[illegible]	[illegible]
[illegible]	[illegible]	3.25	[illegible]	[illegible]	160	[illegible]	[illegible]	[illegible]	[illegible]
[illegible]	[illegible]	4.0	[illegible]	[illegible]	170	[illegible]	[illegible]	[illegible]	[illegible]
[illegible]	[illegible]	[illegible]	[illegible]	[illegible]	[illegible]	[illegible]	[illegible]	[illegible]	[illegible]
[illegible]	[illegible]	[illegible]	[illegible]	[illegible]	[illegible]	[illegible]	[illegible]	[illegible]	[illegible]
[illegible]	[illegible]	[illegible]	[illegible]	[illegible]	[illegible]	[illegible]	[illegible]	[illegible]	[illegible]

5.2.2 Hardness tests of welded plates

Hardness tests were carried out to investigate hardness variations from the parent metal through the HAZ and into the weld metal. A Vickers hardness tester was used with a load of 10kg.

5.2.3 Tensile tests of welded plates

Hounsfield tensile specimens were used to evaluate weld metal tensile properties. The orientation of specimens is shown in Figure 5.4-a. All tests were carried out at ambient temperature. The tensile tests were performed on an Instron servo-hydraulic testing machine of 50 kN capacity at a constant displacement rate. The yield strength, ultimate tensile strength, percentage reduction in area and elongation of all the specimens were measured and results quoted are the means of at least three tests.

5.2.4 Impact tests on welded plates

Sub-size Charpy-V-Notch (CVN) specimens were used to evaluate weld metal impact properties at ambient temperature. The notch orientation was through the thickness of the weld (Figure 5.4-b) so that fracture occurred along the length of the weld. At least three tests were performed on each steel.

5.3 Fatigue tests

Crack growth can occur at K (stress intensity factor) levels much below K_{Ic} (plain -strain fracture toughness

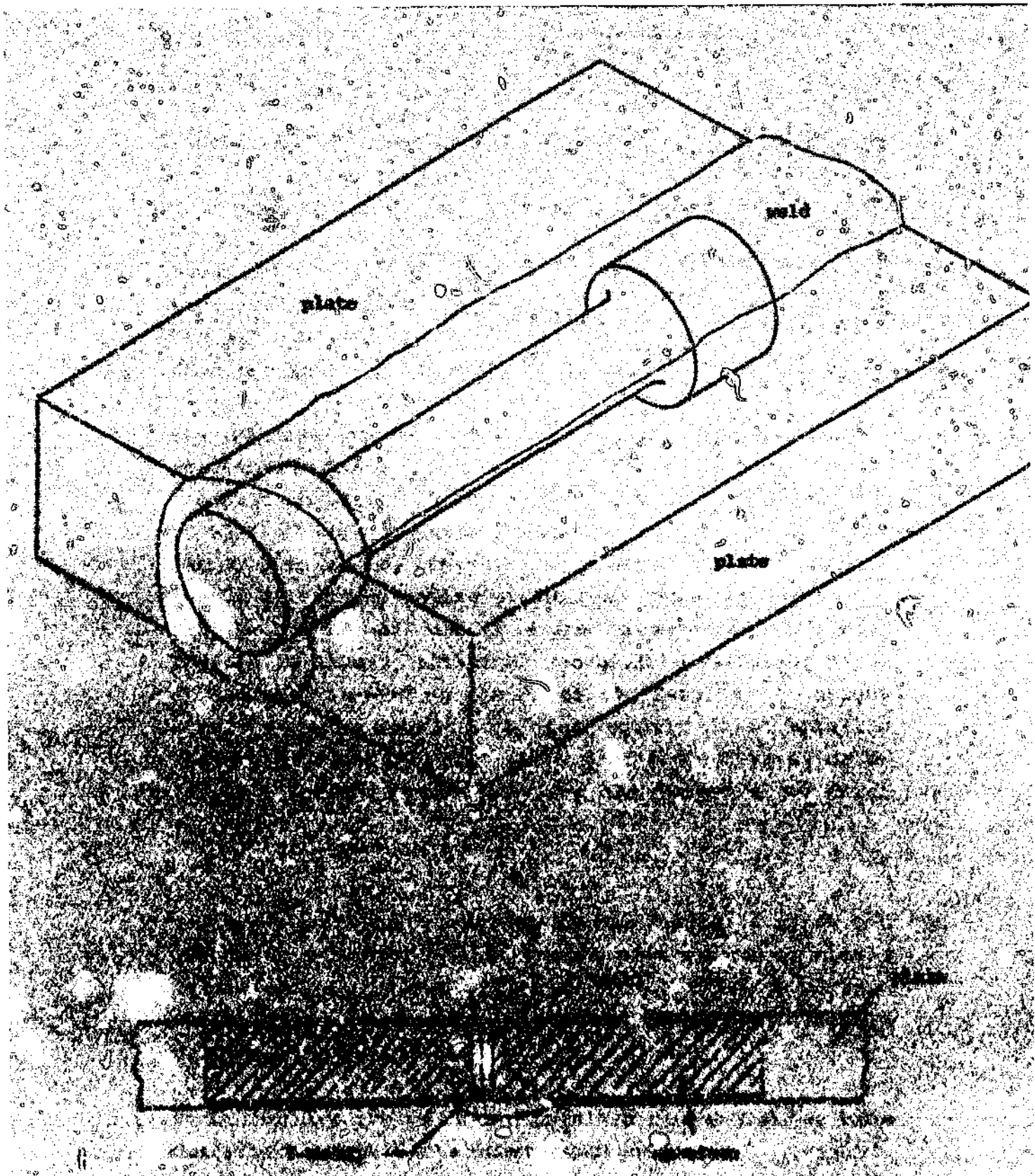

Figure 3.4 The orientation of a Kournfield tensile specimen (a) and sub-size Charpy-V notch specimen (b) in welded plate.

factor) in any structural alloy when cyclic loading is applied. In other words, it is the accumulation of damage from the cyclic plastic deformation in a small zone at a crack tip which accounts for fatigue crack growth at K level much below K_{Ic}. The concentration of damage is increased further when strain hardening occurs and causes the zone of reversed plastic deformation to be smaller than the zone formed during one application of load[11].

The general nature of fatigue crack growth and its description using fracture mechanics can be summarized by the plot shown in Figure 5.3. This figure based on Paris et al [11] shows a logararithmic plot of the crack growth per cycle, da/dN, versus the stress-intensity factor range, ΔK, corresponding to the load cycle applied to the sample. A plot of similar shape is obtained for most structural alloys, although the absolute values of da/dN and ΔK will depend on the material, nature of the crack growth rate tests, and heat treatment. Most structural materials have been found that the crack growth rate versus ΔK are characterized by three regions:

a) Region I which corresponds to low values of da/dN and ΔK. In this region fatigue cracks grow extremely slowly, or not at all if the values of ΔK is below a certain limit. This lower limit of ΔK is called the threshold value and is represented by K_{th}.

b) Region II which is an intermediate region and has been described by the Paris power equation:

$$da/dN = C\,(\Delta K)^n$$

where C and n are material constants.

c) Region III in which crack growth is unstable. The value of ΔK beyond a certain limit corresponds either to

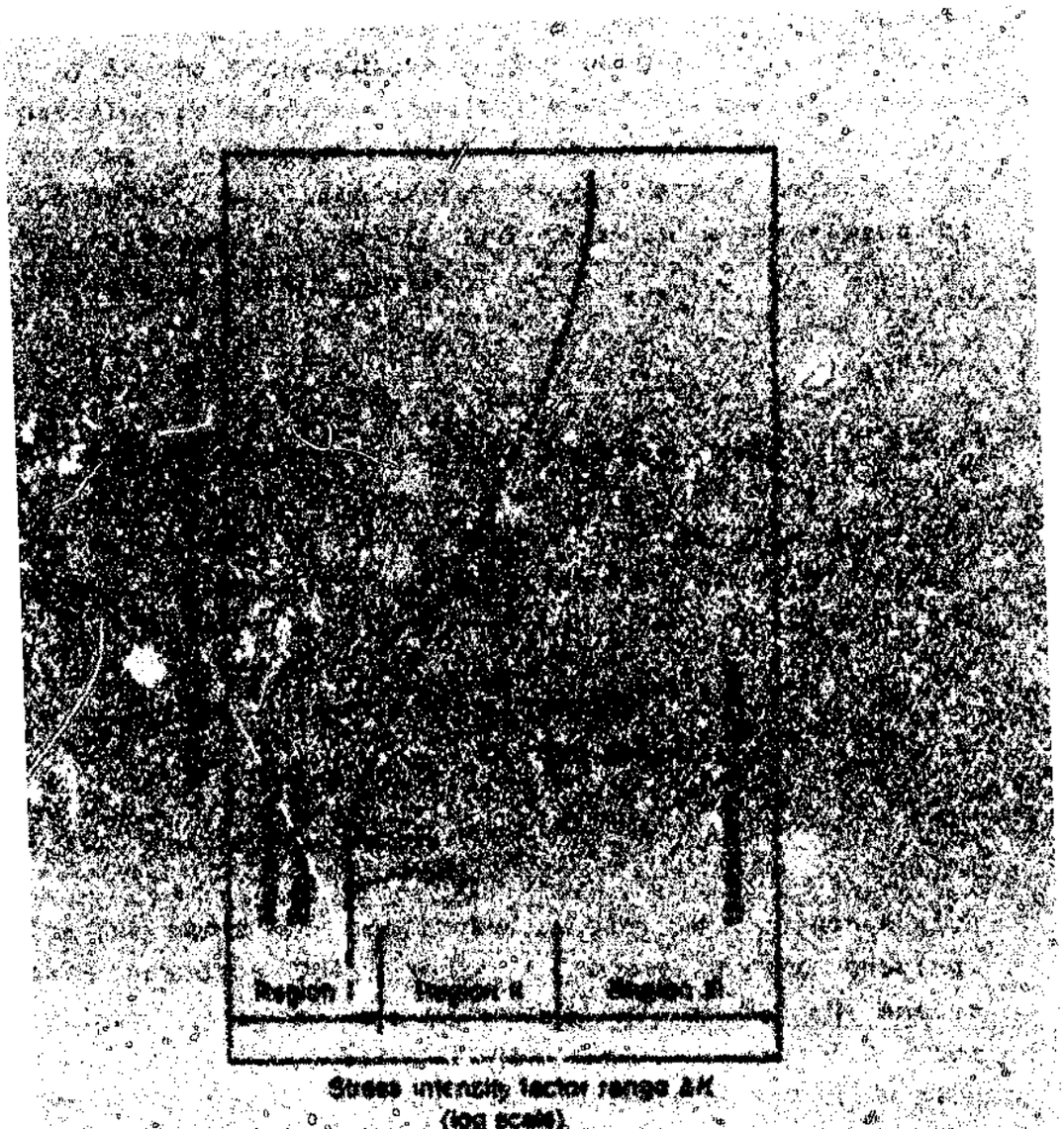

Figure 3.5 Schematic representation of the general nature of fatigue crack growth. (Ref 26)

K_{Ic} or to gross plastic deformation of the specimen.

The crack growth rates and fatigue life of components and structures may be estimated by using Region II of the curve in Figure 5.5. The general limitation of this application is that the power-law representation applies only in the intermediate region of da/dN and ΔK. It is particulary important that the power-law relation not be extended to higher values of da/dN and ΔK than those supported by laboratory test data, because an underestimate of da/dN, and thus an overestimate of fatigue life would result.

5.3.1 Preparation of fatigue test specimens

The specimens for the fatigue growth tests were of the compact tension type (ASTM E647)[47] as shown in Figure 5.6. Specimens were machined from the materials in the as-received condition.

5.3.2 Testing procedure

The specimens were precracked in air, in accordance with ASTM standard E647, prior to crack growth testing. Fatigue testing was performed on a 50 kN Ansler mechanical type machine, Figure 5.7 and 5.8. The operation was controlled at a frequency of 150 Hz. A sine waveform was employed. A R ratio (minimum load/maximum load) of 0.32 was employed in ambient conditions. Fatigue crack extension was measured using a low-power travelling microscopy. The crack length was measured to an accuracy of 0.01 mm. Oblique illumination was used to accentuate the contrast at the crack tip. The end of the test was taken to be the point at which the crack had propagated 15 mm from the notch. At that point the specimen was

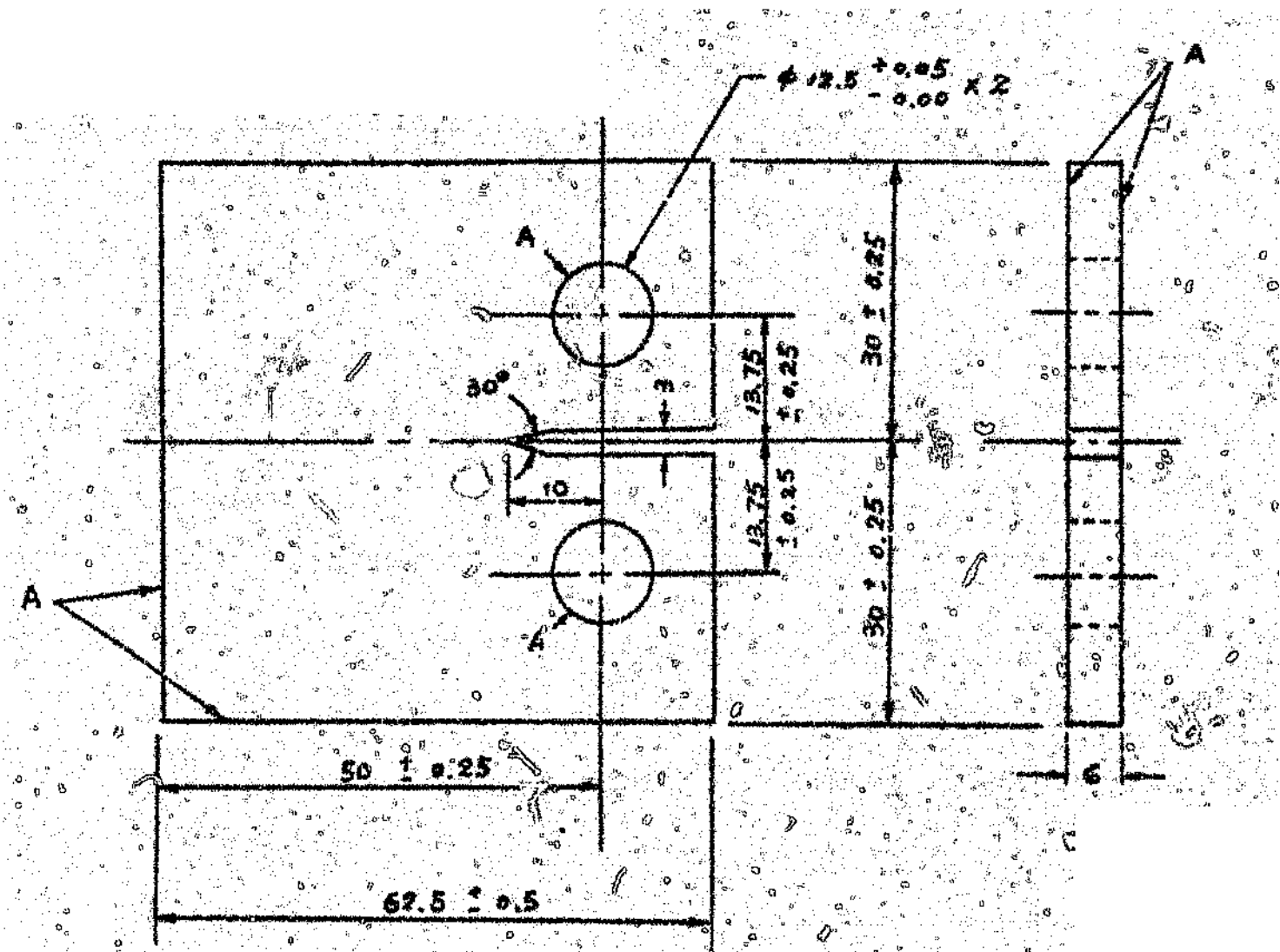

Figure 5.6 The design of Compact-Type (CT) specimens for fatigue crack growth rate testing. (Ref 37)

Figure 5.7 Ansler mechanical type machine of 50kN capacity.

Figure 5.8 General view of the fatigue testing arrangement in air.

overloaded to failure for examination of the fracture surface by scanning electron microscopy (SEM).

The stress intensity factor ΔK was calculated from the following equation[37]:

$$\Delta K = [\ \Delta P\ (\ 2+\ \alpha\ )\ /\ BW^{1/2}(\ 1\ -\ \alpha\ )^{3/2}\ ]\ (\ 0.886\ +\ 4.642\alpha\ -\ 13.32\alpha^2\ +\ 14.42\alpha^3\ -\ 5.62\alpha^4\ )$$

where $\alpha = a/w$

ΔP : fatigue load range = Pmax - Pmin

B : specimen thickness

W : specimen width

a : crack length

The final result is therefore a curve of log da/dN versus ΔK for the test.

5.4 Corrosion fatigue tests

There are countless combinations of physical and chemical testing environments which can affect crack growth in structural alloys. For a few conditions[38], an increase in the K value is required for crack growth at a designed rate, but generally the K value is decreased when specimens are exposed to service environments other than normal laboratory air. The general variables in any testing environment can include variation in loading temperature, rate of loading, and chemical environment. As might be expected, temperature generally increases the kinetics of environmental attack and diffusion of embrittling species, so growth rates increase at higher temperatures.

The major difficulty and limitation of measuring crack growth as affected by testing environments is in accurately producing and maintaining the specified test conditions during the laboratory test. The proper use of high and low loading rates, high and low temperature chambers, and environmental chambers can greatly increase the time and cost required to obtain laboratory test results.

Fatigue testing in [illegible] lythionic acid solution was carried out on a 250 kN E.S.H. servo-hydraulic testing machine coupled to an electronic controller, Figure 5.9. An environmental cell was used for the tests, Figure 5.10. A hydrogen sulfide indictor was used during the tests for reasons of safety. The maximum allowable concentration of hydrogen sulfide in the air for an 8-hour work day is 10 ppm, which is well above the level detectable by smell. Exposure to high concentrations of hydrogen sulfide can be fatal.

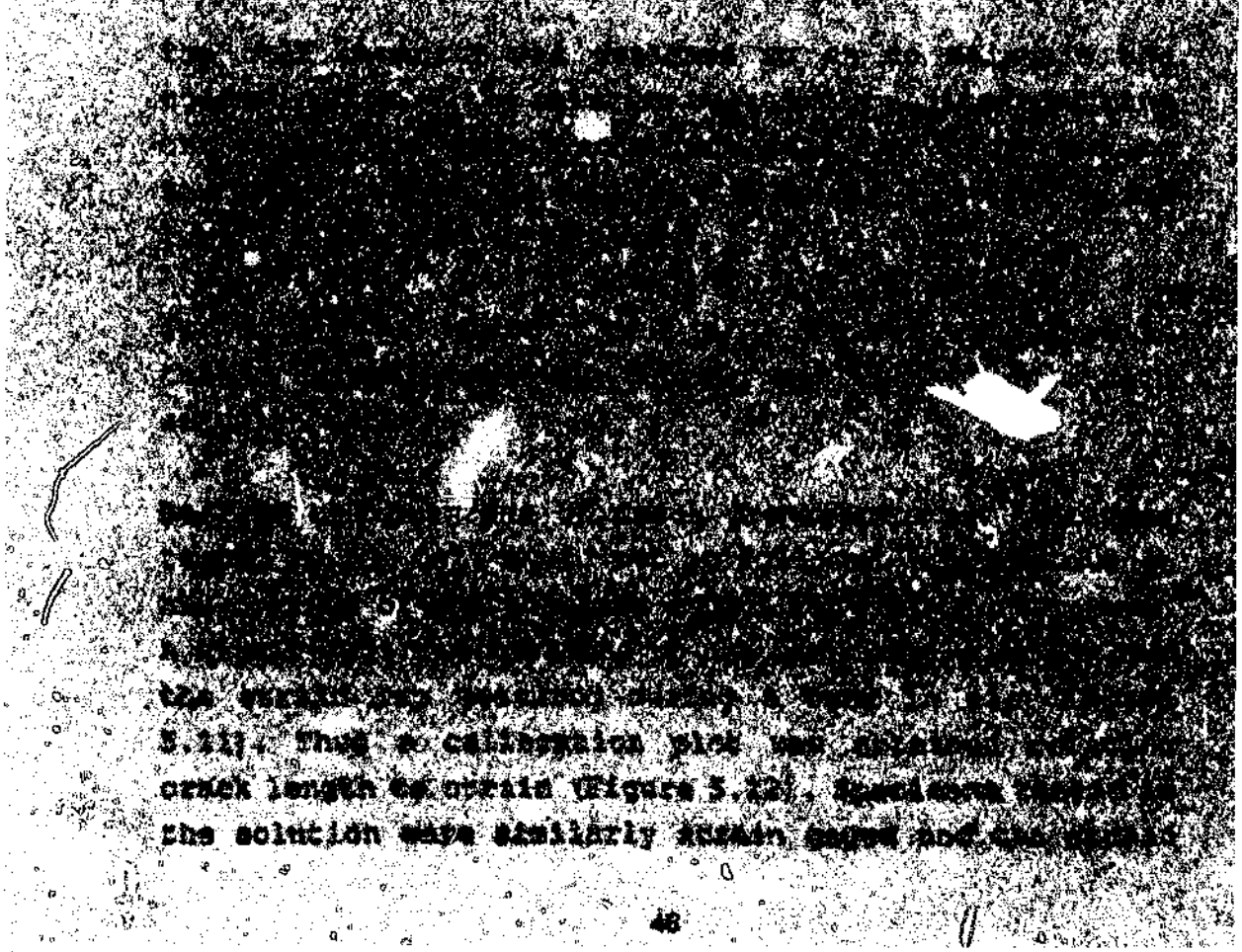

Figure 5.9 Servo-hydralic testing machine of 250 kN capacity and electronic controller.

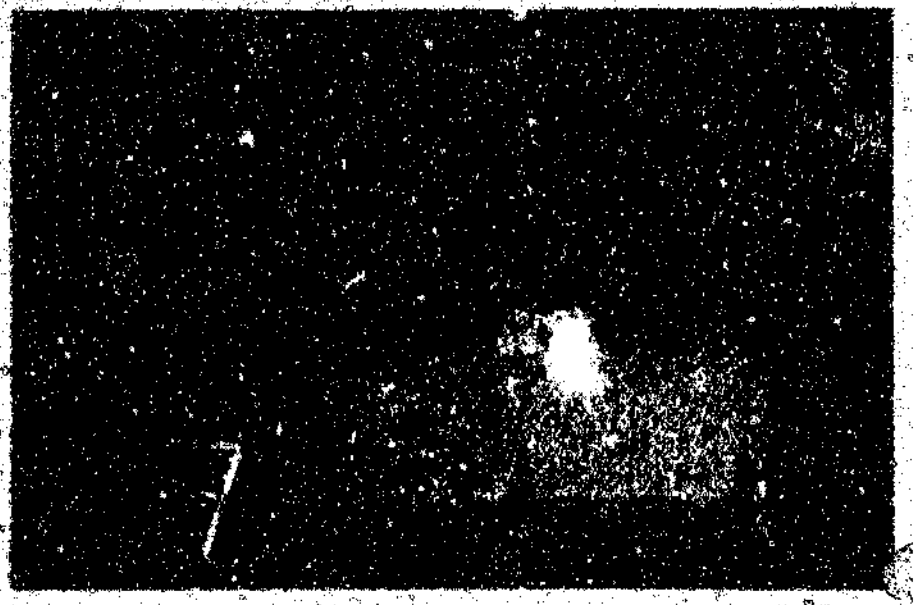

Figure 5.10 General view of the environmental cell.

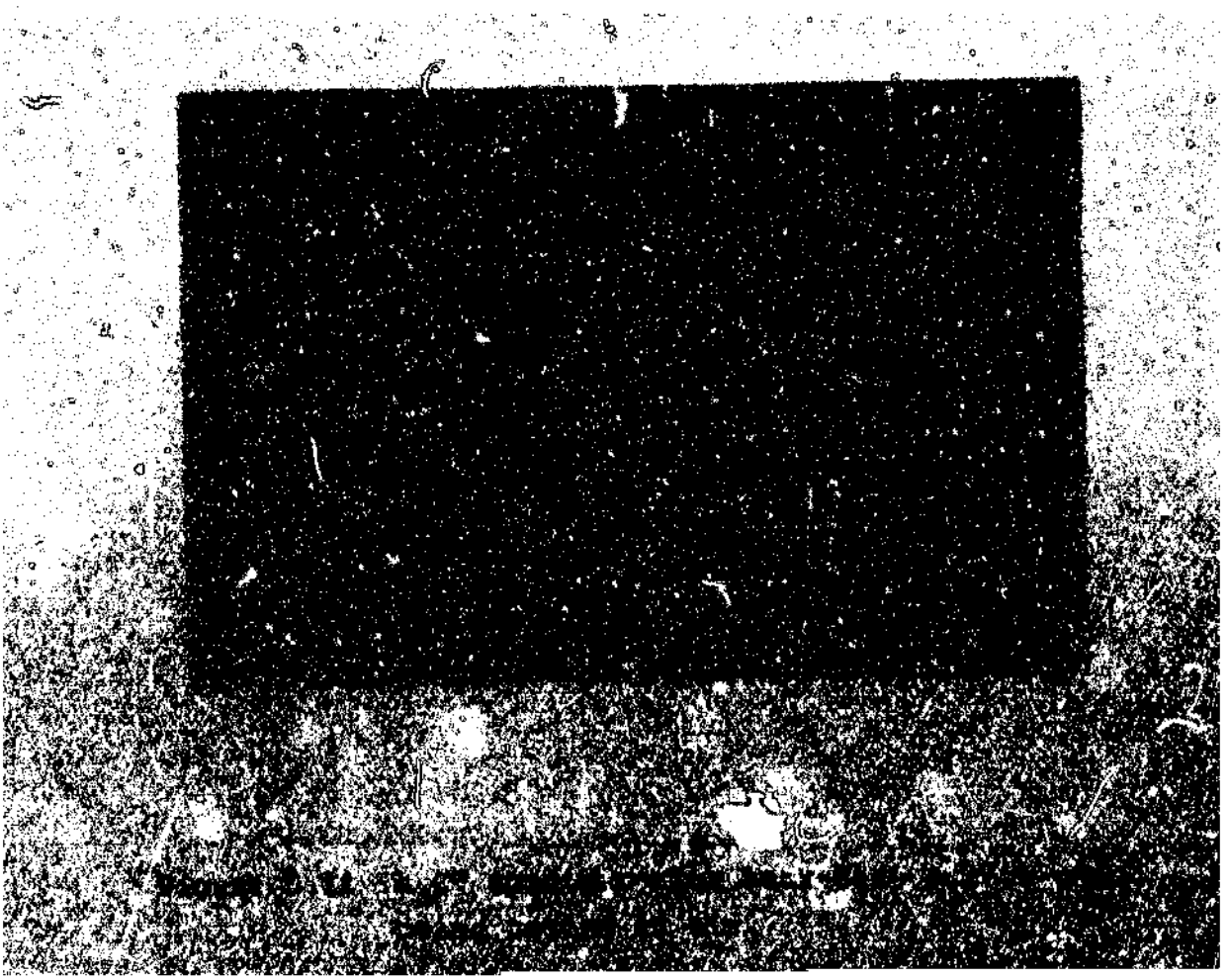

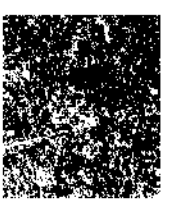

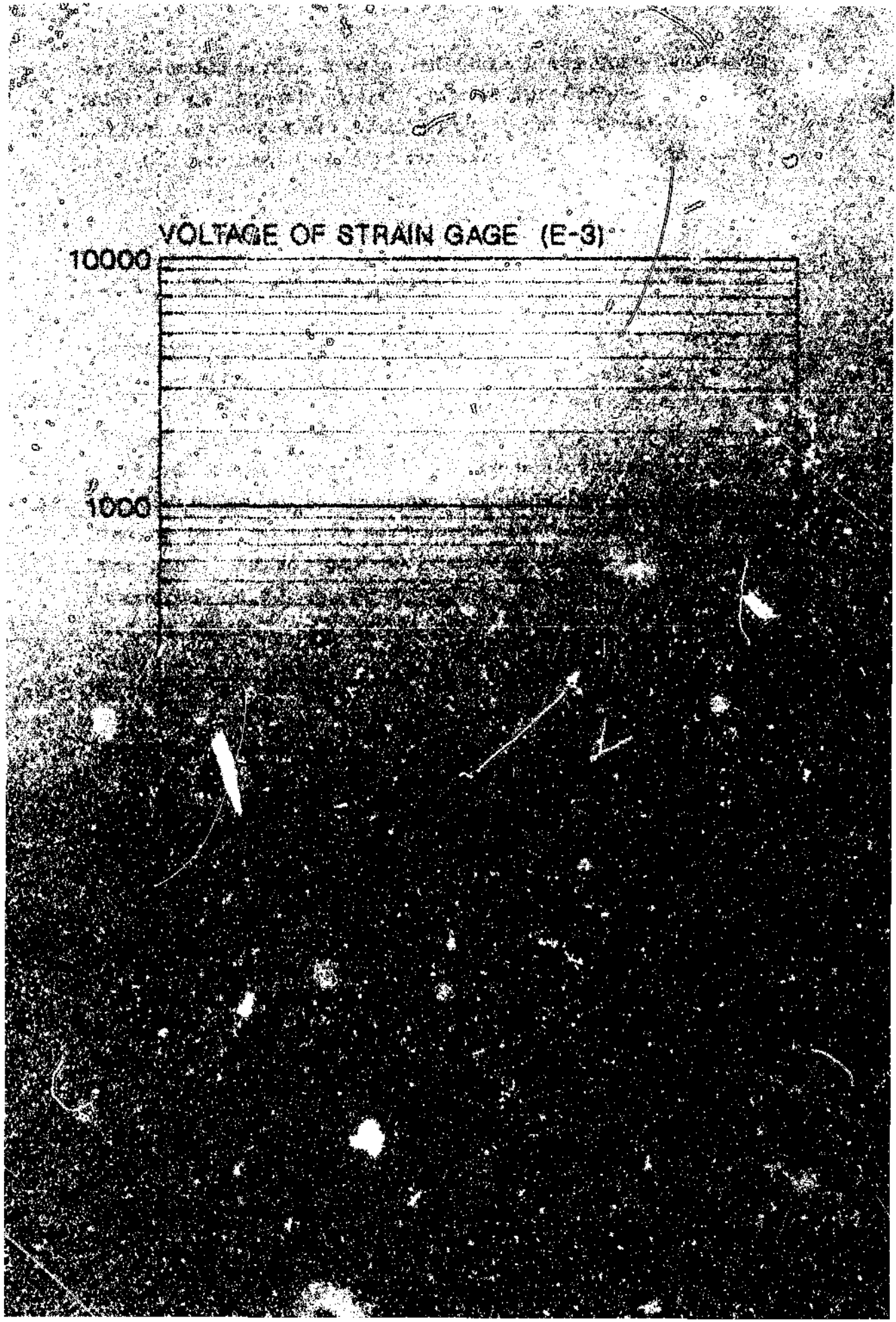
VOLTAGE OF STRAIN GAGE (E-3)
10000
1000

drying, all dust was removed with filtered compressed air. They were also carbon coated to enable examination of certain non-metallic inclusions present on the fracture surface that would otherwise have charged up when bombarded with the electron beam. This also enabled qualitative analyses to be carried out of inclusions by Energy Dispersive X-ray Analysis (EDAX).

3.7 X-Ray diffraction analyses

X-ray diffraction analyses were carried out on the scale from the Cortan wagon after pulverizing in order to determine the phases present. Analyses were also carried out on samples which had been corrosion fatigue tested in order to determine the nature of surface precipitates.

Diffraction patterns were obtained which [illegible] using a goniometer whose movement and diffracted [illegible]

Figure 6.1 The view of 3CR12 plate with pitting corrosion.

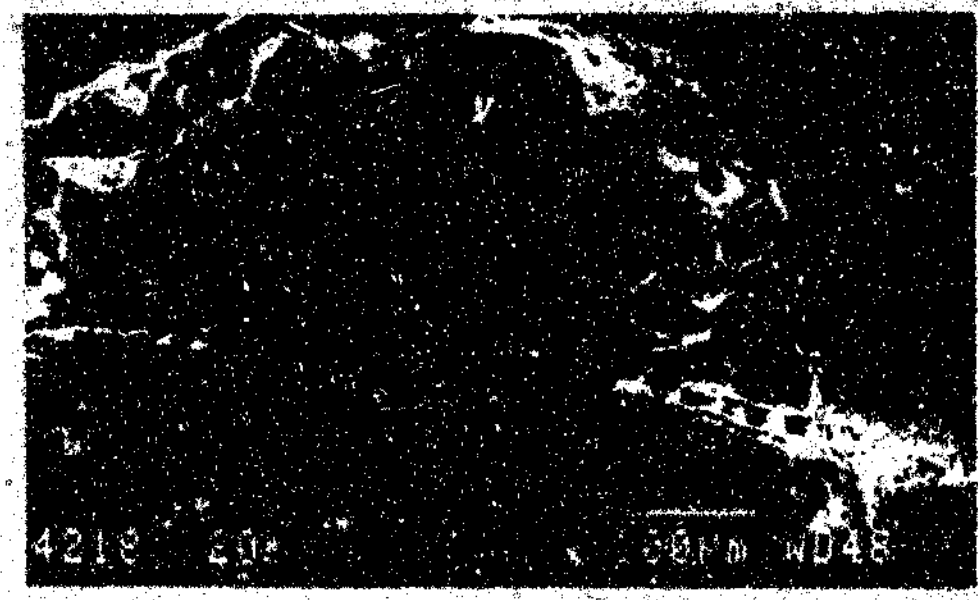

Figure 6.2 A pit of the surface of 3CR12 plate.

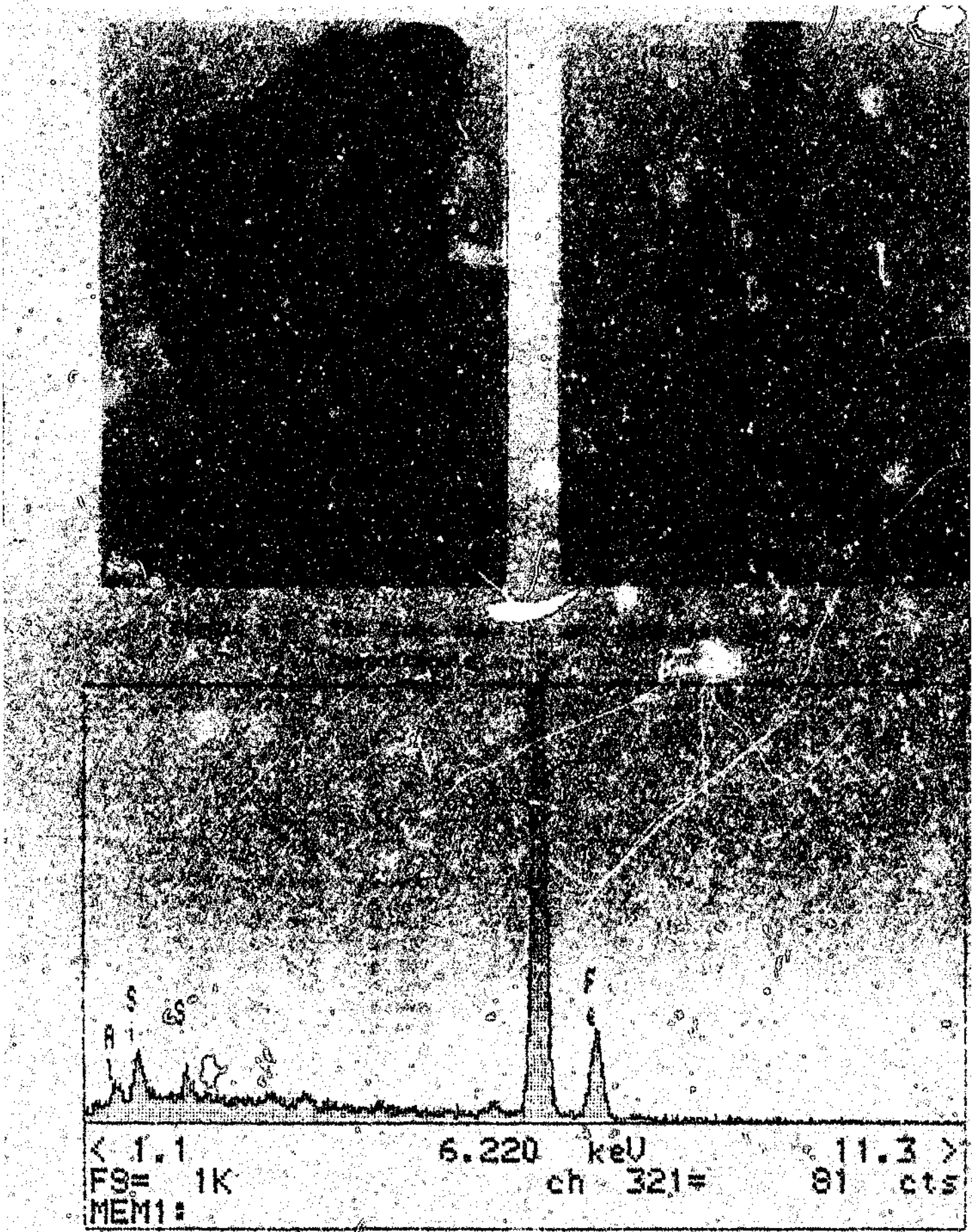

Figure 6.6 Spectrum of the surface of scale from Colton scale.

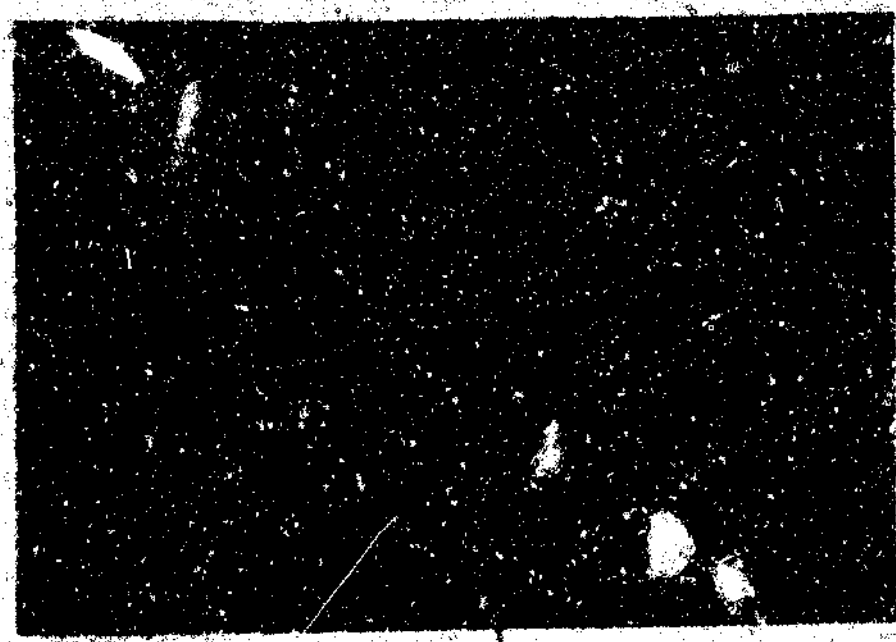

Figure 5.13 Arrangement for bubbling sulphur dioxide through distilled water.

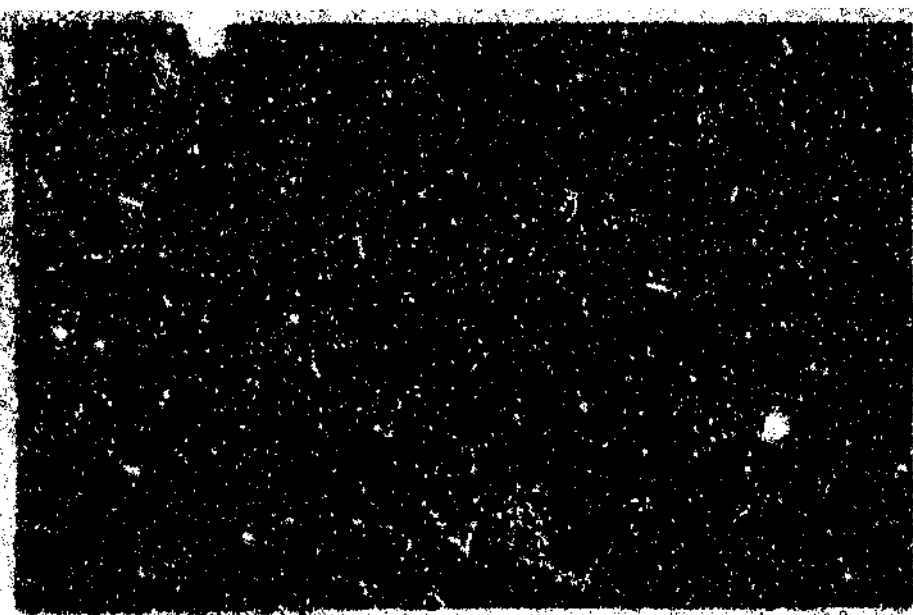

Figure 5.14 Arrangement for bubbling H_2S gas through the solution of sulphurous acid.

The formula to produce H_2S (g) is

$$FeS + 2HCl \rightarrow H_2S\ (g) + FeCl_2 \text{ ---------- (2.2)}$$

Thus 1 mole FeS reacting with 2 moles HCl produce 1 mole H_2S and 1 mole $FeCl_2$. To produce 0.1200 mole H_2S, 0.1200 mole FeS must react. 0.2412 mole HCl (0.1206 x 2). The molecular weight of FeS is 87.911 g. Therefore 0.1206 mole FeS is equivalent to 87.911 x 0.1200 = 10.5494 g [illegible]

The concentration of HCl was 32%.

i.e. 32 gm HCl in 68 gm H_2O

Figure 3.1f Strain gage and strain gage bridge coated with moist-proofing wax.

[redacted]

followed by mounting in resin. The mounted specimens were then ground on 1200 grit finishes on SiC paper. The samples were washed and dried followed by degreasing in alcohol in an ultrasonic cleaner. The ground surface of the samples was coated with lacquer film, [illegible] leaving a small area of the surface exposed. The exposed surface area which was usually 0.2 to 0.25 cm².

[illegible] Testing procedure

The electrochemical tests were carried out by using an [illegible]

[illegible]

fatigue test specimens were also examined in the SEM.

Preparation consisted of cutting the relevant pieces to the required size, followed by ultrasonic cleaning in an organic solvent to remove all traces of lubricant from the cutting operation. The corrosion fatigue testing specimens were cleaned by using Derestan™ cleaner-rust remover and brushing to remove rust from the fracture surface. The specimens were mounted onto aluminium holders using a graphite/alcohol suspension, and after

Figure 3.10 Typical electrochemical polarization cell illustrating location for the working electrodes (graphite rods) (1), reference electrode (2), and the sample (3).

6 RESULTS

6.1 Examination of 3CR12 plate

It can be seen from Figure 6.1 that the 3CR12 plate taken from the wagon showed extensive pitting after being in use for three months. Various sections were taken from this plate and examined in a scanning electron microscope equipped with an EDS facility. Examination of sections through the plate revealed the detailed appearance of the pits (Figure 6.2). A severe form of attack commonly referred to as "mud-cracking" was also observed in [illegible] (Figure 6.3).

[illegible] on the surface of the plate and in the pits [illegible] of sulphur as indicated in the [illegible]

[illegible] examined is given in Figure [illegible] very [illegible] plate [illegible] has [illegible] sulphur [illegible] than that [illegible] the presence of [illegible] EDS analyses of [illegible] concentration of

[illegible] Diffraction. The [illegible] is shown in Figure 6.7. It can be [illegible] major peaks was gamma iron oxide (γ-Fe_2O_3 also called Maghemite).

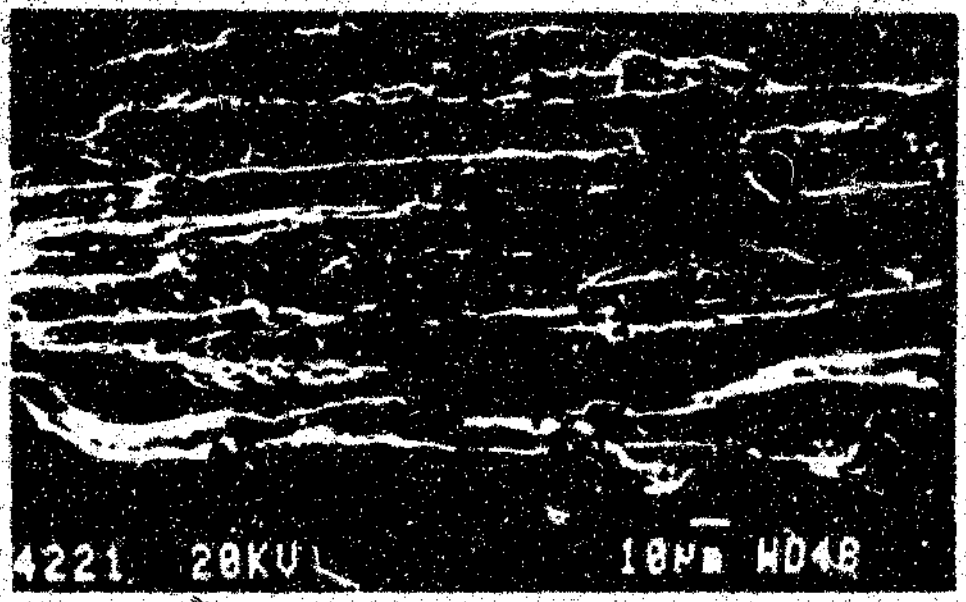

Figure 6.3 "Mud-cracking" on the surface of 3CR12 plate.

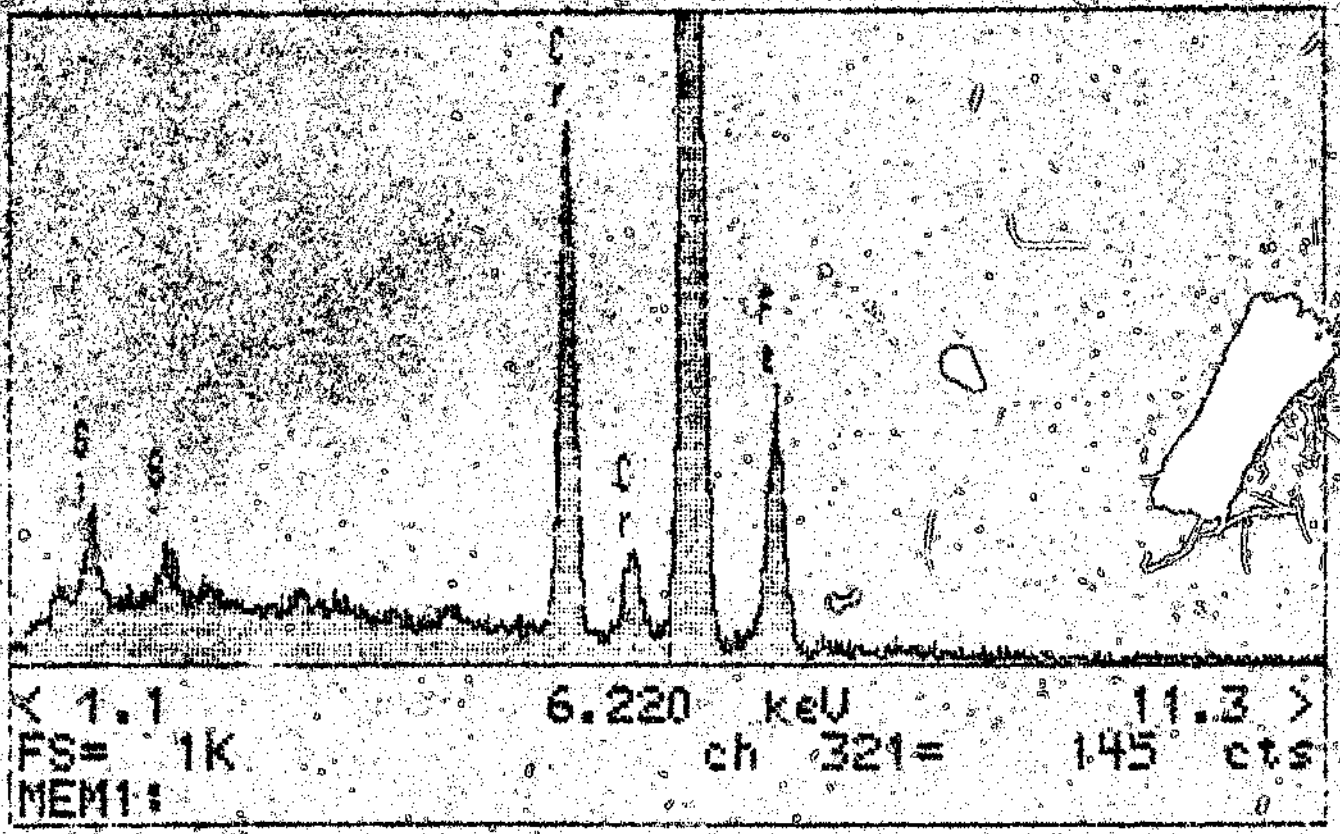

Figure 6.4 Spectrum obtained from the surface of 3CR12 plate.

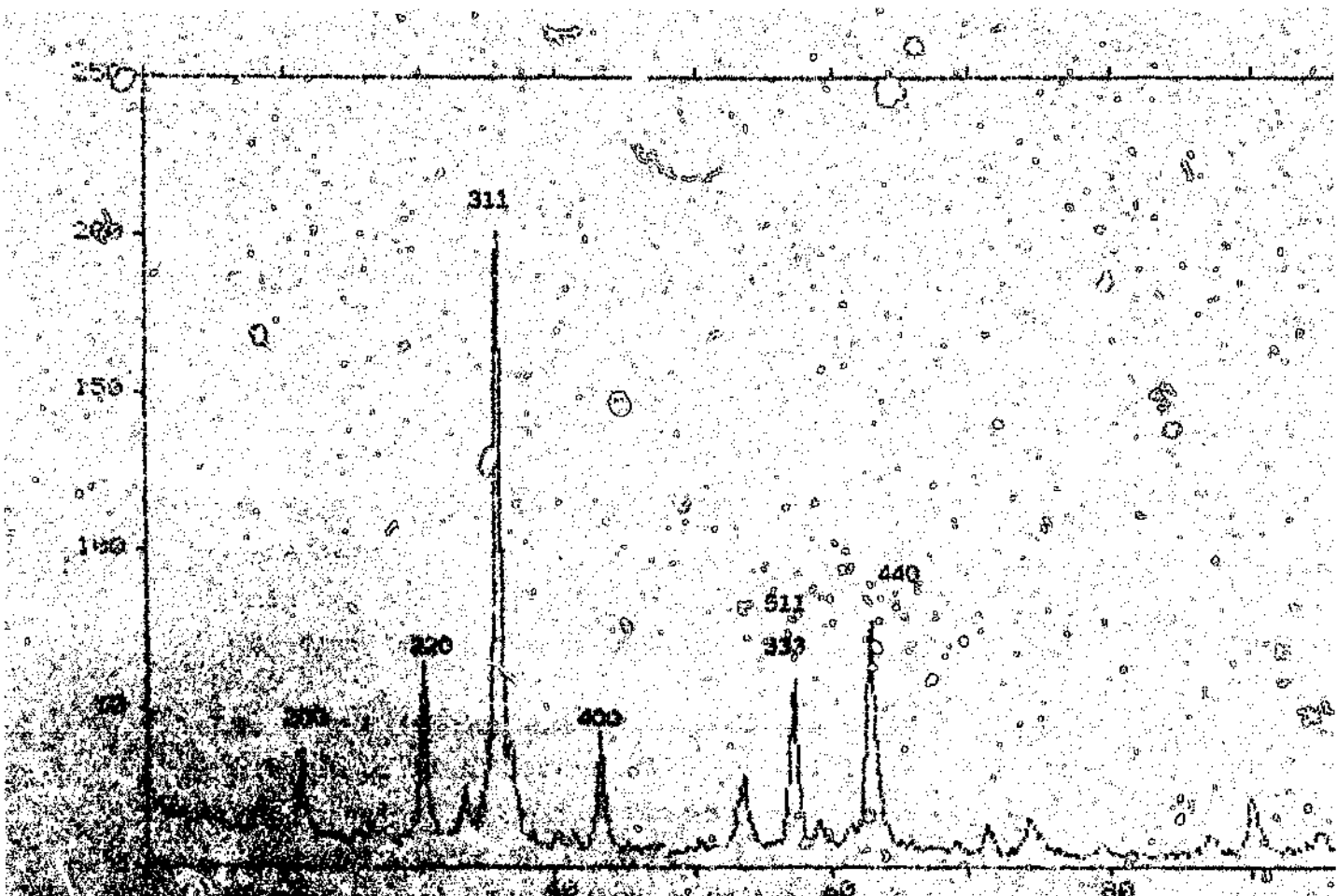

peak No.	2θ	d-spacing	FWHM	peak height (counts)	background (counts)	I/Imax (%)	significance
1	[illegible]	[illegible]	[illegible]	[illegible]	33	12.98	1.47
2	[illegible]	[illegible]	[illegible]	52	13	20.83	2.11
3	2.6939	33.238	0.240	13	13	7.01	0.78
4	2.5236	35.544	0.408	185	23	100.00	4.30
5	2.0927	43.195	0.320	59	7	28.76	1.87
6	1.7188	53.523	0.504	16	8	10.00	1.74
7	1.6056	57.185	0.480	49	10	26.49	2.16
8	1.4799	62.735	0.560	66	12	35.47	3.04
9	1.3229	71.225	0.480	10	5	5.54	0.85
10	1.0898	89.955	0.480	15	6	8.22	0.83
11	1.0465	94.795	0.640	10	6	5.54	0.77

Figure 6.7 X-ray diffractogram of the scale from Corten steel.

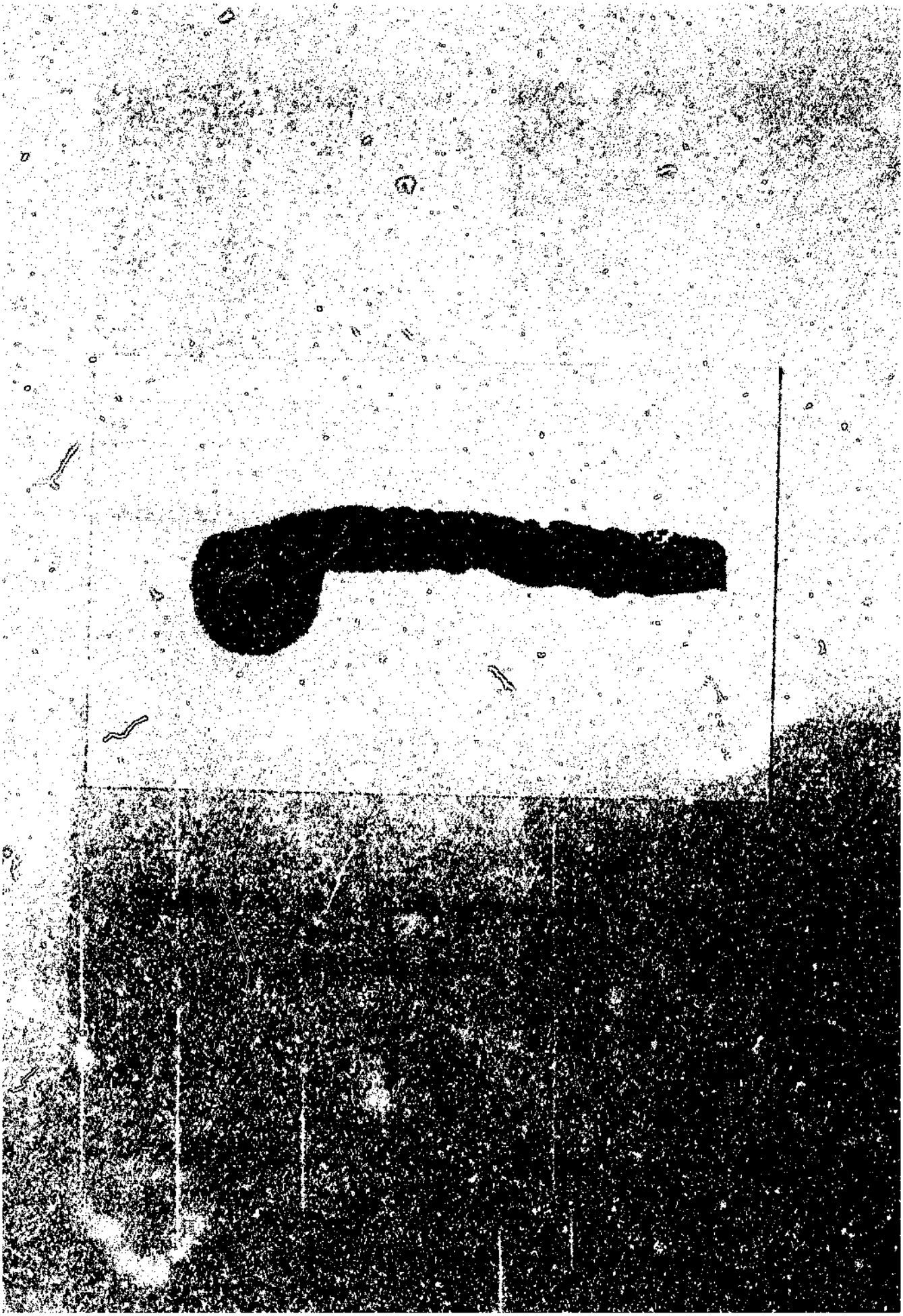

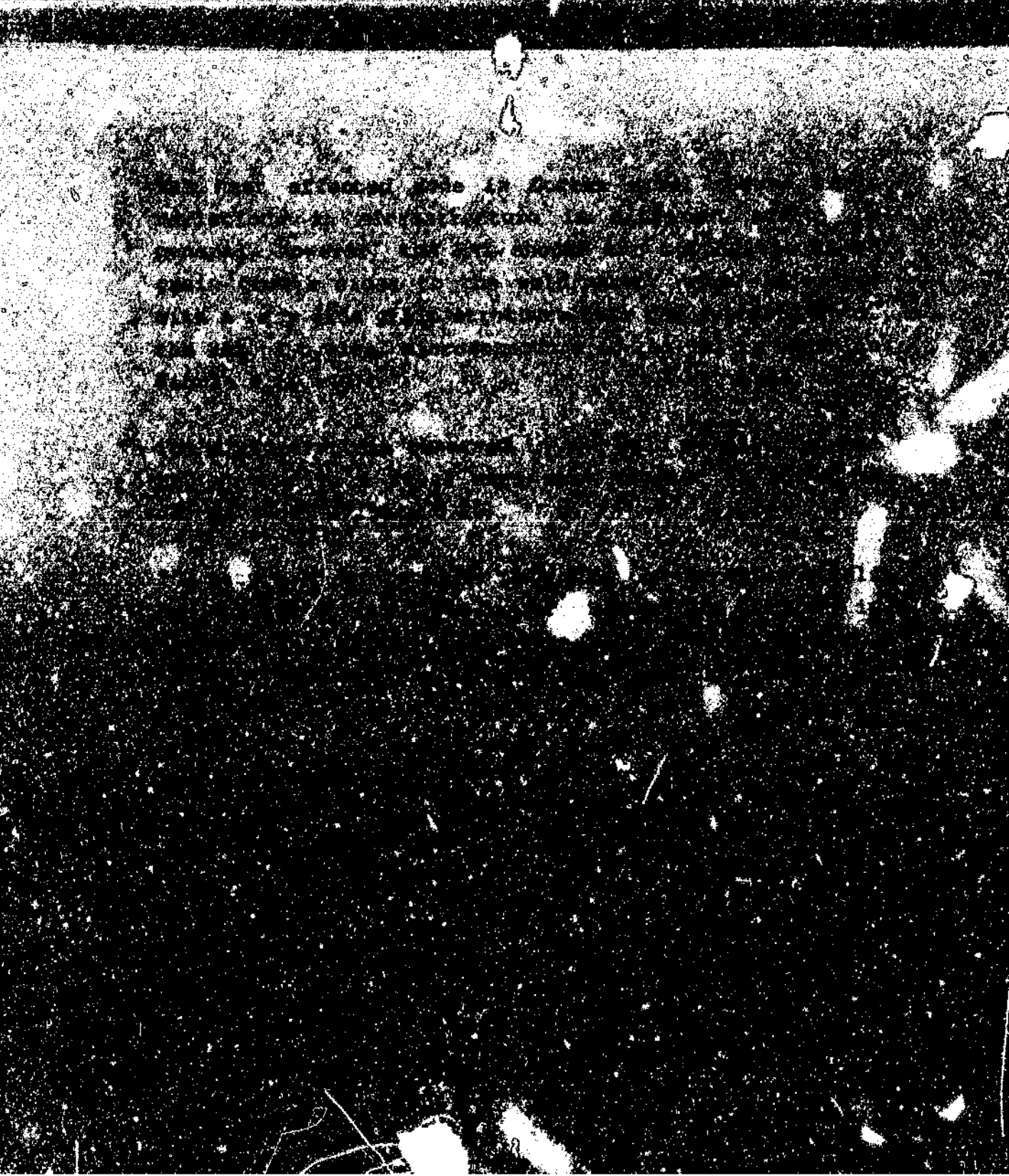

6.3 The microstructure of the materials and welded joints

Sections of the three steels studied and of their welded joints were prepared and examined microscopically.

Steel 3CR12 showed a banded dual-phase microstructure of ferrite and martensite after etching (Figure 6.8). Intermetallic carbonitride particles were observed in this material. In some areas these particles occurred in the form of clusters (Figure 6.9).

Both the Corten and mild steel used were of adequate cleanness with regard to non metallic inclusions. The Corten steel showed stringers of MnS particles in the polished condition (Figure 6.10). Transverse section of this material showed that the inclusions were of limited size and fairly evenly dispersed (Figure 6.11). Similar sections taken through the mild steel showed very small amounts of MnS inclusions.

Etching of Corten revealed a relatively coarse microstructure of ferrite and pearlite (Figure 6.12). The microstructure of the mild steel also consisted mainly of ferrite with small amounts of pearlite (Figure 6.13).

Examination of the weld joints in the three steels showed that these were generally sound with regard to the presence of porosity and inclusions.

Small amounts of porosity and non metallic inclusions were also present in the 309L weld deposit used with steel 3CR12 (Figure 6.14).

Small amounts of porosity were observed in polished sections of the weld in Corten steel. The maximum size of the pores was of the order of 0.5 mm (Figure 6.15). Small amounts of slag were also observed in the weld in Corten

Figure 6.8 Steel 3CR12 showing a banded dual-phase microstructure of ferrite (bright) and martensite (dark).
Etched, Vilellas, 400X.

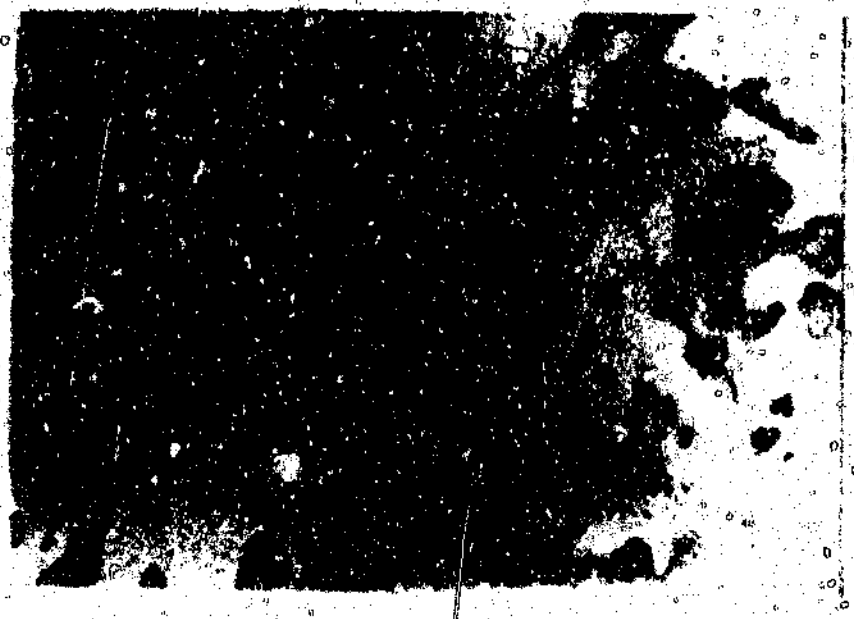

Figure 6.9 Titanium carbonitride particles in steel 3CR12.
Etched, Vilellas, 1000 X.

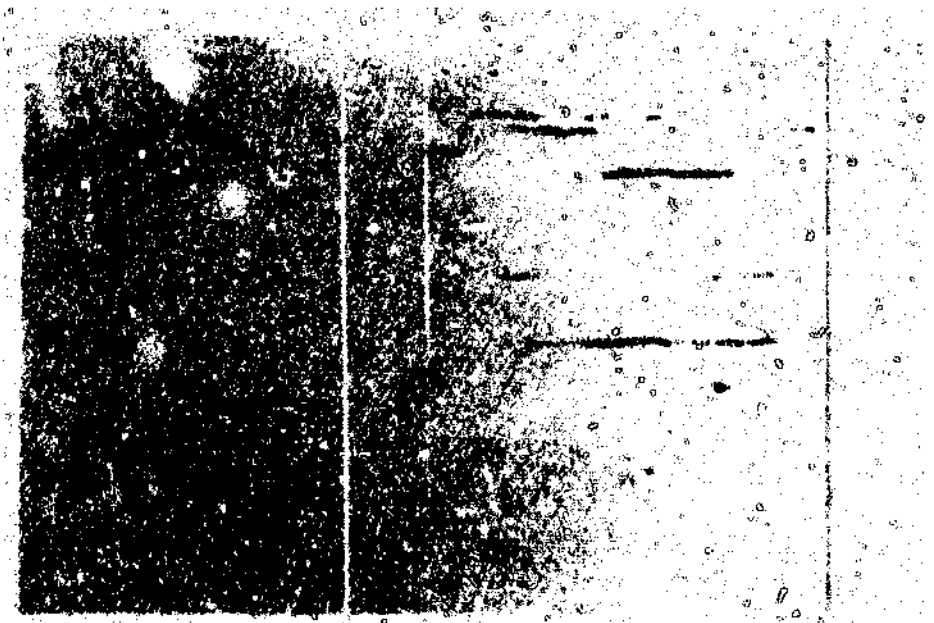

Figure 6.10 Non metallic inclusions (MnS) in a longitudinal section of Corten steel. Polished, 400 X.

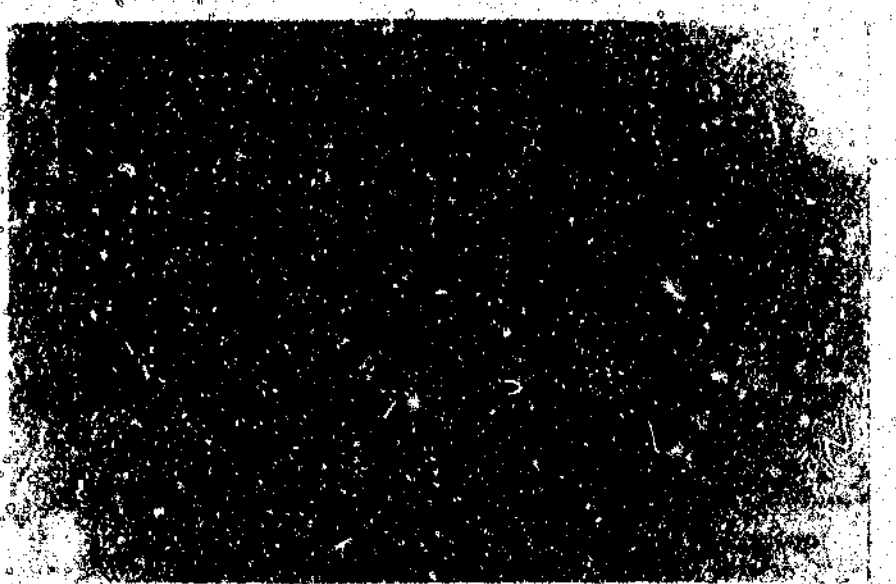

Figure 6.11 MnS inclusions in a transverse section of Corten steel. Polished, 100 X.

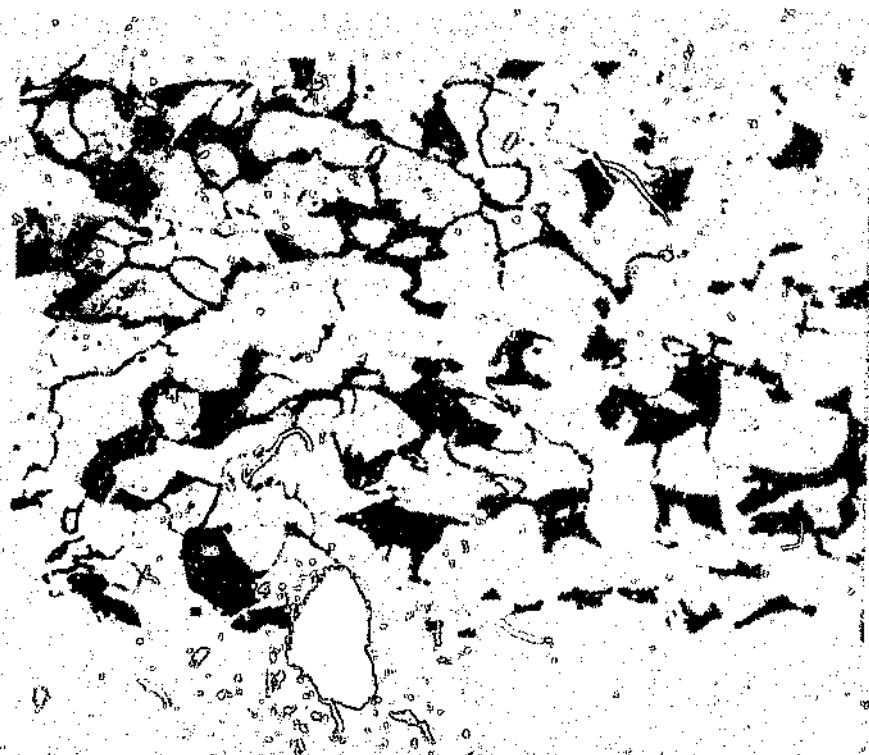

Figure 6.12 Microstructure of Corten steel. Etched, Nital, 400 X.

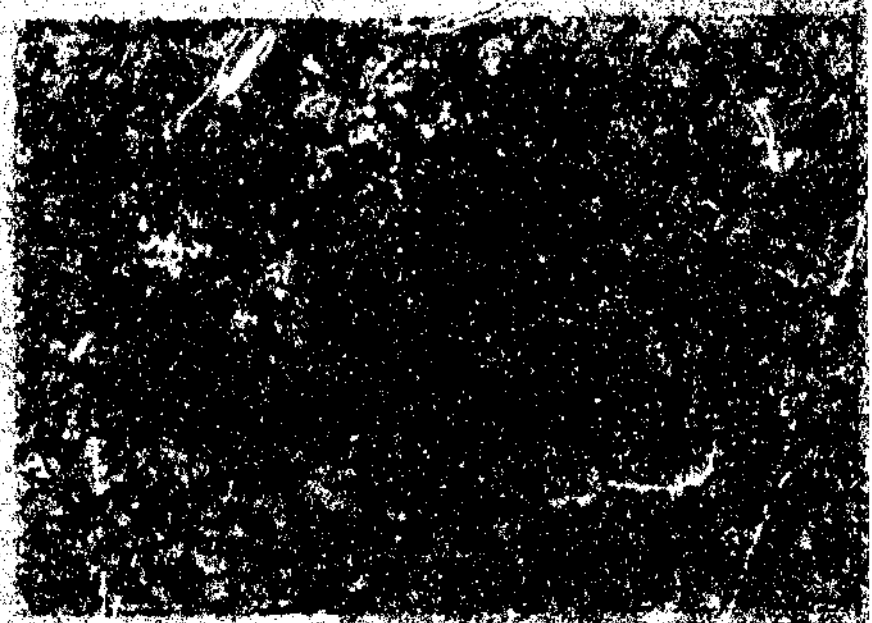

Figure 6.13 Microstructure of mild steel. Etched, Nital, 400 X.

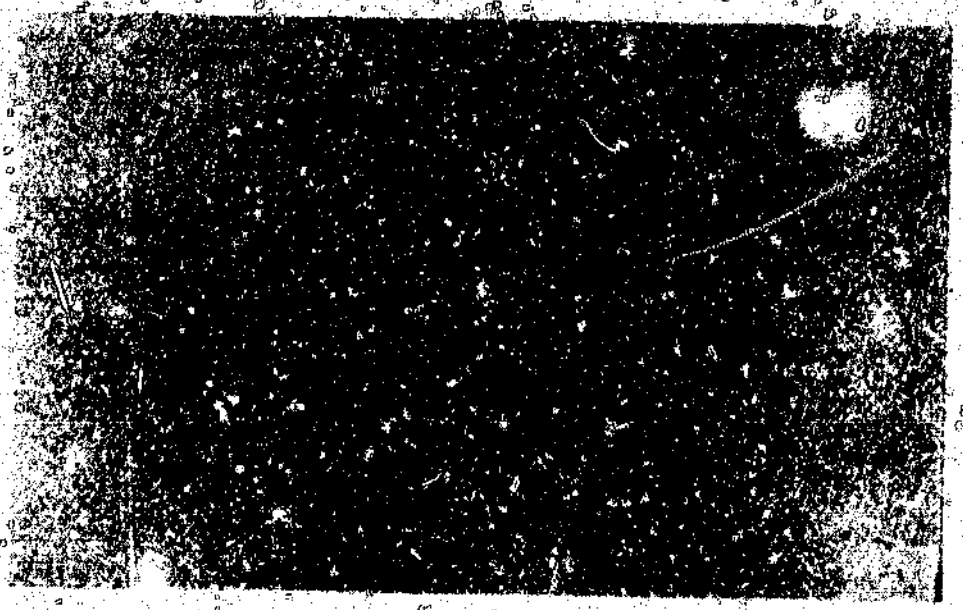

Figure 4.14 Porosity and non metallic inclusions in the vein deposit of Sagl. Reichenau [96 M].

steel (Figure 6.16).

The welding procedure used with plates of the three steels was similar. 3CR12 plate was welded by depositing a run on one side of the prepared junction then turning the plate over and depositing another three beads on the other side. Corten was welded in exactly the same manner. The mild steel plate was welded in a similar fashion but only three weld runs were used in this case.

The microstructure observed in the weld metals and the heat affected zones were those expected of the materials used and the welding conditions employed.

The microstructure of the weld deposit and the HAZ in 3CR12 steel are shown in Figure 6.17. The last weld run to have been deposited showed a dendritic structure of austenite with a more or less continuous network of interdendritic delta ferrite (Figure 6.17 - a). The reheating of weld metal by subsequent bead deposition caused the network of delta ferrite to break up to a considerable extent and form globules (Figure 6.17 - b and c).

The heat affected zone in 3CR12 showed significant grain growth (Figure 6.17 - d). General views of the weld and parent metal microstructures are shown in Figure 6.18.

The weld metal in Corten steel had an acicular ferritic microstructure typical of as cast metal which cooled down rapidly (Figure 6.19 - a). This microstructure was only present in the last weld run to have been deposited. The microstructure of the other three runs had been modified by the repeated thermal cycles during deposition of subsequent runs (Figure 6.19 - b and c). The effect of reheating was to produce a fine equiaxed ferrite structure in the weld metal.

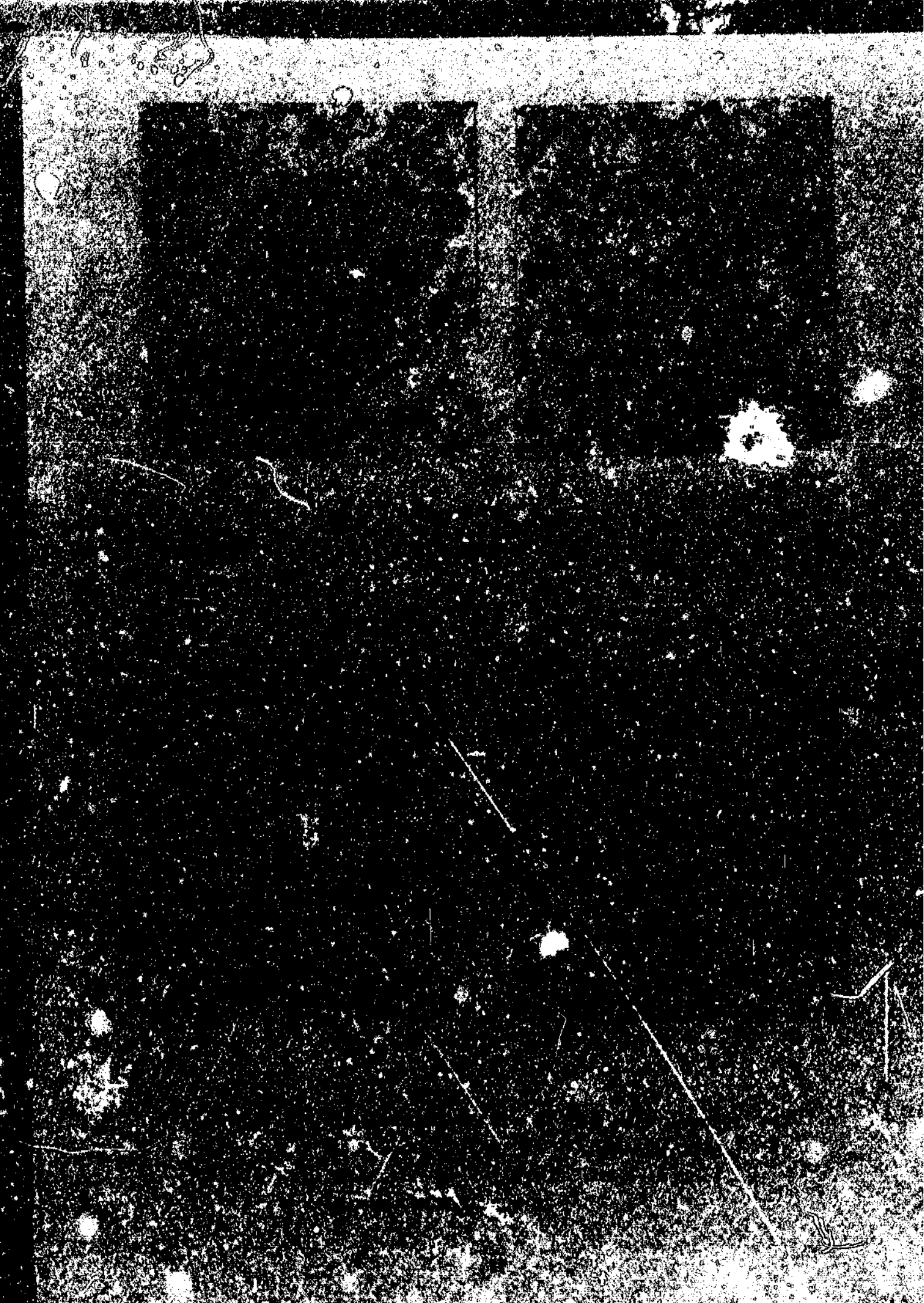

Figure 6.22 Spectrum of an alanine irradiation in the Gammacell.

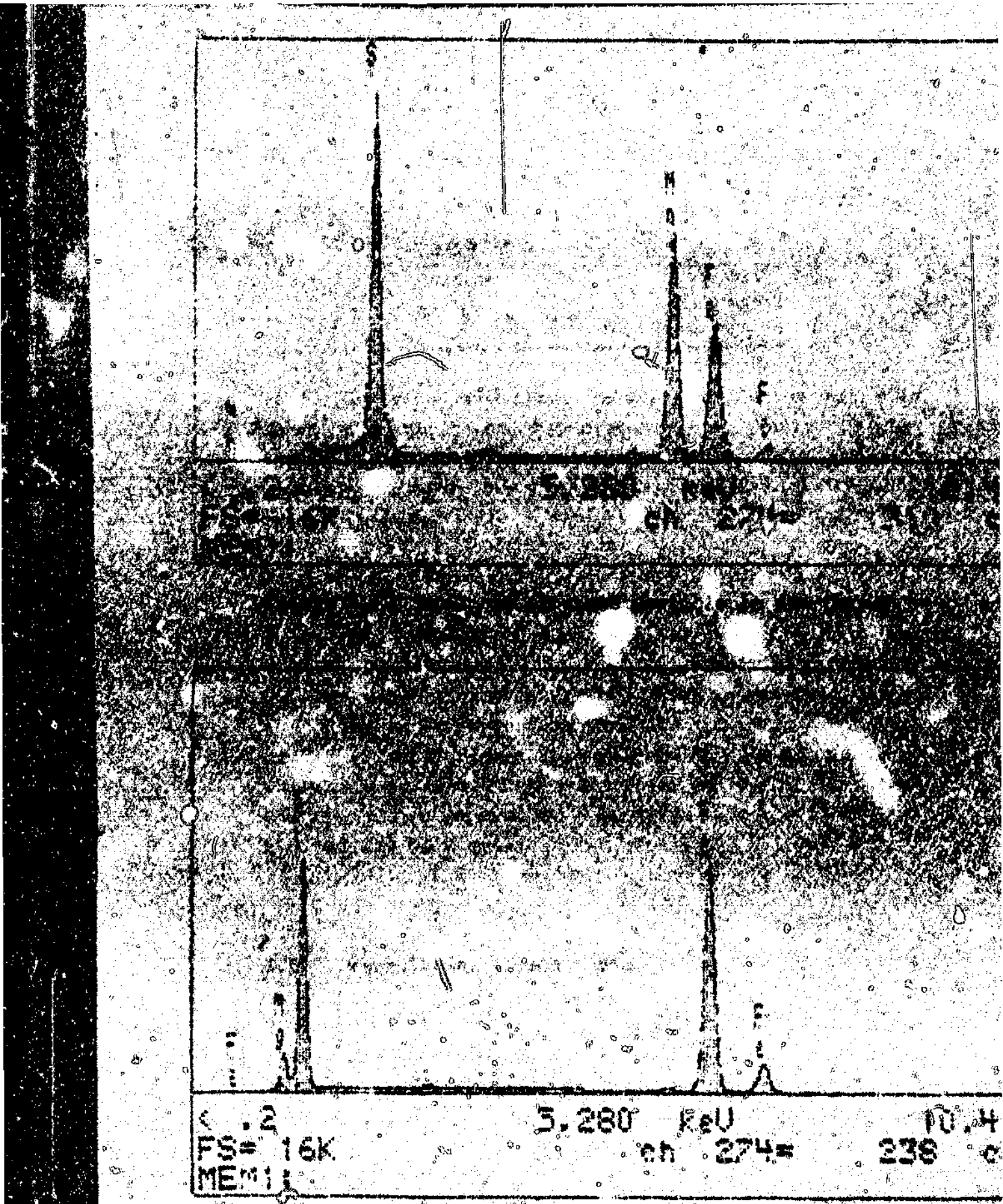

Figure 6.24 Spectrum of a complex oxide particle in the mild steel.

Steel	HV10
3CR12	206
Corten	156
Mild	157

It can be seen from these values that Corten and mild steels had the same hardness due to their similar carbon and carbon equivalents. 3CR12 has a somewhat higher hardness [illegible] to its greater carbon equivalent.

6.3 Tensile and Impact tests

The results of the tensile and impact tests for the three steels are shown in Table 6.1 and Figure 6.26. It can be seen that Corten had intermediate tensile properties between those of 3CR12 and mild steel. From Figure 6.26 it can be seen that the welded samples exhibited improved yield stress values.

The 3CR12 specimens taken from the parent metal showed some delamination effects as can be seen from Figures

Vickers hardness

Table 6.1 Tensile and impact test results

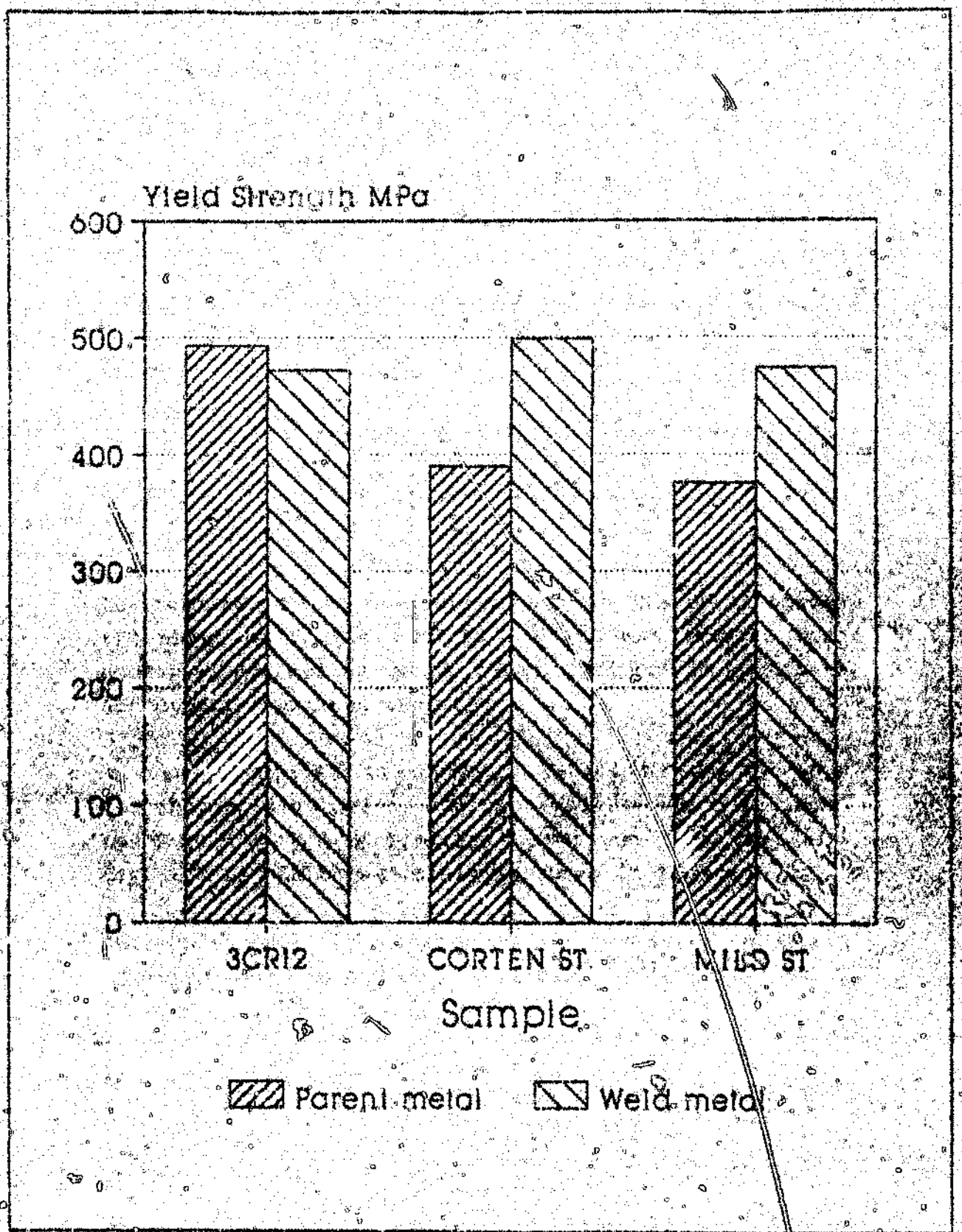

Figure 6.26 Comparison of yield strength of 3CR12, Corten and mild steels.

6.27 and 6.28. The specimens taken from the weld joint in the 3CR12 failed in the cup-and cone fashion (Figure 6.29) and showed mostly a dimpled fracture surface (Figure 6.30). In some areas of the welded specimens some cleavage effects were apparent. Figures 6.31 to 6.34 show the fracture surfaces of the tensile test specimens of Corten and mild steel both in the parent metals and the weld deposits. The fracture surfaces of mild steel and Corten were similar. The specimens failed in the cup-and cone fashion and exhibited a dimpled fracture surface typical of ductile materials.

for Figure 6.12.

was found and applied to the results to obtain equations for stage II of the crack propagation process. The equations generated were as follows.

3CR12	$da/dN = 3.00 \times 10^{-9}(\Delta K)^{3.038}$	(1)
Corten steel	$da/dN = 8.49 \times 10^{-13}(\Delta K)^{5.38}$	(2)
mild steel	$da/dN = 1.74 \times 10^{-10}(\Delta K)^{4.14}$	(3)
3CR12 weld	$da/dN = 4.51 \times 10^{-13}(\Delta K)^{5.47}$	(4)
Corten weld	$da/dN = 3.42 \times 10^{-12}(\Delta K)^{4.11}$	(5)
mild steel weld	$da/dN = 1.73 \times 10^{-10}(\Delta K)^{4.02}$	(6)

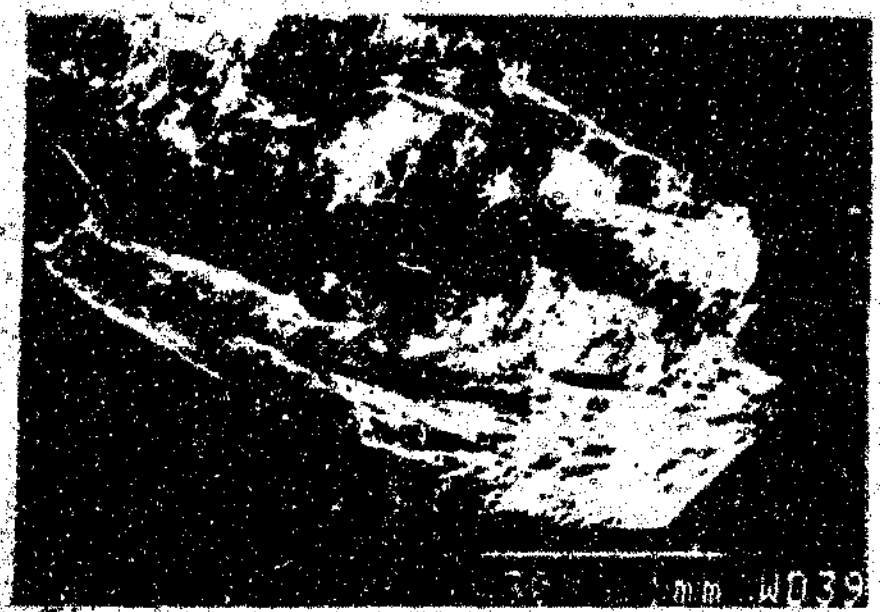

Figure 6.27 Fracture surface of a tensile test specimen of 3CR12 steel showing delamination.

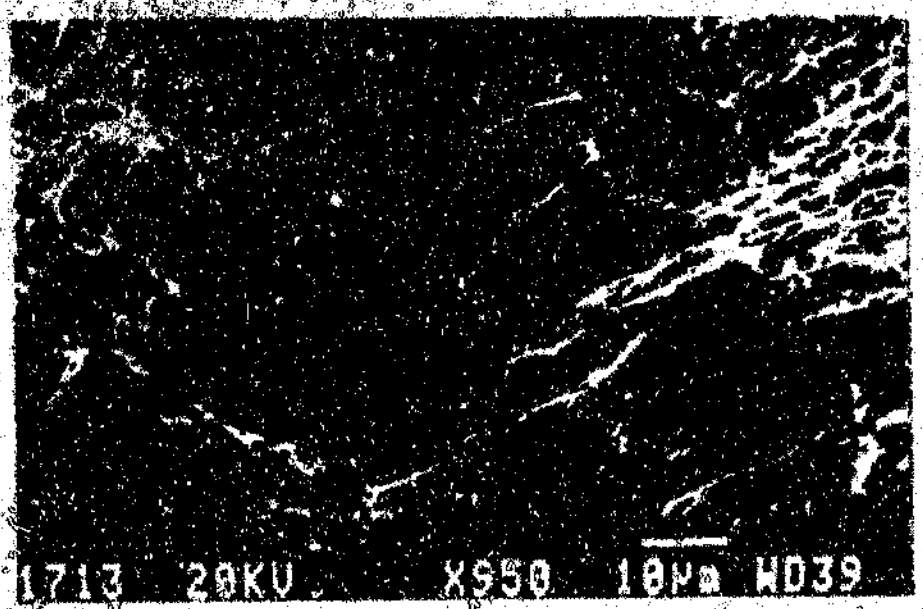

Figure 6.28 Fractograph of 3CR12 tensile specimen showing typical ductile fracture.

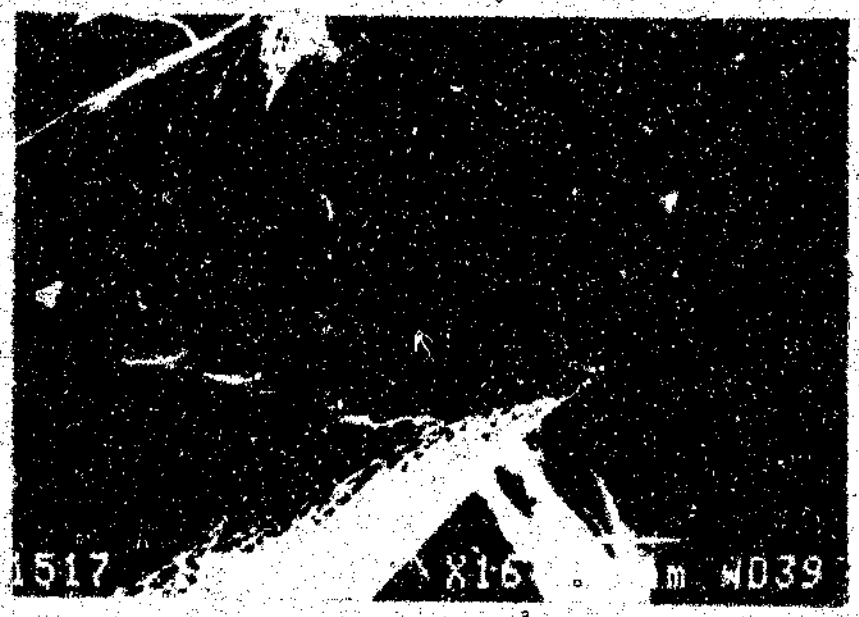

Figure 6.29 Fracture surface of the weld deposit between 3CR12 plates.

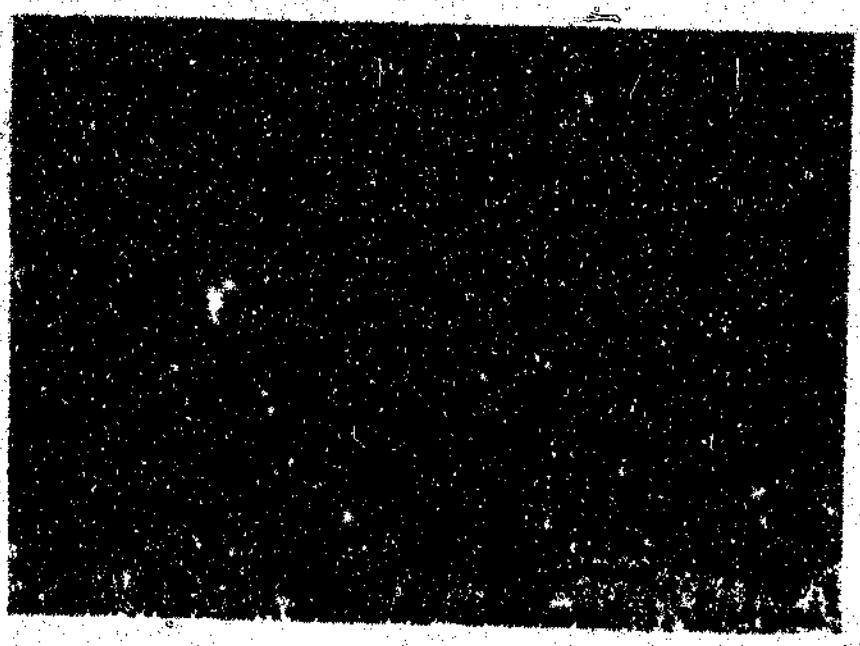

Figure 6.30 Ductile fracture surface of the weld metal between 3CR12 plates.

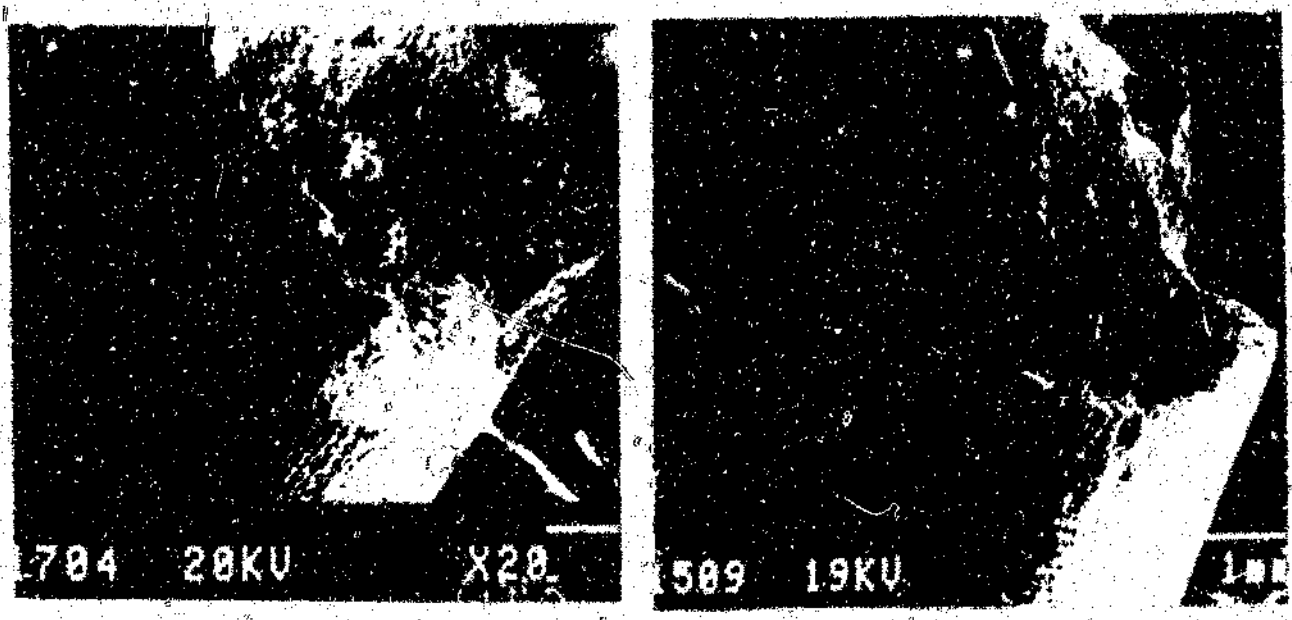

a b

Figure 6.31 Fractured tensile specimens in (a) Corten steel and (b) weld deposit in Corten steel.

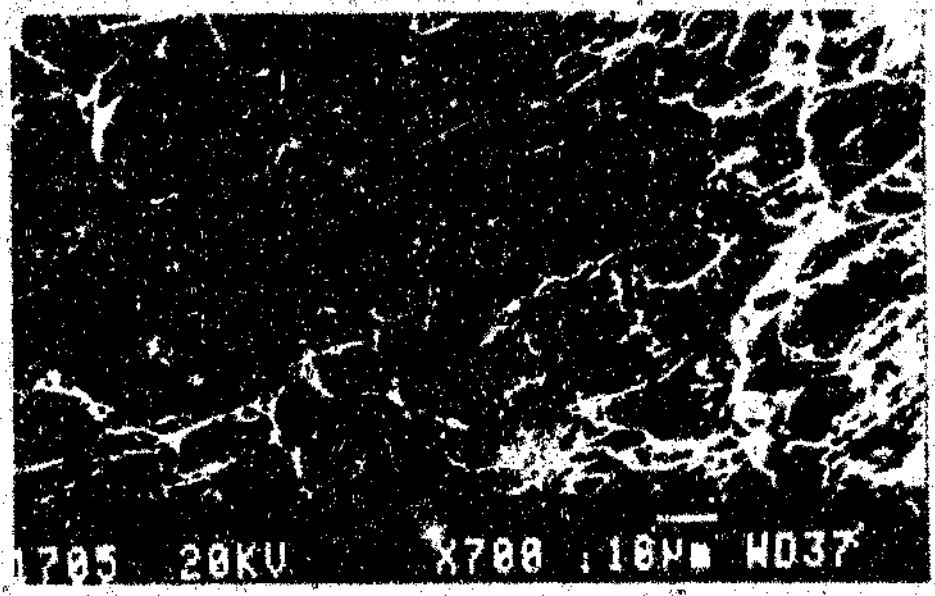

Figure 6.32 Ductile fracture surface of tensile specimen in Corten steel.

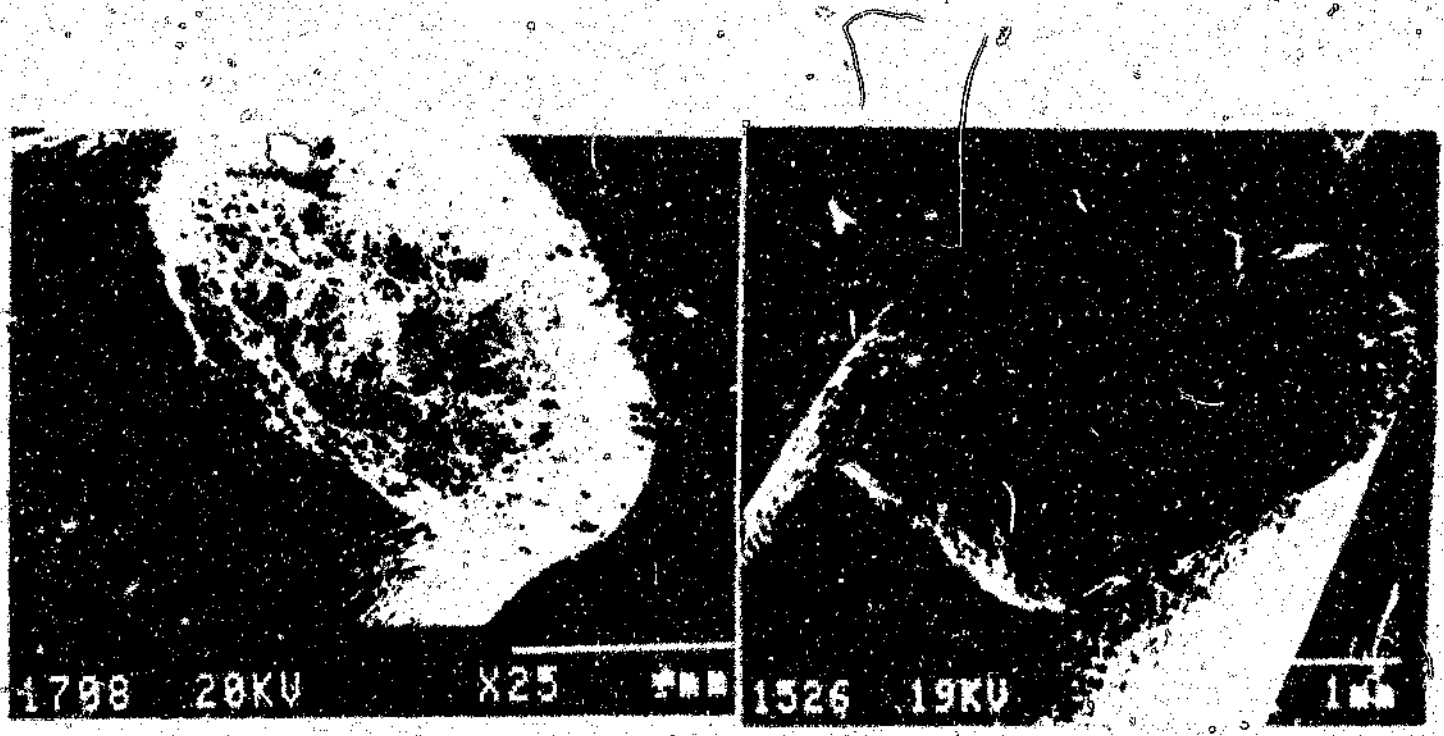

a b

Figure 6.33 Fractured tensile specimens in (a) mild steel and (b) weld deposit in mild steel.

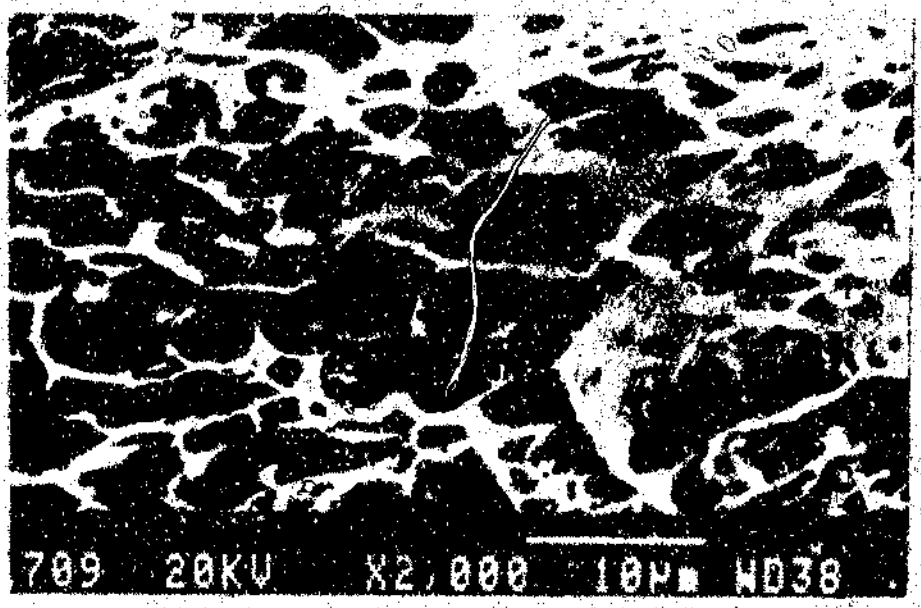

Figure 6.34 Ductile fracture surface of mild steel tensile specimen.

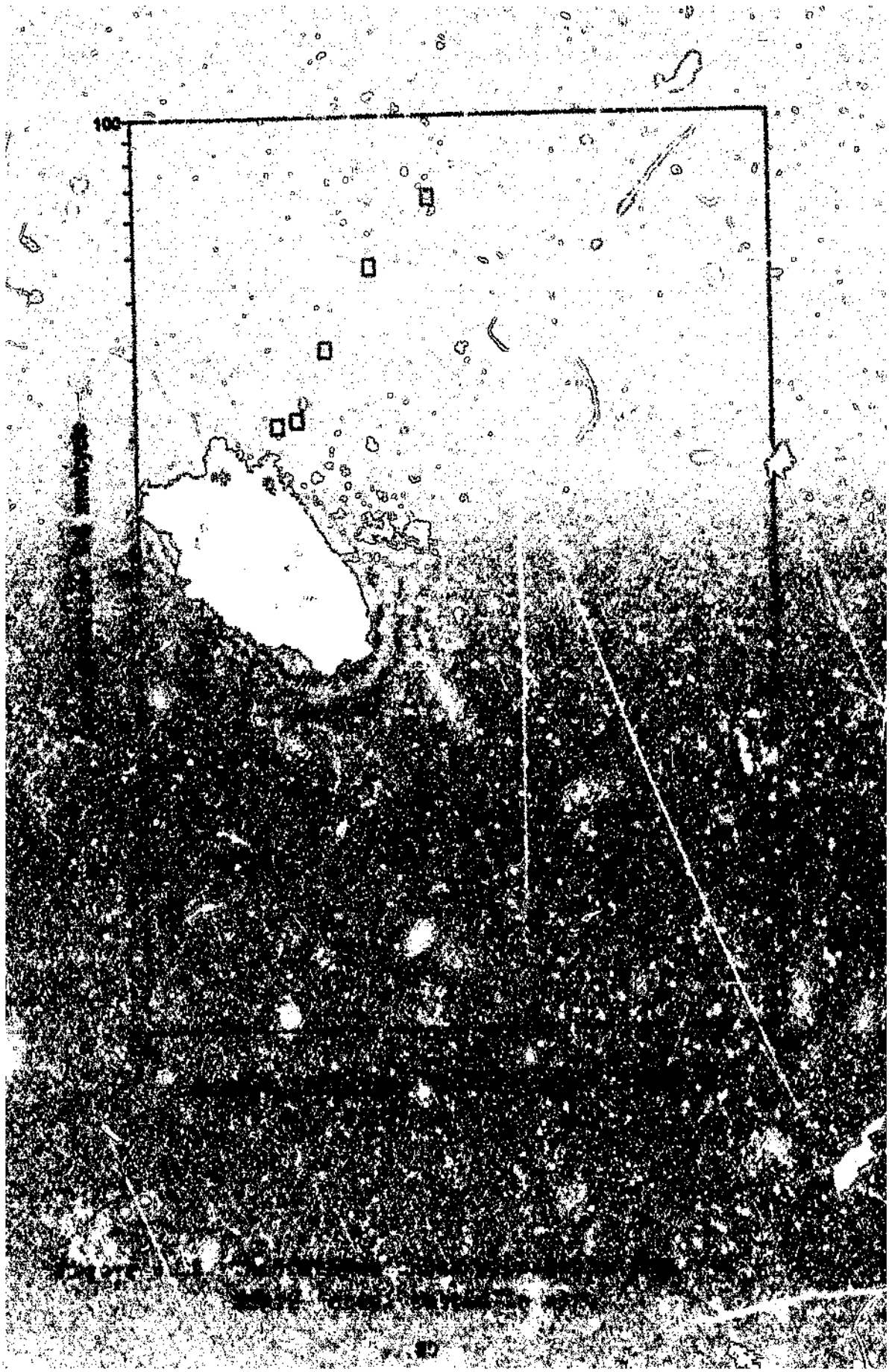
100

Figure 5.43 Comparison of fatigue crack propagation rates for 3CR12, Cortan and mild steel at ΔK=25.

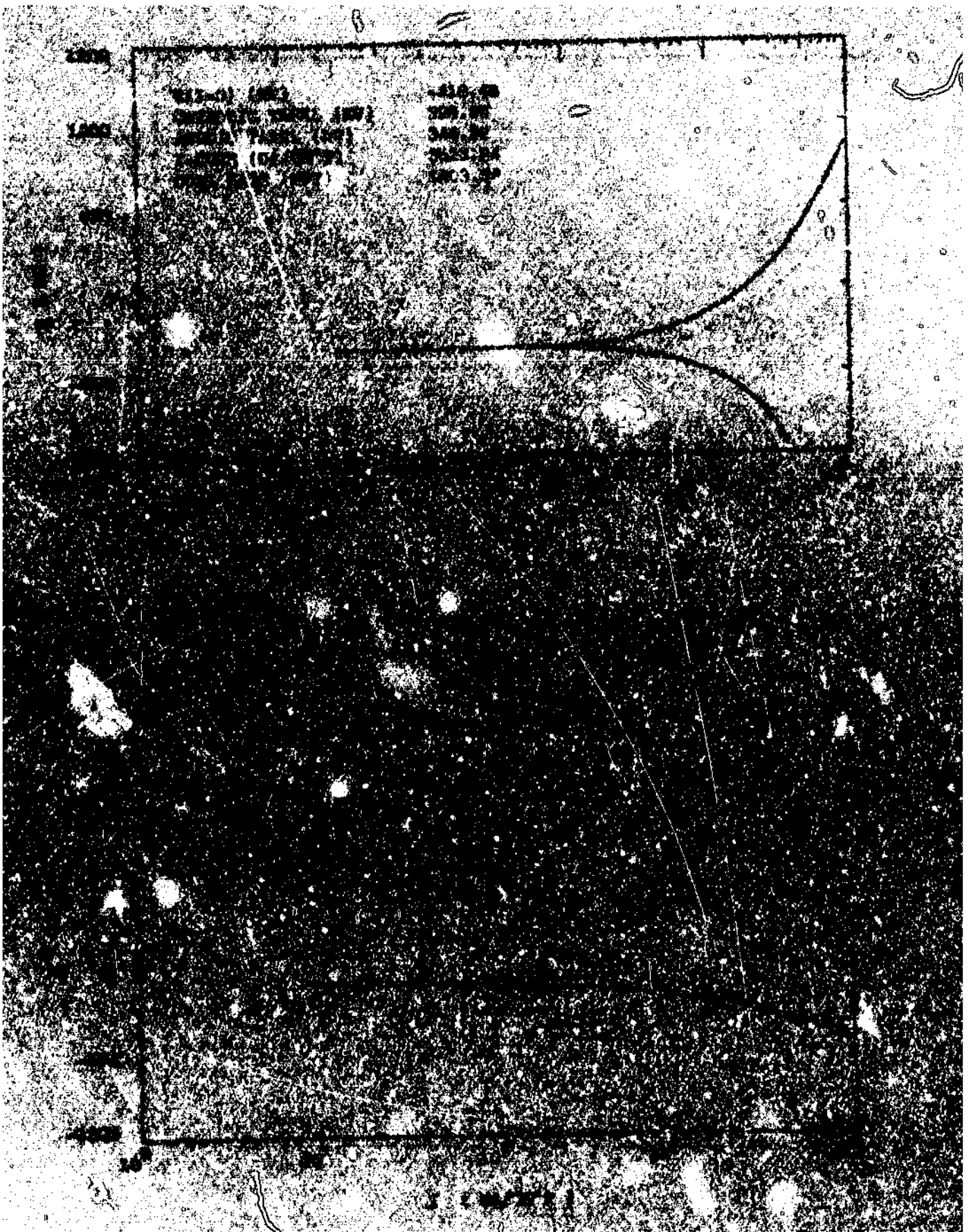

Figure 8.17 Potentiodynamic polarisation scan of the weld deposit in 3CR12.

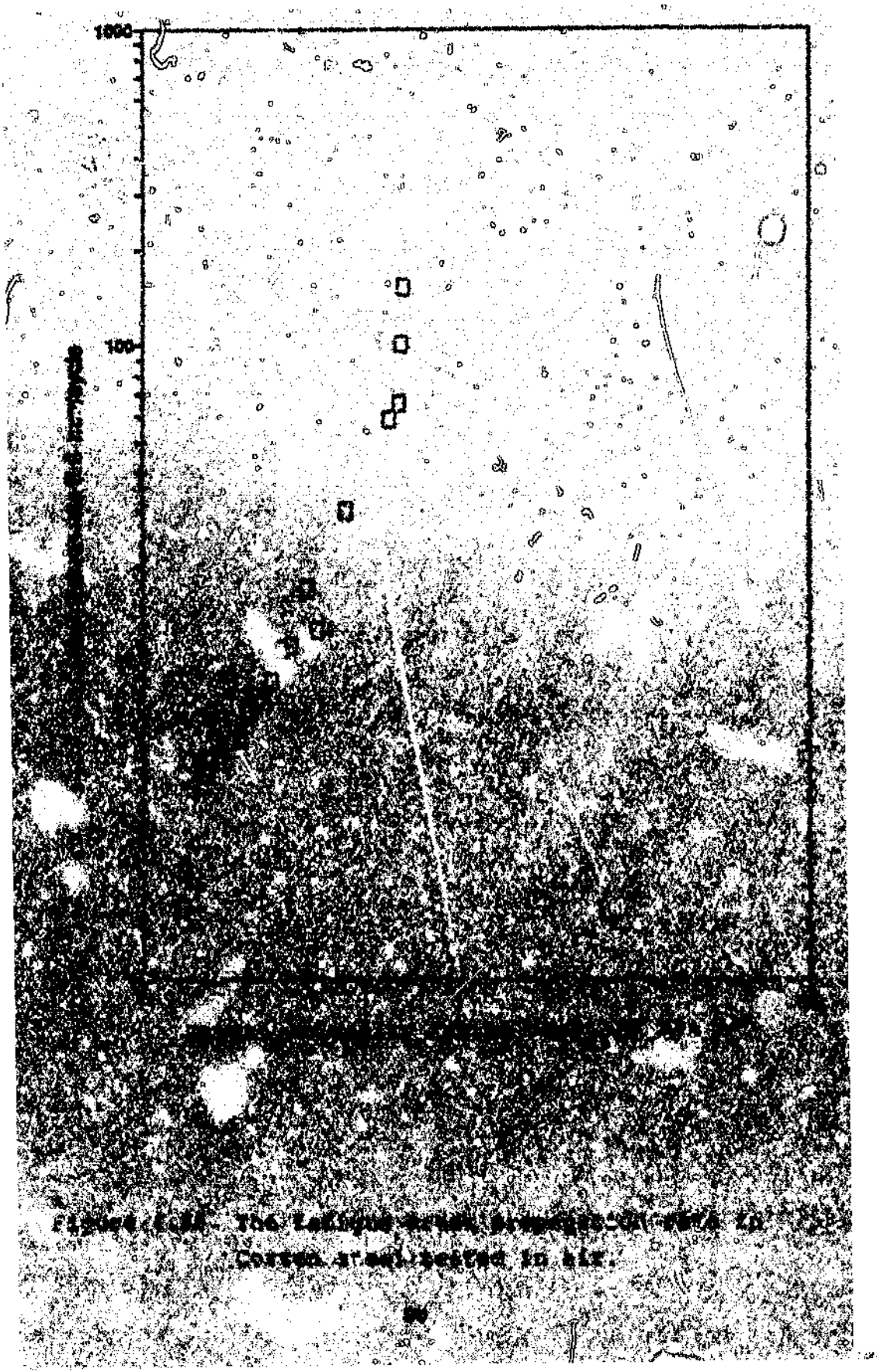

Figure 6.6 - The Lexington series, drawdown-CDA-1974 Zn
Corsen at equilibrium in air.

Figure 6.37 The relationship between [illegible] and [illegible] tested in air.

1000
100
Cycles to failure (Nf) - E-6 stainless

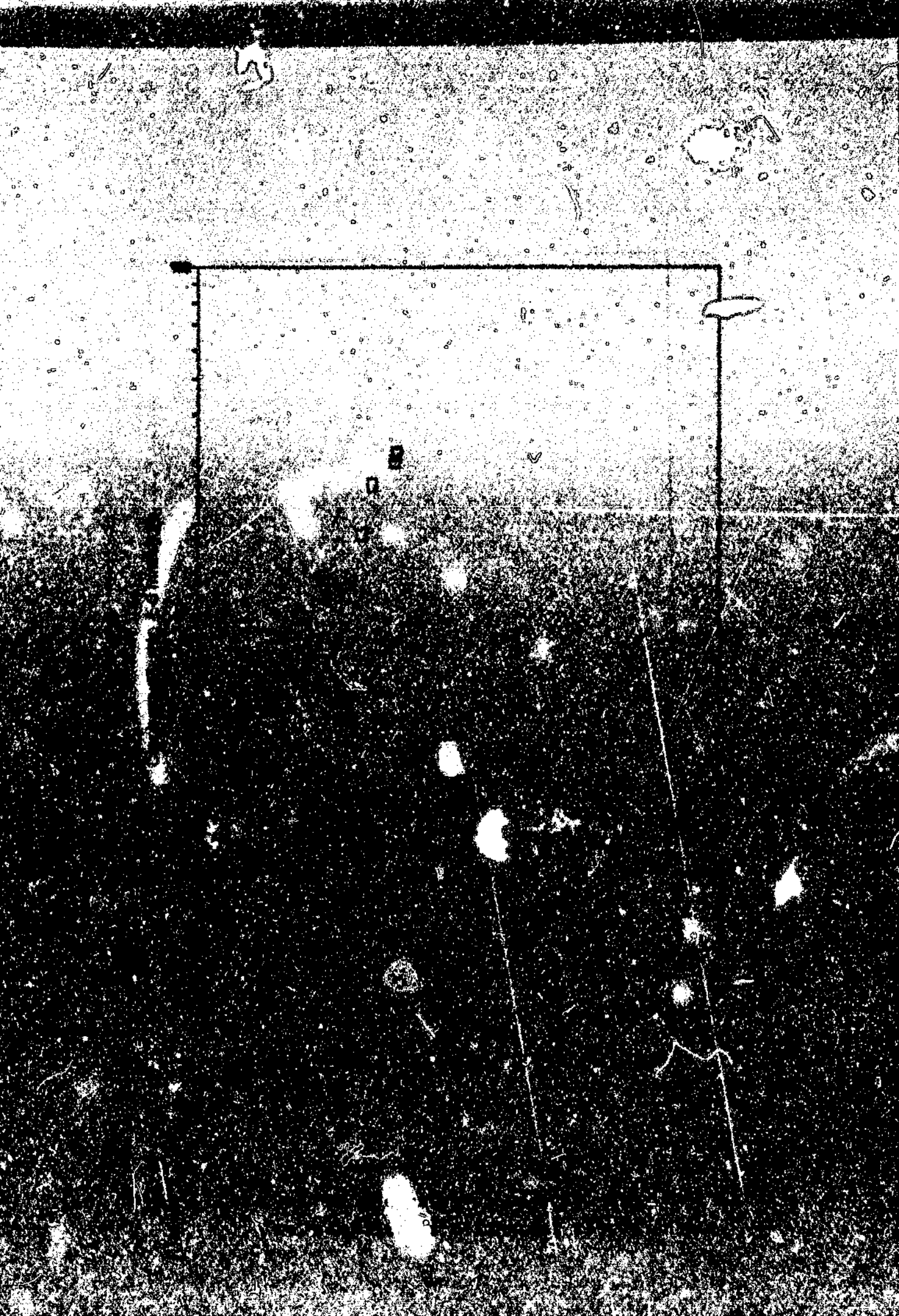

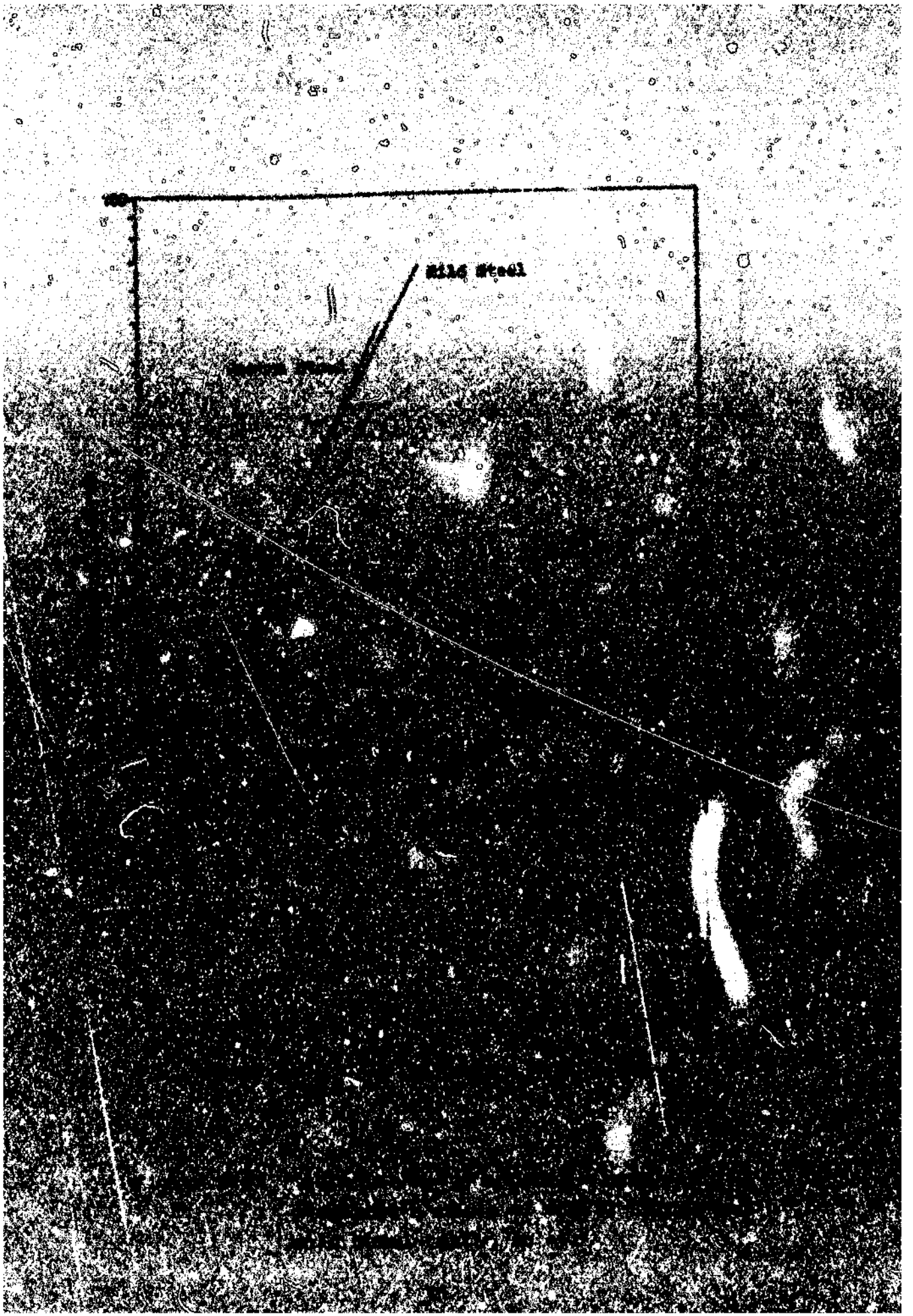
#16 Steel

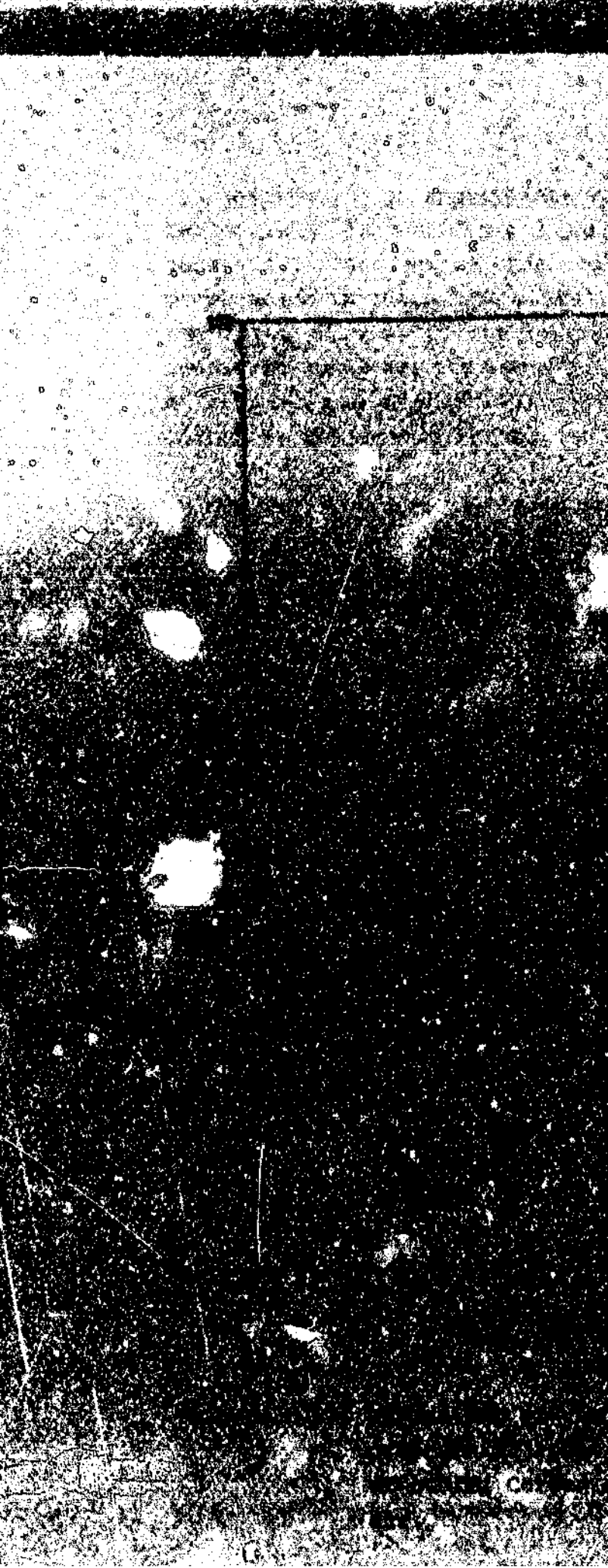

By substituting an appropriate value of stress intensity factor, ΔK, in equations 1 to 6, Figure 6.43 may be generated. This shows the relative rates of crack propagation in the parent plates and the weld deposits of the three alloys. It can be seen that in the unwelded condition 3CR12 has the lowest crack propagation rate and 316 steel the highest. The crack propagation rate in [illegible] is comparable to that in 3CR12.

[illegible] the crack propagation rate of [illegible]

[illegible] two steels in [illegible] the Cleland steel had a [illegible] rate in polythionic acid [illegible] contrary to expectation. The [illegible] that the two materials had [illegible] compositions and that the technique is not very sensitive to small changes in chemical composition.

Figure 4.43 Potentiodynamic polarisation scan of Corten steel.

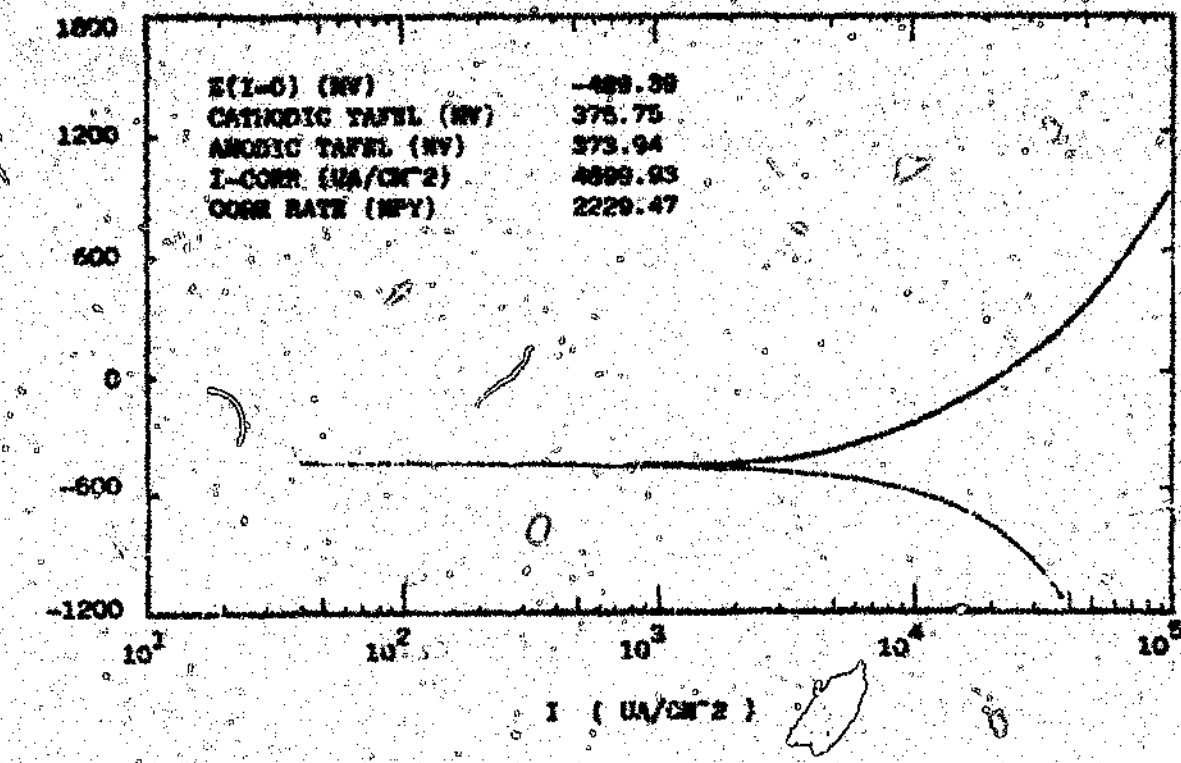

Figure 6.48 Potentiodynamic polarisation scan of the weld deposit in Cortan steel.

Figure 6.49 Potentiodynamic polarisation scan of the weld deposit in mild steel.

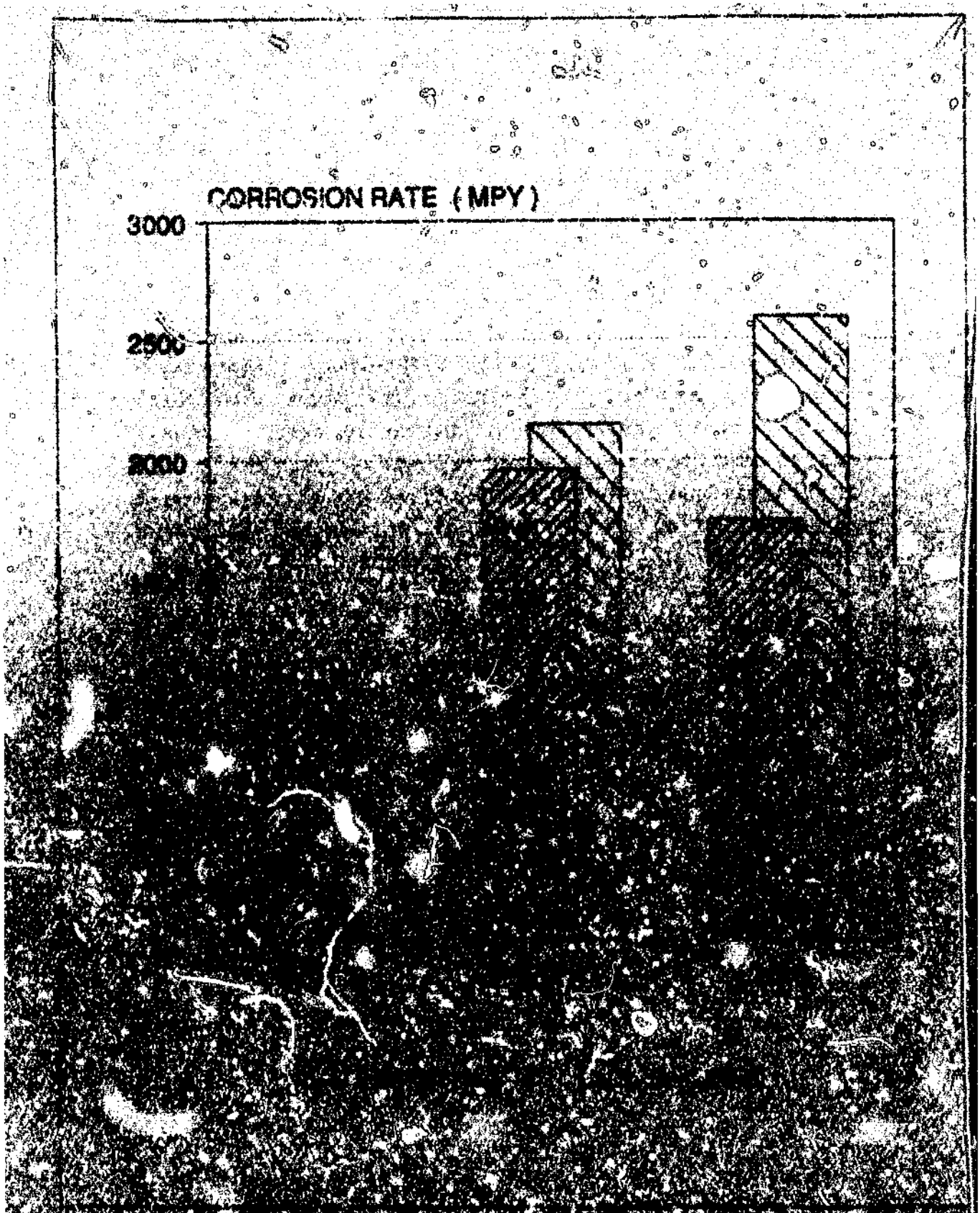

Figure 6.20 Comparison of effect of temperature on corrosion rate of mild steel

The weld deposits in Corten and mild steel had a higher corrosion rate than the parent metals. This was probably due to the as cast-type of microstructure of the weld deposits which is inhomogeneous and is therefore attacked more severely by the aggressive solution.

Corroded surfaces were examined by scanning electron microscopy. Steel 3CR12 was severely attacked by the polythionic acid solution and exhibited the "mud-cracking" type of attack (Figure 6.51). This type of attack was due to the preferential dissolution of the martensitic lathes in the material and was similar to [illegible]

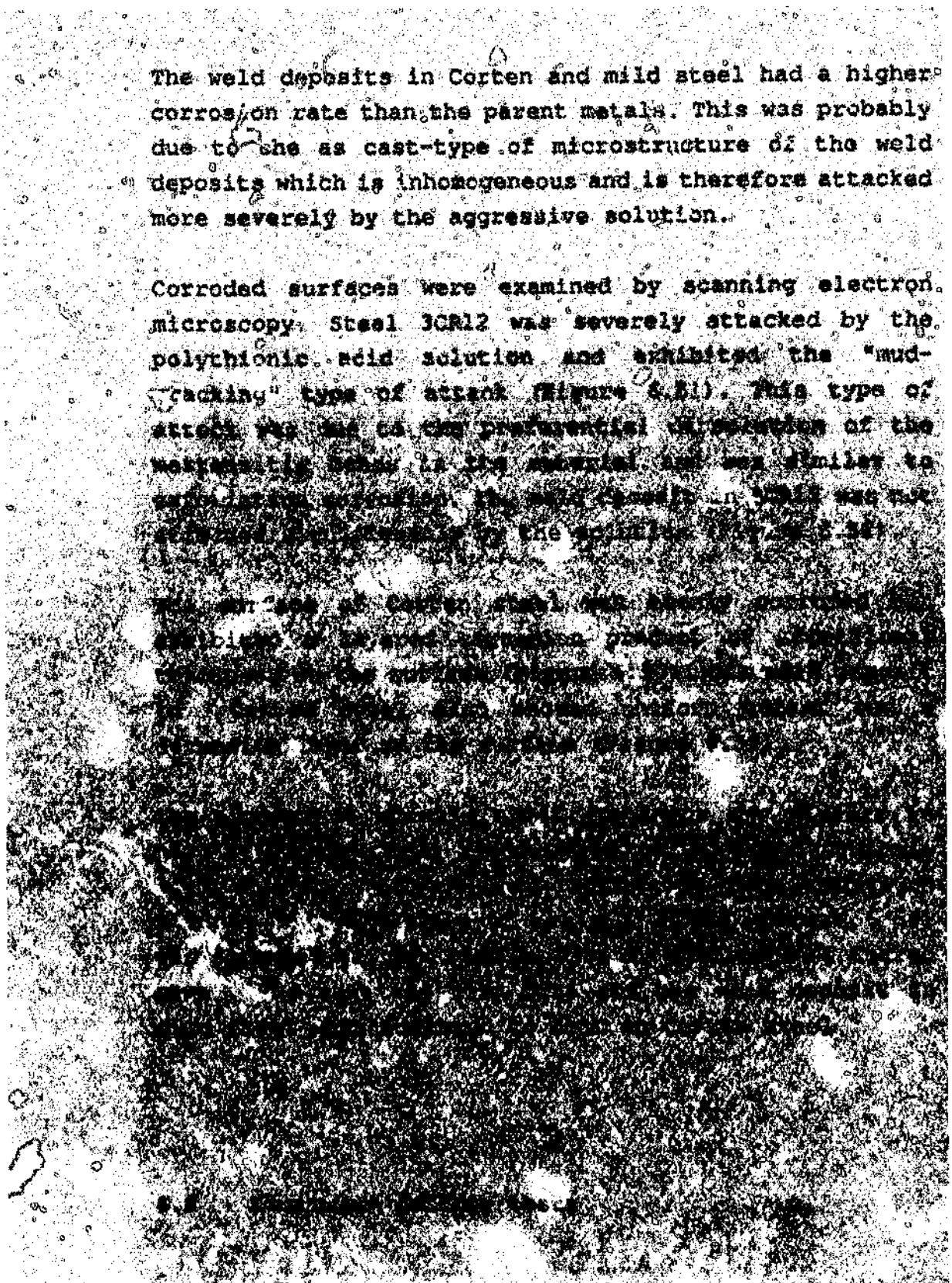

The results of corrosion fatigue tests in the polythionic acid solution in both unwelded and welded samples are presented in Figures 6.57 to 6.62. Figure 6.63 shows a comparison of the fatigue crack propagation rates of

Figure 6.54 The corroded surface of the weld deposit in Corten steel.

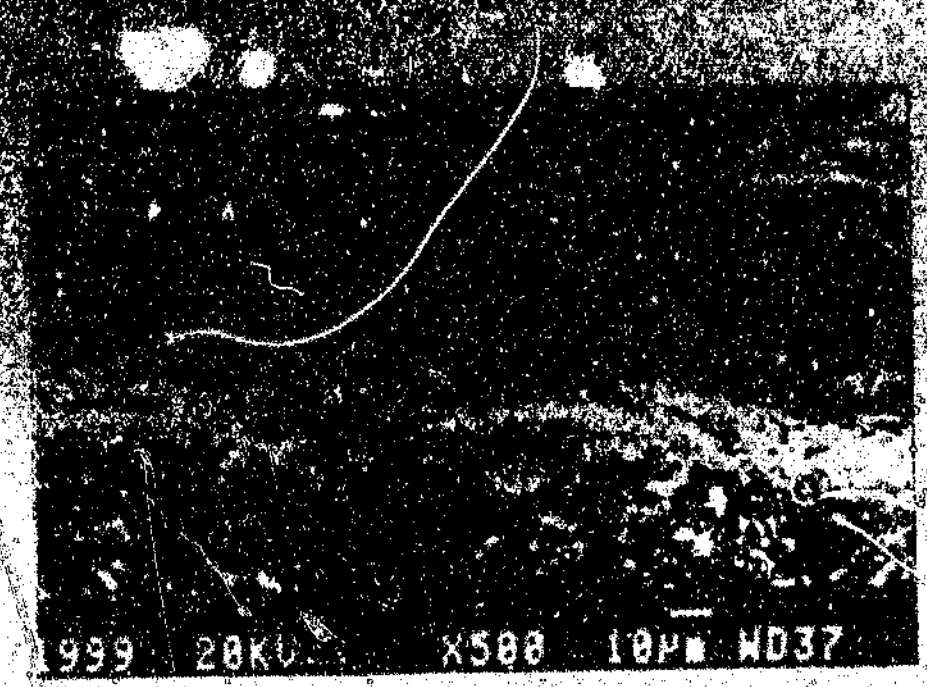

Figure 6.56 The corroded surface of the weld deposit in mild steel.

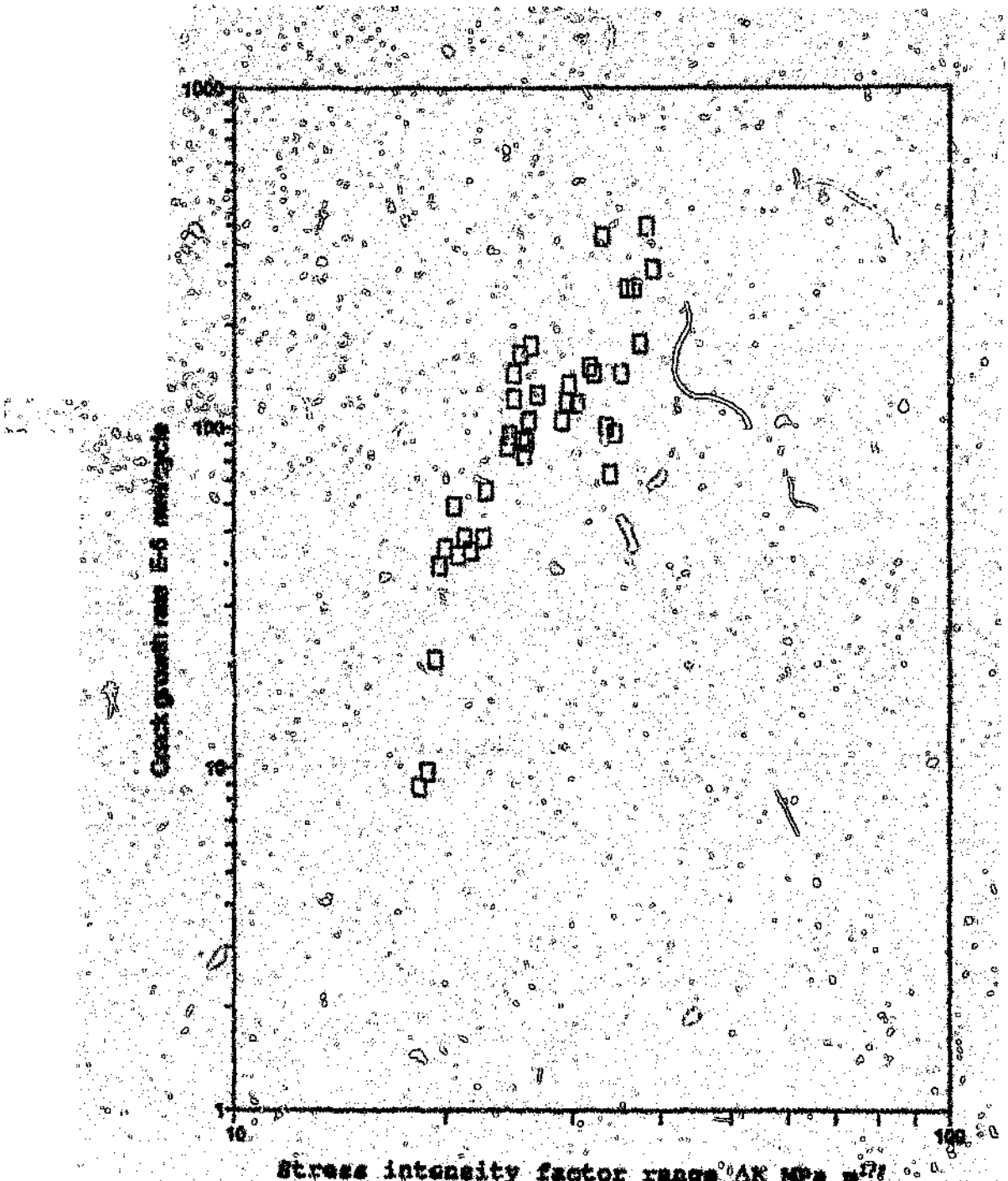

Figure 6.57 The corrosion fatigue crack propagation rate in 3CR12.

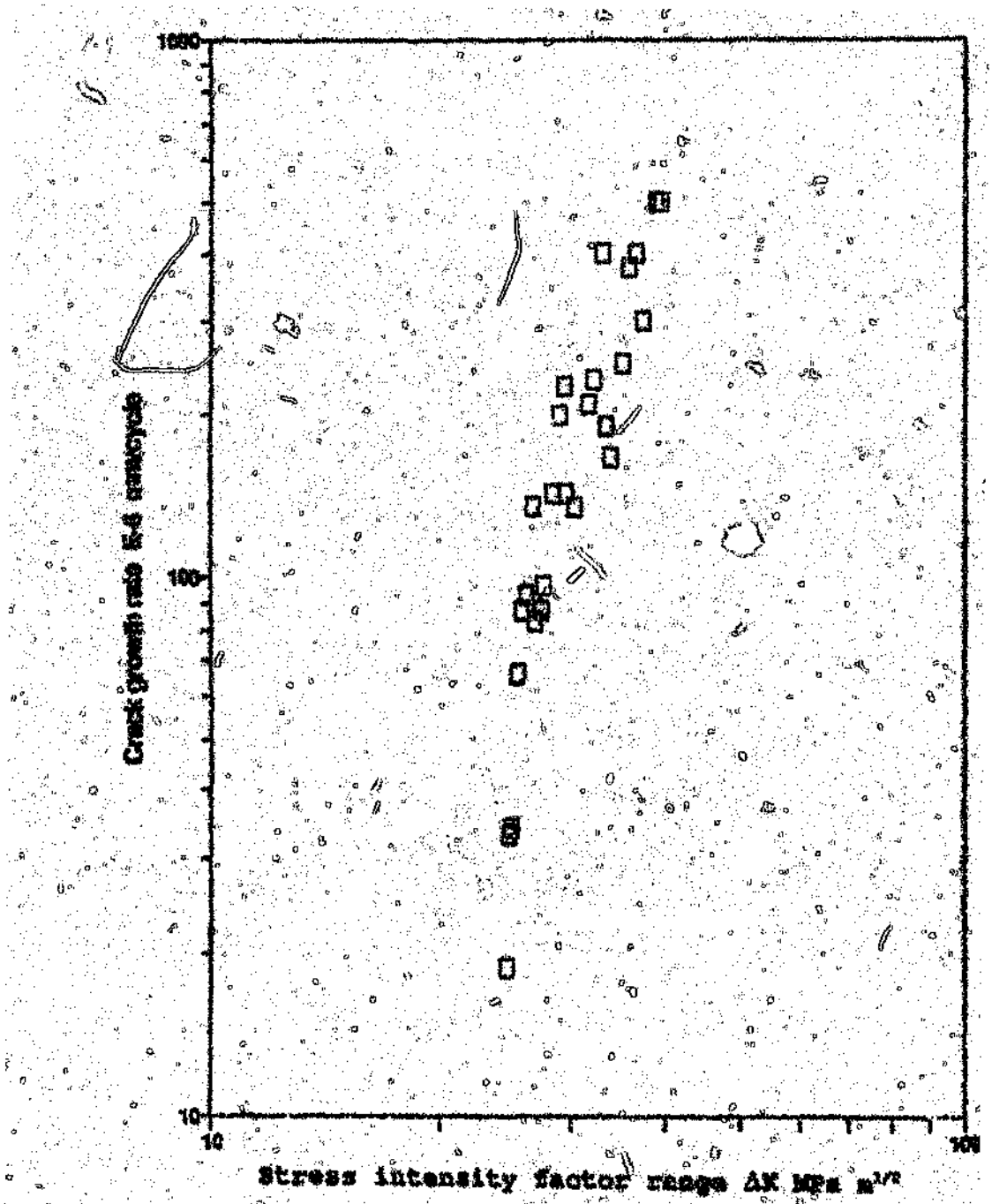

Figure 6.58 The corrosion fatigue crack propagation rate in Corten steel.

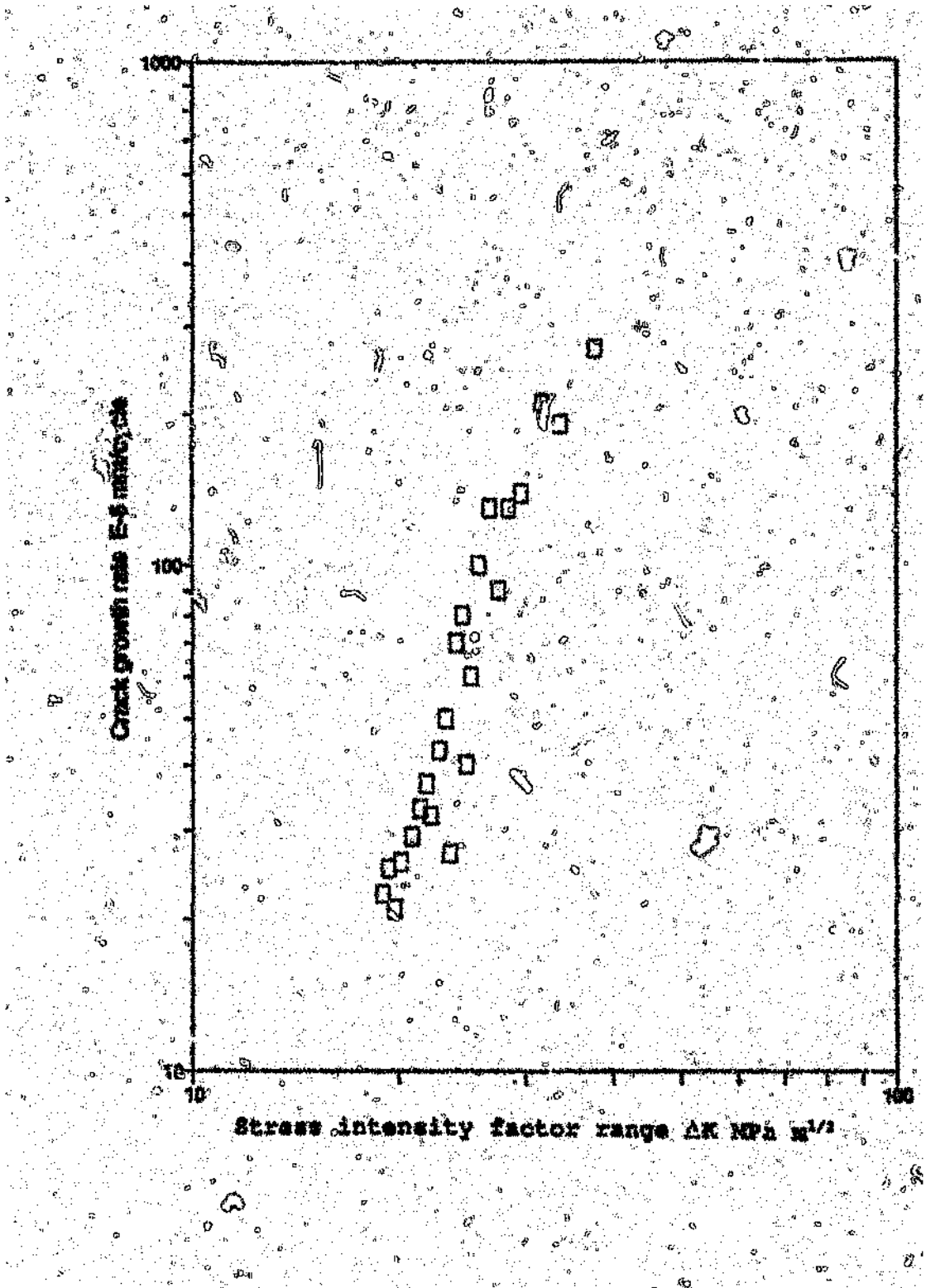

Figure 6.59 The corrosion fatigue crack propagation rate in mild steel.

Figure 6.18


1056

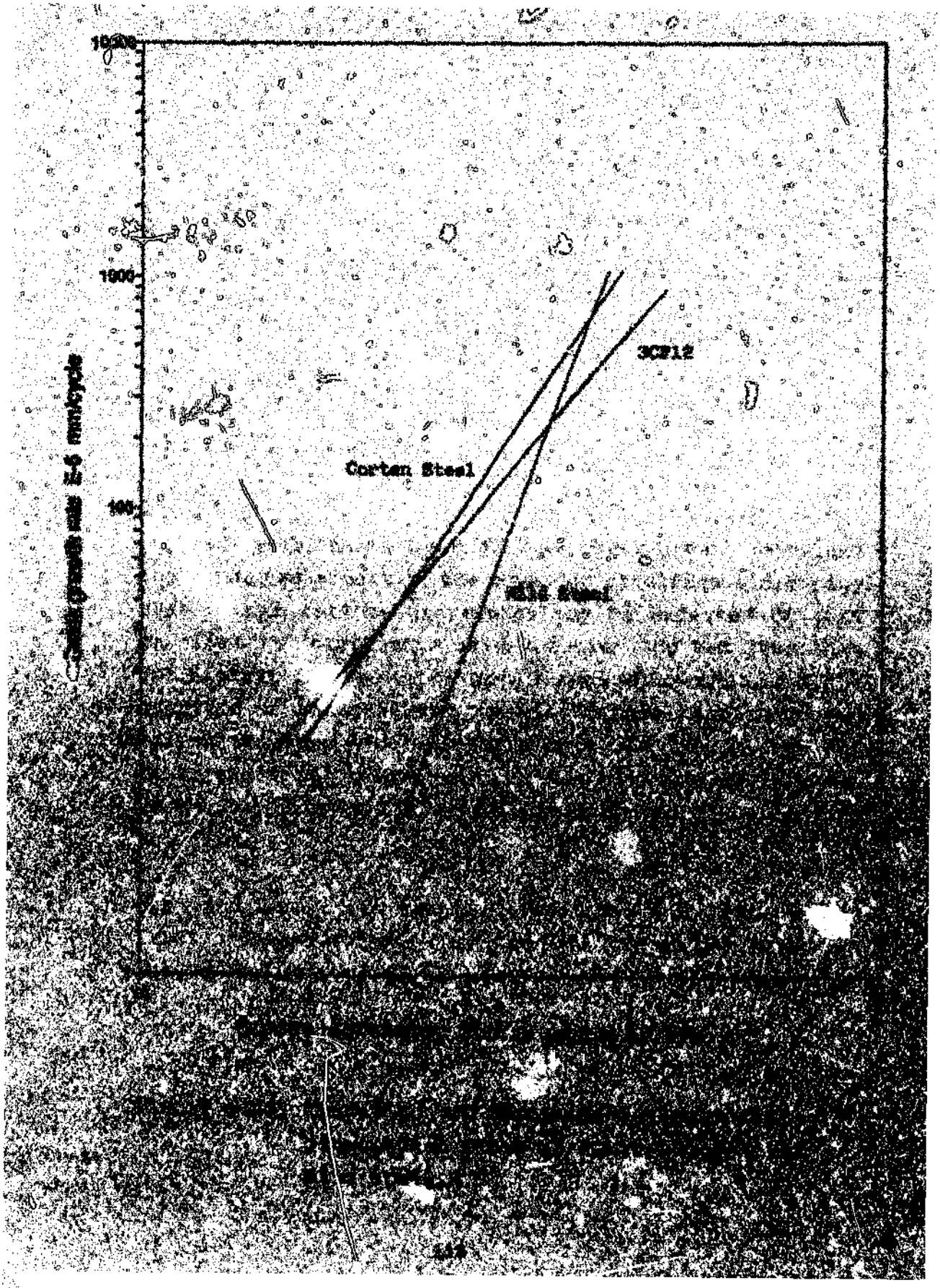
1000
3CR12
Corten Steel
mild steel

3CR12, Carbon and mild steel in stage II of the cracking process for constant amplitude. Figure 5.45 shows a comparison of the fatigue crack propagation rates in the weld deposits of the three steels during stage II of the tests.

Regression analysis was applied as before to obtain equation for the rates of crack propagation during stage II of the process for the parent metals and their weld deposits. The equations generated were as follows.

3CR12 $da/dN = 3.61 \times 10^{-9}(\Delta K)^{3.02}$ ---- (7)

Carbon steel $da/dN = 1.50 \times 10^{-11}(\Delta K)^{4.73}$ ---- (8)

Mild steel $da/dN = 2.15 \times 10^{-9}(\Delta K)^{3.1}$ ---- (9)

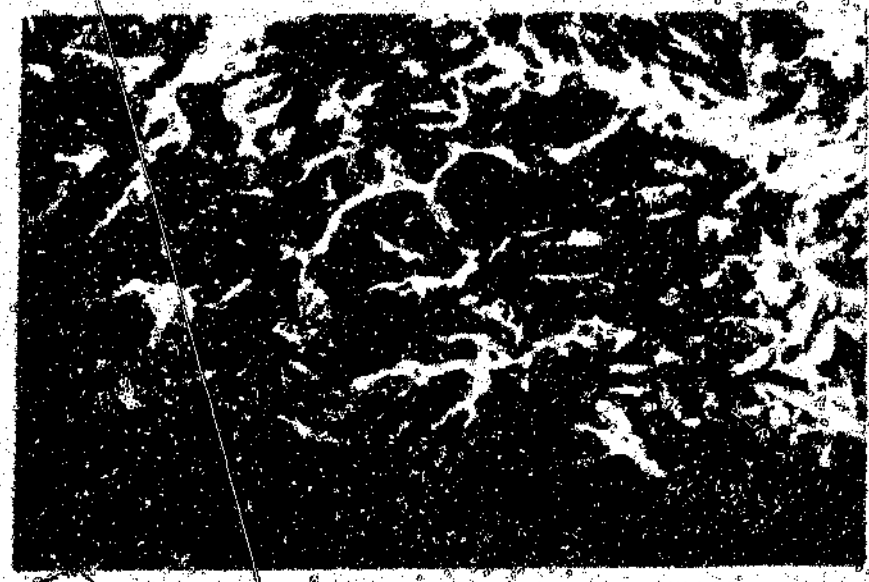

Figure 6.70 Fatigue fracture surface of the weld deposit in mild steel tested in air.

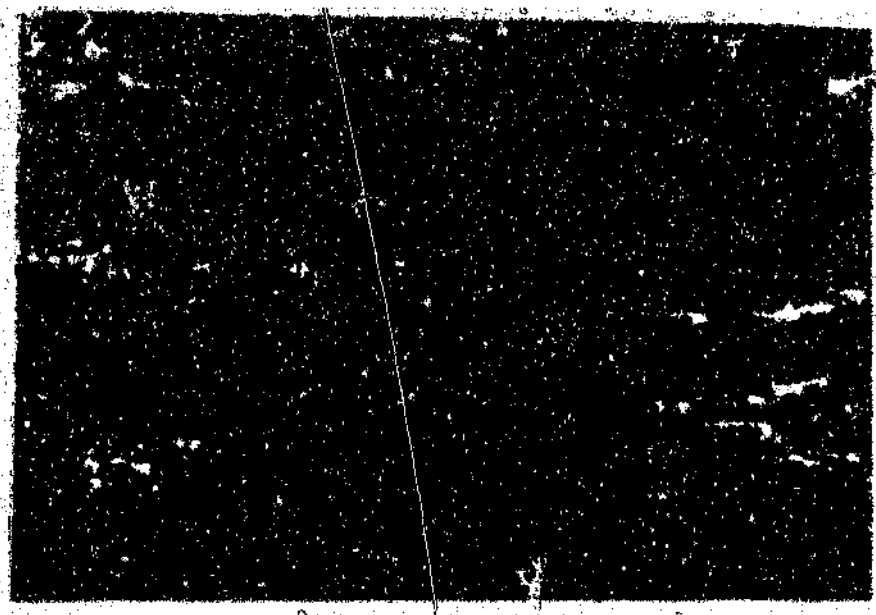

Figure 6.71 "Mud-cracking" in the corrosion/fatigue fracture surface of steel 3CR12.

4.6 Fractographic Examination

The largest portion of a fatigue fracture consists of stage II crack growth, which generally occurs by transgranular fracture and is characterized more by the magnitude of the alternating stress than by the mean stress or the microstructure. Fatigue fracture surfaces usually exhibit crack arrest marks which are perpendicular to the local crack growth direction. Each of these arrest lines is a record of the position of the crack front at some point during the propagation of the fatigue crack through the material.

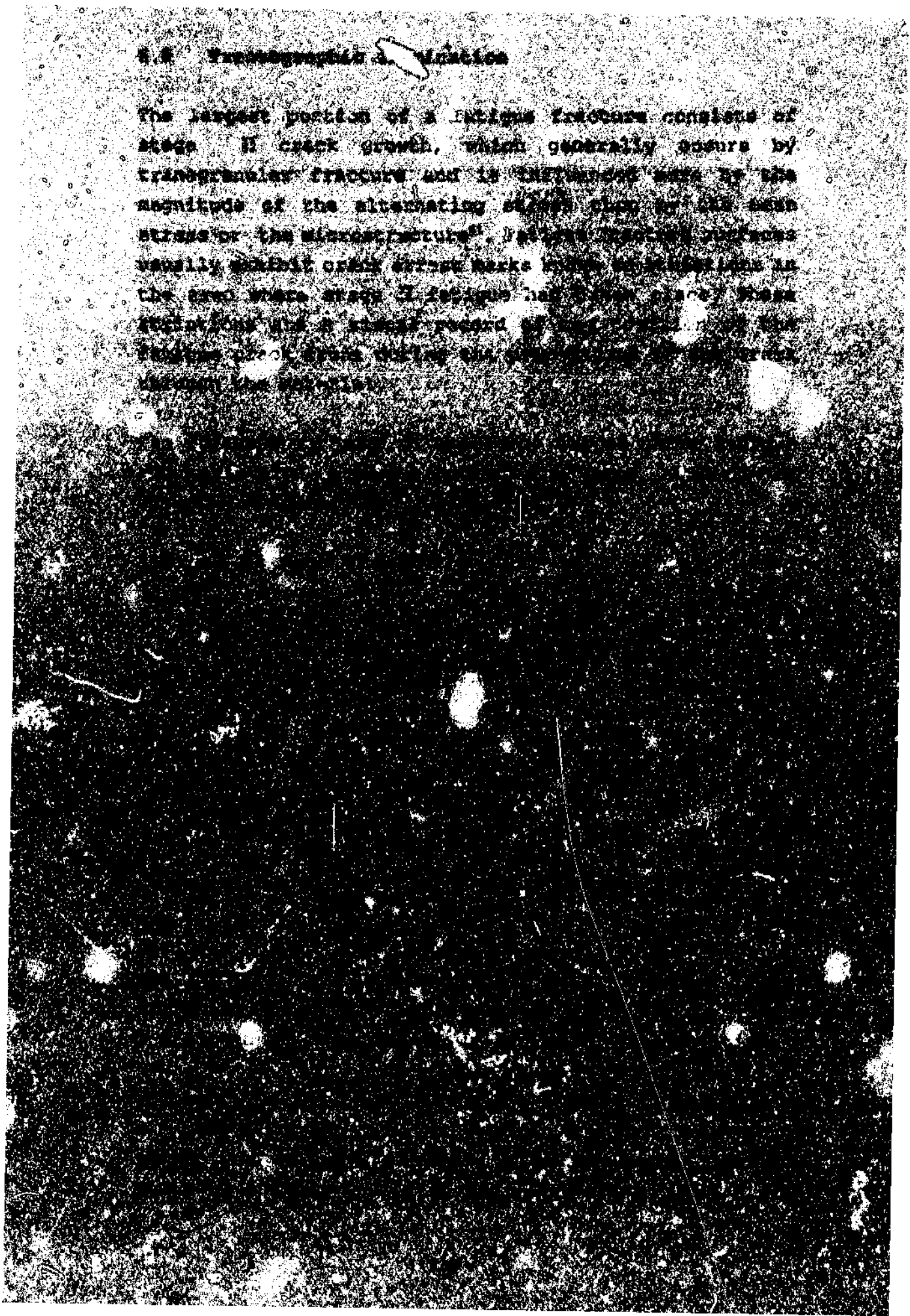

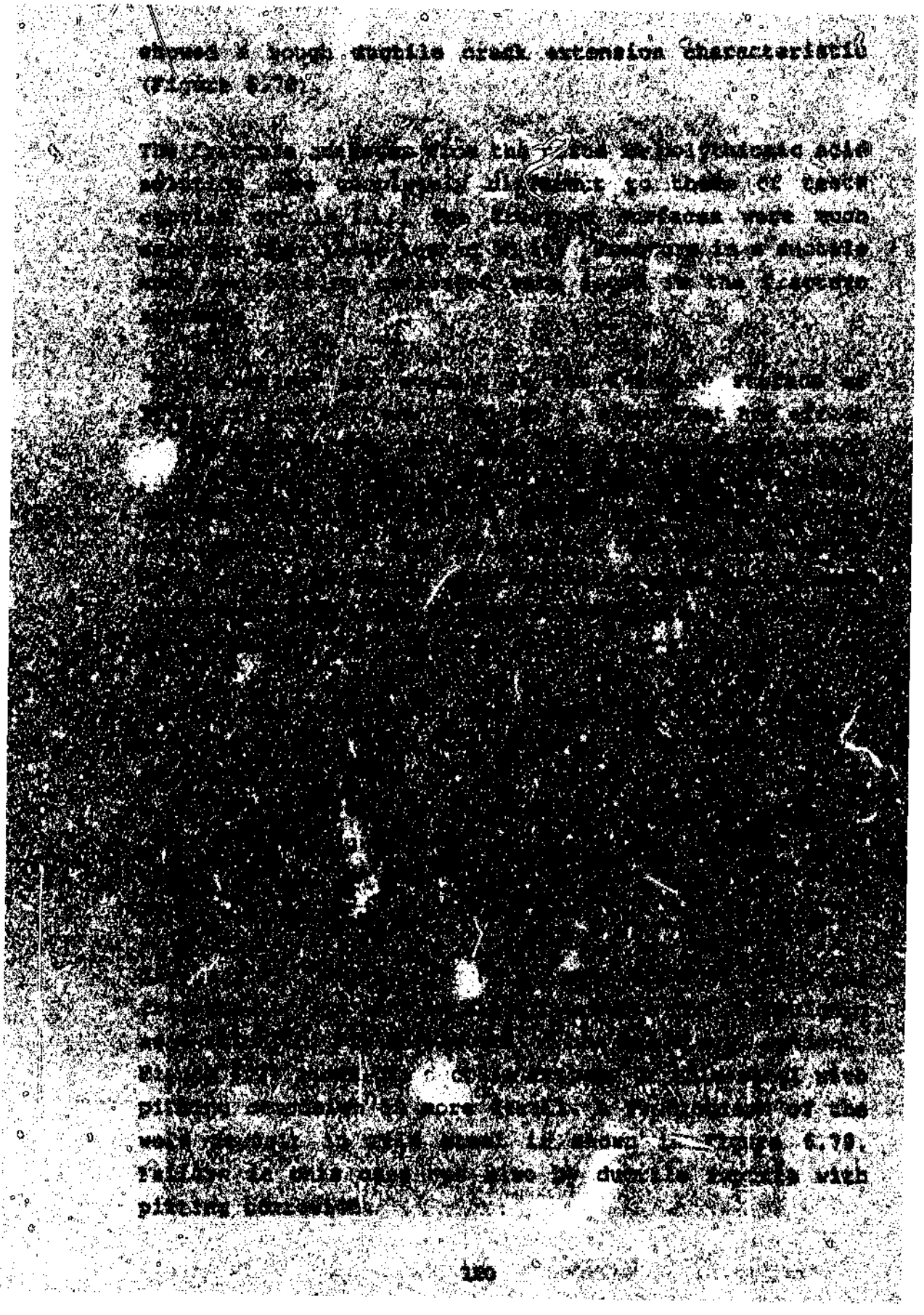

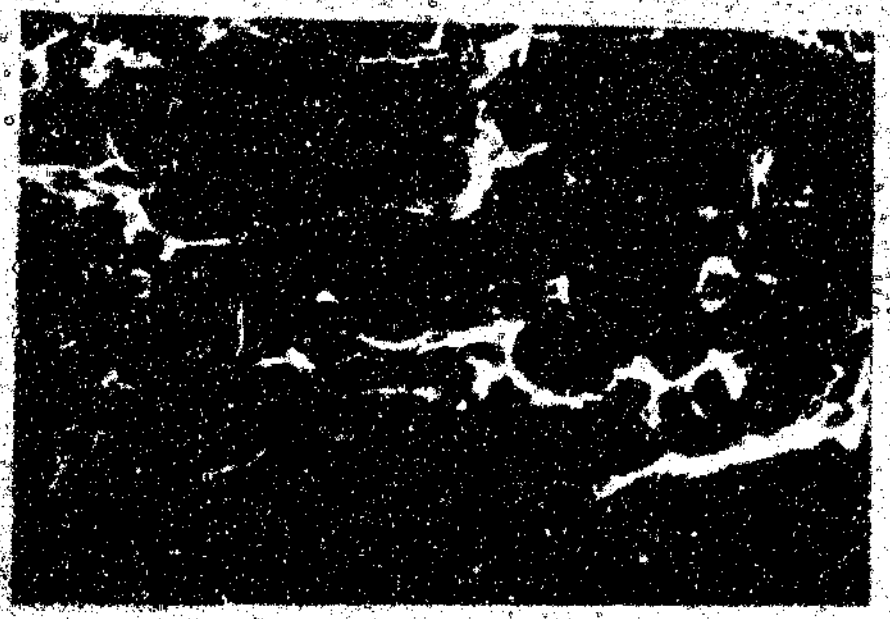

Figure 6.72 Corrosion fatigue fracture surface of steel 3CR12 with spherical inclusions in the weld surface.

Figure 6.73 Titanium carbonitride particles on the corrosion fatigue fracture surface of steel 3CR12.

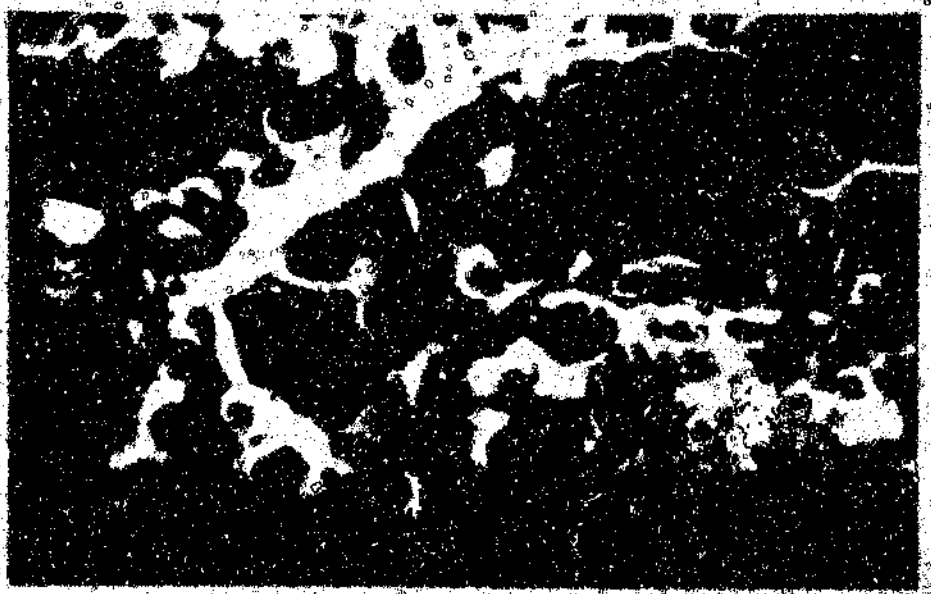

Figure 6.74 Corrosion fatigue fracture surface of steel 3CR12 in the weld deposit.

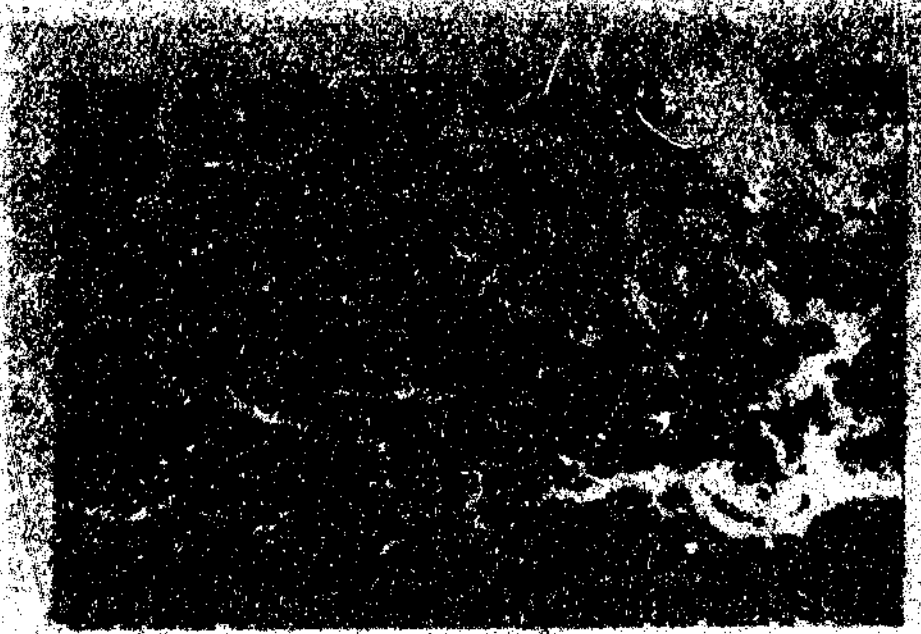

Figure 6.75 Corrosion fatigue fracture surface of Corten steel tested in the polythionic acid solution.

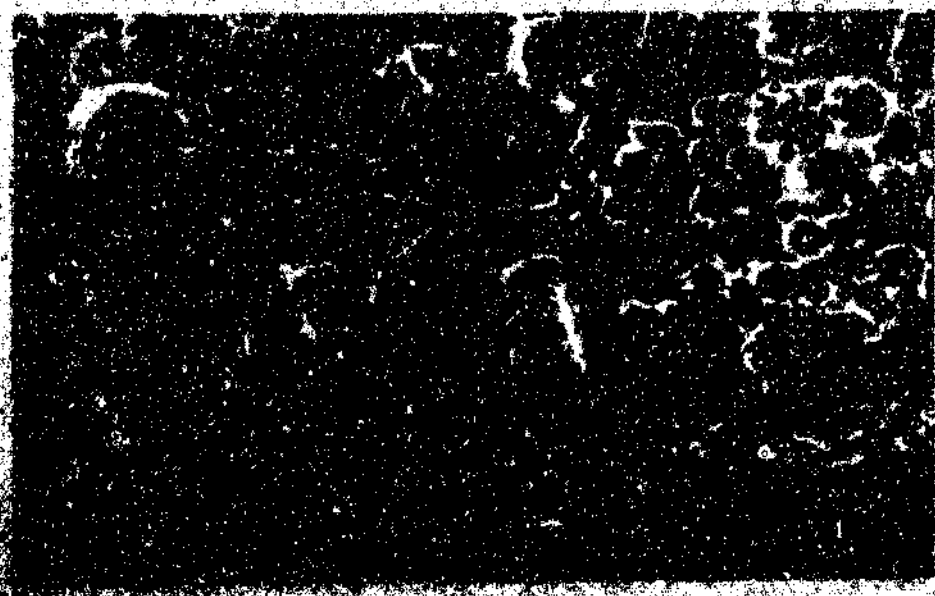

Figure 6.76 Corrosion fatigue fracture surface of carbon steel in the weld deposit.

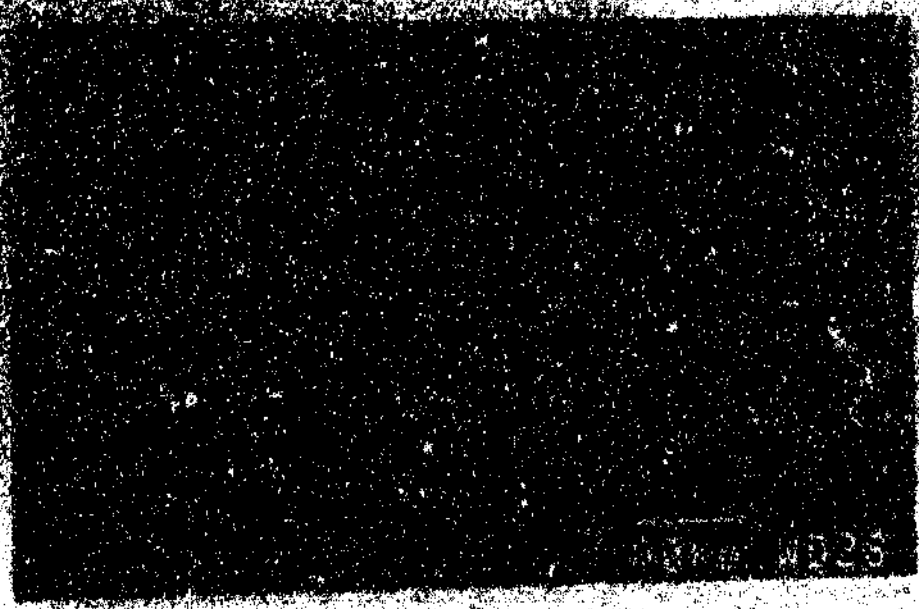

Figure 6.77 General view of corrosion fracture surface of mild steel tested in the polythionic acid solution.

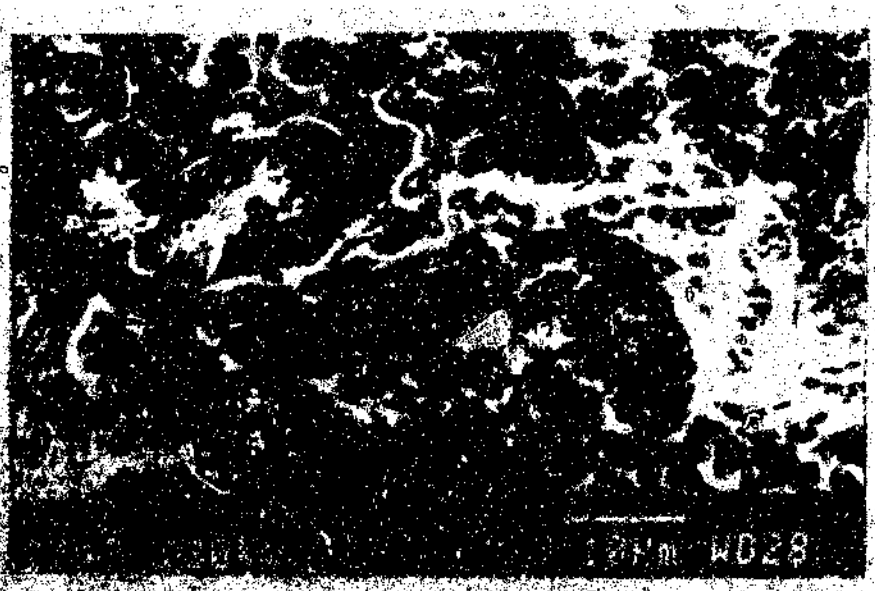

Figure 6.78 Corrosion fatigue fracture surface of mild steel.

Figure 6.79 Corrosion fatigue fracture surface of the weld deposit in mild steel.

6.10 X-Ray diffraction analyses

X-ray diffraction is a powerful technique for investigation surface phenomena such as thin films on metals. The materials used in this study were analyzed by this method, after testing under corrosion fatigue conditions, to test for the presence of sulphur on the surface of specimens. All of the alloys showed α-iron and sulphur as the major phases. The diffractogram of 3CR12 is shown in Figure 6.80 while Figure 6.81 shows a detailed view of the peaks due to reflections from sulphur on the surface. Figures 6.82 and 6.83 show the diffractograms obtained with Corten and mild steel respectively. It is evident that here the thickness of the layer of sulphur on the surface was greater precluding high intensity peaks for the underlying α-iron.

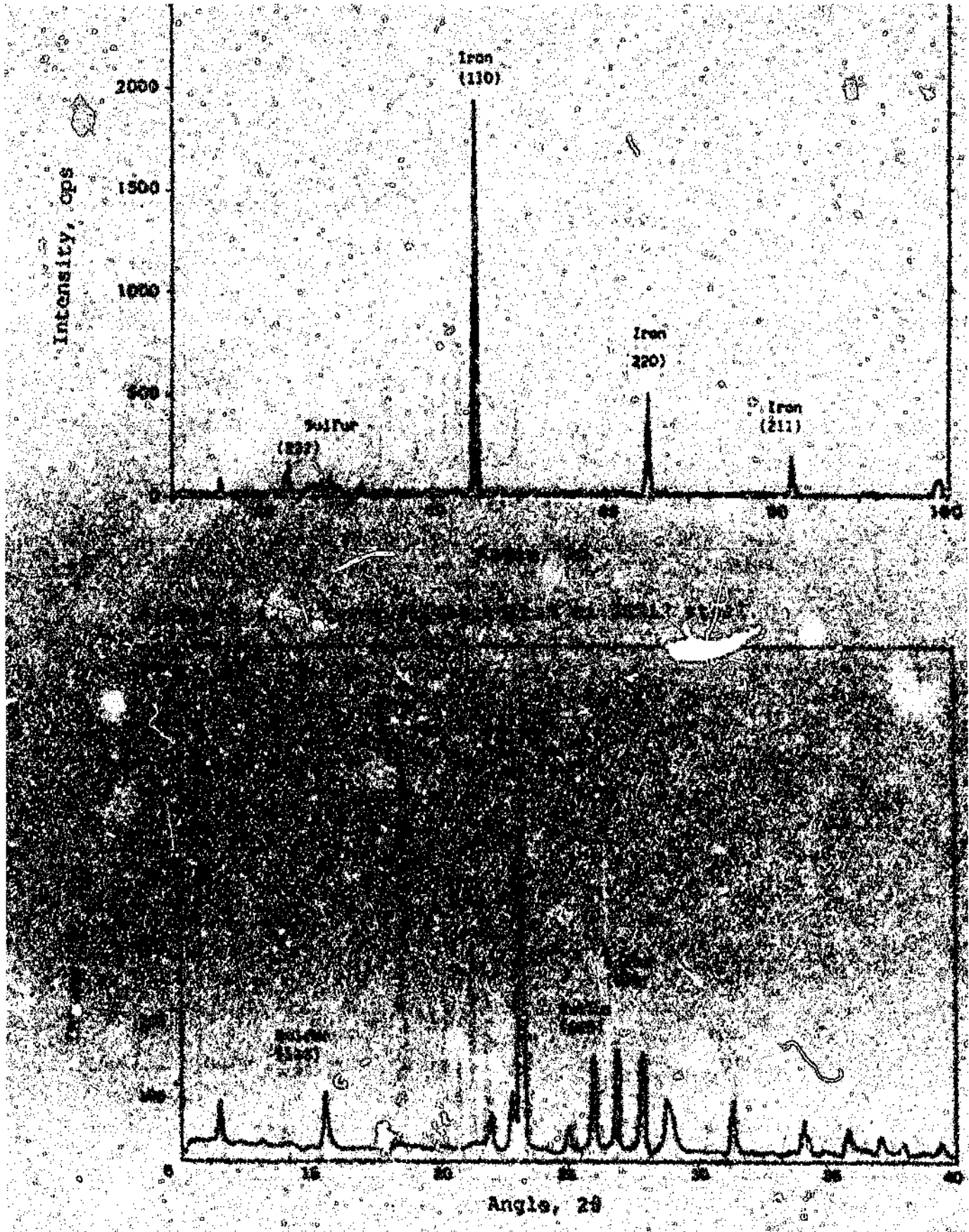

Figure 6.81 Detailed X-ray diffractogram steel 3CR12 between Bragg angles of 10 and 40 degrees 2θ.

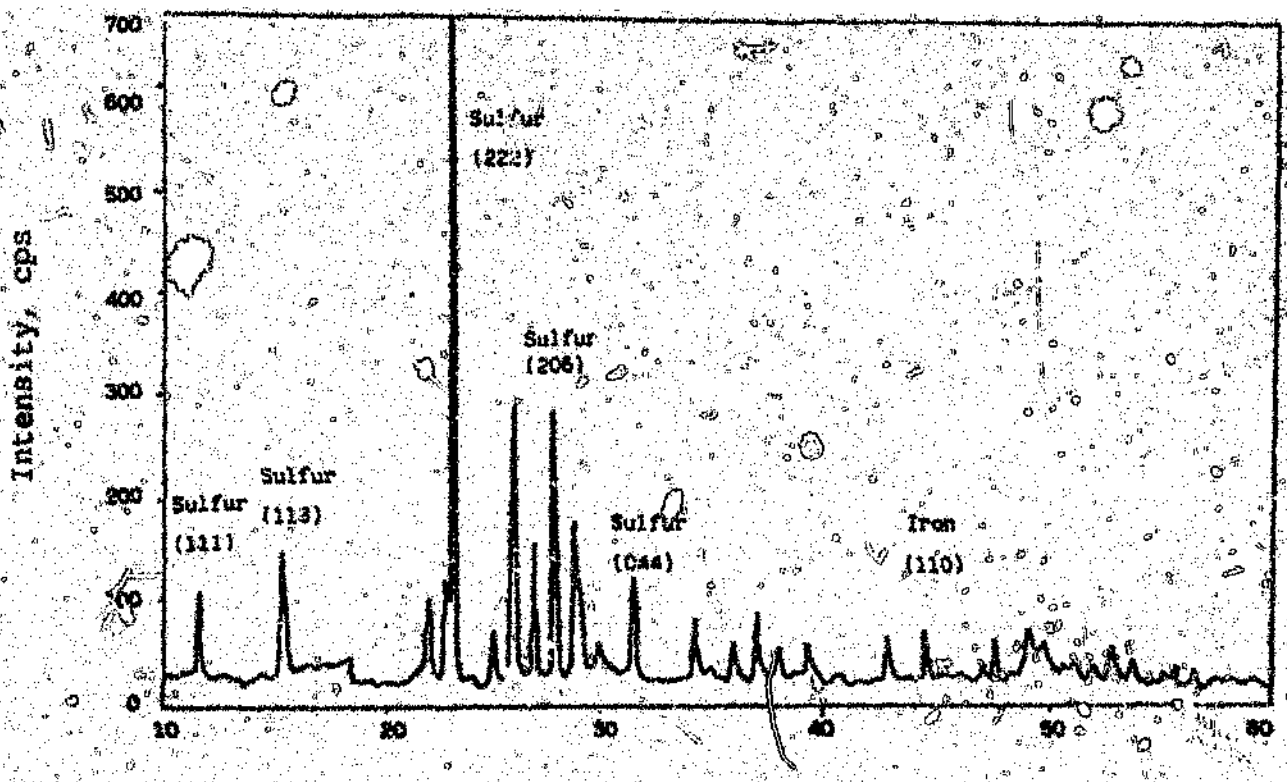

Figure 6.82 X-ray diffractogram of Corten steel.

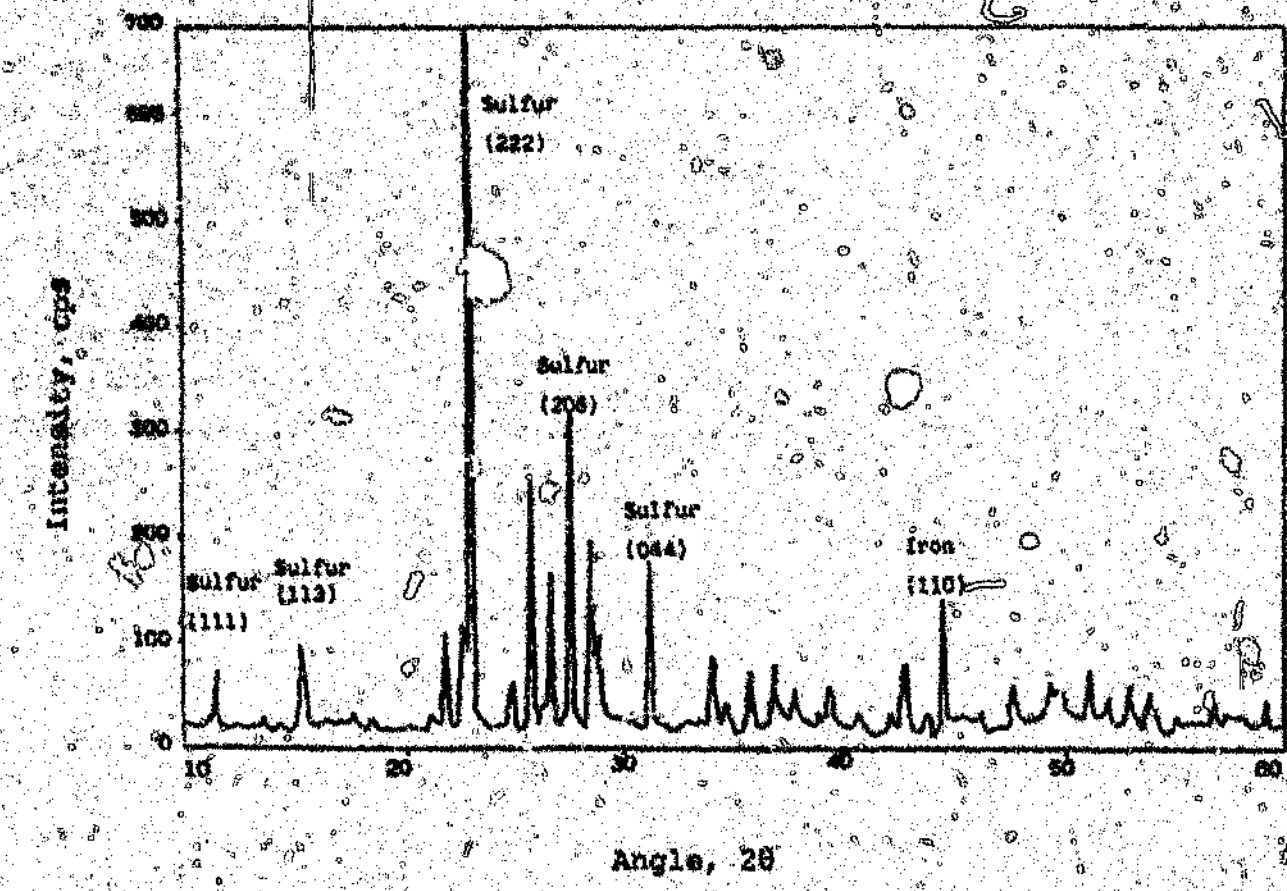

Figure 6.83 X-ray diffractogram of mild steel.

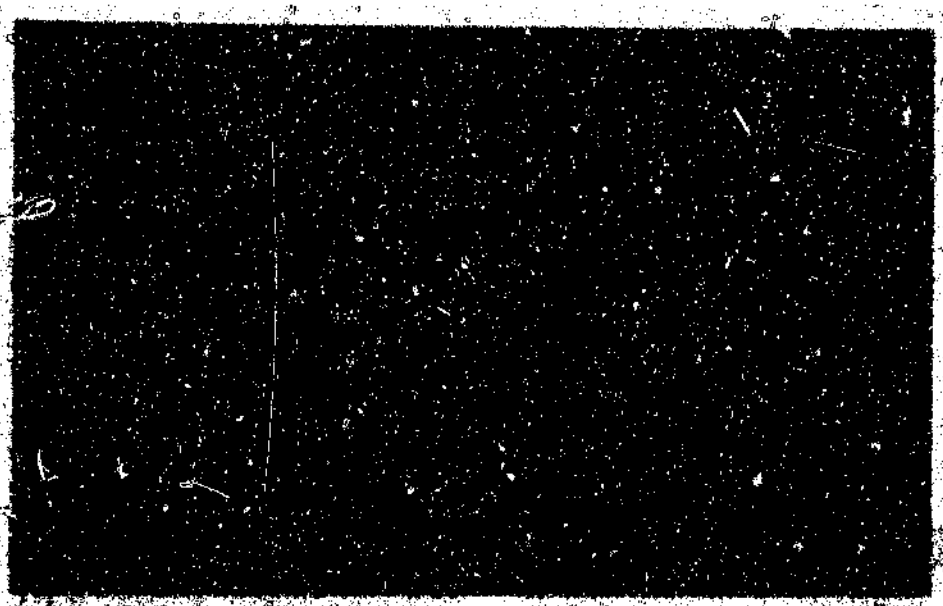

Figure 6.66 Fatigue fracture surface in the weld deposit of test 3213.

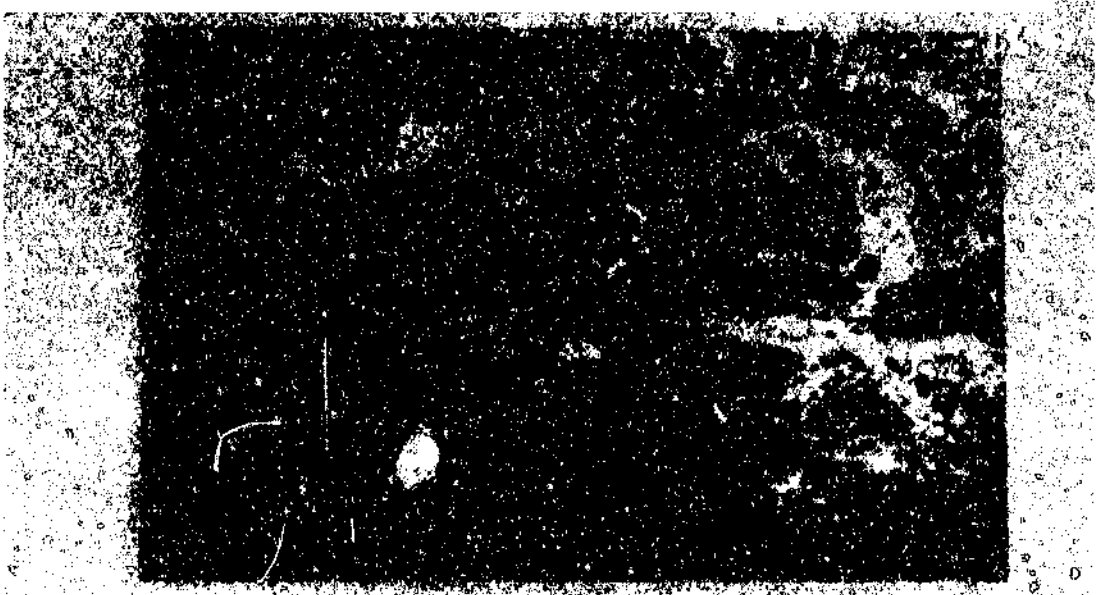

Figure 6.67 Fatigue fracture surface of Corten steel tested in air.

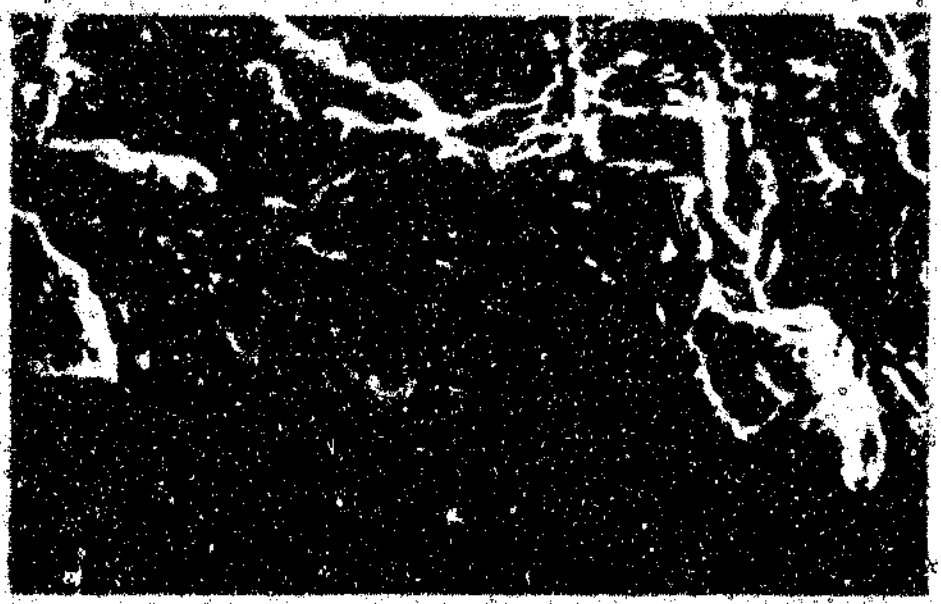

Figure 6.68 Fatigue fracture surface of the weld deposit in Corten steel tested in air.

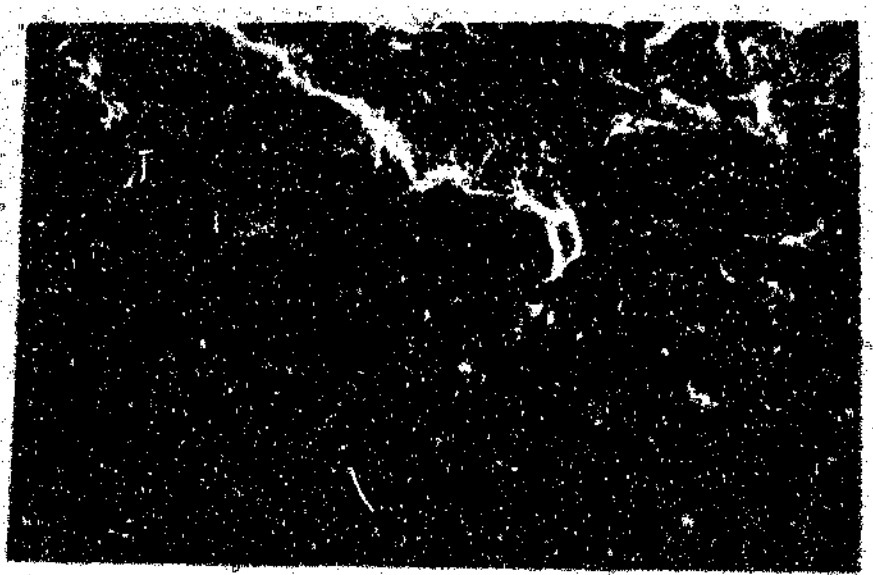

Figure 6.69 Fatigue fracture surface of mild steel parent metal tested in air.

7.2 Corrosion properties

Accelerated electrochemical corrosion tests were conducted on three steels, namely 3CR12, mild steel and Corten using the potentiodynamic technique in a polythionic acid solution. The results obtained from this technique were very high when compared to the exposure test results obtained after two years at various sites, see Table 2.4.

It was found that 3CR12 has a lower corrosion rate than the other two steels in both the welded and unwelded condition. The corrosion rates of the weld deposit in mild steel and Corten were found to be higher than the corrosion rates of the parent plates (Figure 6.30). This difference in the corrosion rates can be related to the inhomogeneous as cast microstructure of the weld deposit which could be preferentially and more severely attacked in the aggressive environment.

7.4 Corrosion Fatigue Properties

Crack propagation rates, under conditions of corrosion fatigue for 3CR12, Corten and mild steel were investigated in a polythionic acid solution. The results of the fatigue crack growth tests in polythionic acid do not follow the same trend as was observed in the mechanical properties or from the fatigue tests carried out in air. A possible reason for this is that it appears that the failure crack growth rate is dependent on the corrosivity of the test solution. This phenomenon can be seen when comparing results obtained for Corten and mild steel in both the welded and the unwelded conditions, see Figures 6.58, 6.63 and 6.64. This shows that alloys which exhibit a high corrosion rate will have a high fatigue crack growth rate.

An interesting phenomenon was observed in that the alloys tested in polythionic acid exhibited a much slower initial (Stage I) fatigue crack growth rate than would be expected if the alloys had been tested in air. The secondary crack growth rate (Stage II) was however found to be more rapid than would be expected if the alloys had been tested in air.

7.3 Summary

From these results we can conclude that 3CR12 was a very good choice for the material of construction of the coal wagons from a fatigue and mechanical properties point of view, however the person who selected this material was either not aware of, or overlooked the microbial corrosion problem. As a result of the microbial corrosion problem the use of 3CR12 is not recommended for coal wagons carrying high sulphur coals. At this stage it should be pointed out that 3CR12 coal wagons have been used successfully for a number of years on the Sishen-Saldanha line to [illegible]

7 DISCUSSION

7.1 The mode of failure of coal wagons

All of the 3CR12 coal wagons in this investigation were used to transport coal from the Eastern Transvaal area to a coal Depot at Richards Bay. These wagons were all stationed at a marshalling yard at Ermelo in the Eastern Transvaal. These wagons are supplied with coal from various mines in the area and a delay of one to two days from the time of commencing loading of the wagons to the time of departure of the wagons is normal. After off loading the coal at Richards Bay the wagons wait another one to two days before returning empty to Ermelo where they would be left on a siding until needed again. From this it can be seen that for the majority of time the coal wagons are empty.

From the previous investigation it is evident that a corrosion process is responsible for the damage observed. On closer examination several factors were found that could have caused this corrosion problem. Firstly the residual corrosive mine water which is carried over to the wagons with the coal during the process of loading the wagons. In recent tests conducted by SATS it has been shown that these mine waters contain a large number of bacterial species. Under certain conditions some of these bacteria, better known as sulphate reducing bacteria (SRB) can cause accelerated pitting corrosion to occur. Pitting is a form of localised corrosive attack resulting from damage to the passive layer on the stainless steel.

Another possible source of a corrosive medium could be from rain water, but the contribution of this to the corrosion problem is considered to be insignificant.

In the past Corten was used to manufacture the wagons. This steel suffered extensive general and uniform corrosion attack resulting in thick layers of rust being removed from the wagons during loading and unloading of the coal. Pitting corrosion was however never observed in the corten coal wagons. This observation is in agreement with what was said earlier because

corten does not have a protective oxide layer that protects it from corrosion like 3CR12.

The 3CR12 coal wagons did not show any appreciable amounts of general corrosion indicating that the choice of this alloy to prevent general corrosion was correct. However the possibility of pitting corrosion has been overlooked and it is now necessary to determine what is causing the pitting corrosion.
On closer examination mud cracking of the corrosion product was observed under the SEM, but unfortunately this does not tell us anything about the corrosion processes that are taking place. Instead it is rather related to the fact that the volume of the corrosion product is greater than that of the base material and this leads to mud cracking.

An EDS analysis of the corrosion product on the corroded 3CR12 wagons indicated that sulphur was present in the corrosion product (Figure 6.4). This once again tends to indicate that microbial corrosion was the probable cause of the corrosion damage. The source of the sulphur contamination in the coal wagons was traced back to the coal which is relatively high in sulphur. This high sulphur content would provide the "food source" for the SRB which would produce organic sulphur compounds resulting in the corrosion problem observed.

A schematic representation of the sulphur cycle is shown in Figure 7.1[43]. This schematic indicates how the SRB can short circuit the process by going directly from S^{2-} to SO_4^{2-} and vice versa to ultimately form organic sulphur compounds such as sulphuric acid.

Microbial corrosion is normally associated with the presence of tubercles on the corroded surface as is shown schematically in Figure 7.2[43]. However no tubercles were observed in this case. A possible reason for this is probably that they were scraped off the metal surface during the loading and off loading operations.

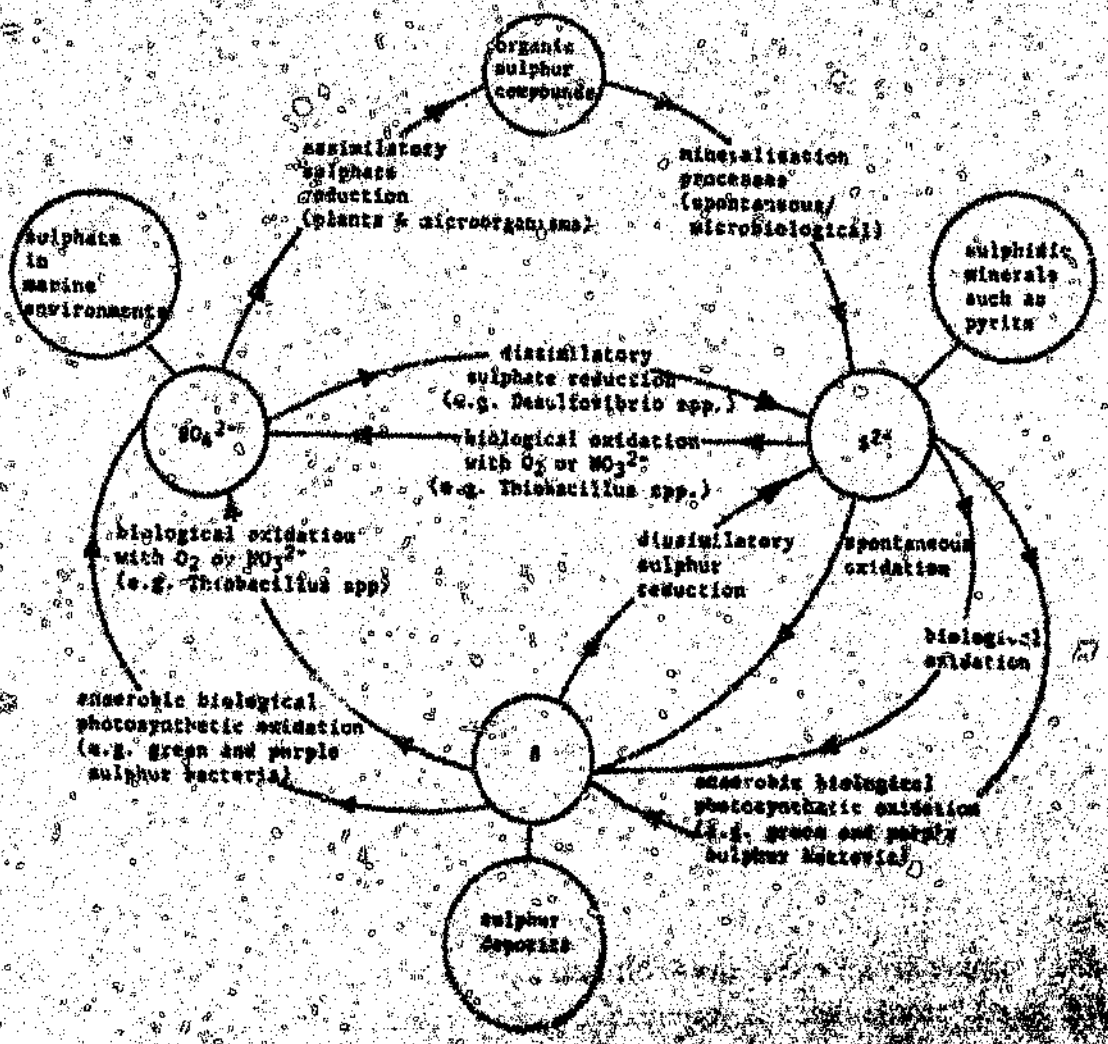

Figure 7.1 Schematic representation of the sulphur cycle. (Ref 42)

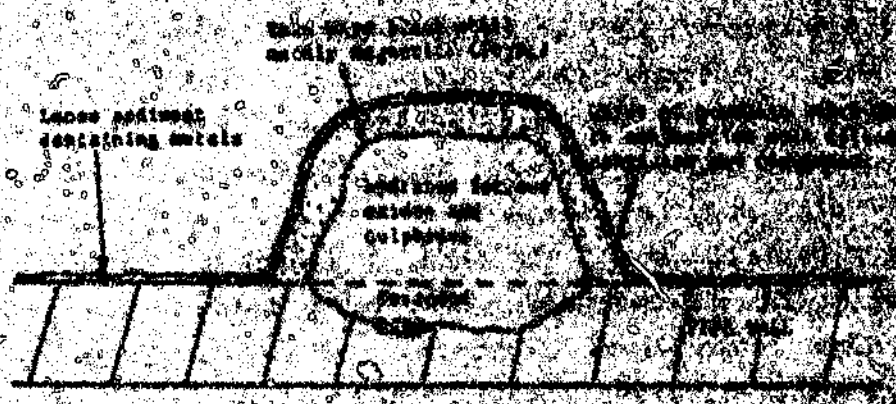

Figure 7.2 Cross-section through a tubercle. (Ref 43)

The severe corrosive nature of the polythionic acid might be due to the high sulphur content of this acid which would tend to accelerate the corrosion process.

7.3 Fatigue Properties in Air

Fatigue tests were carried out on 3CR12, Corten and mild steel plates. The fatigue properties of these alloys containing welds were also examined. The fatigue properties of steels are generally related to their strength as is seen when Figures 6.26 and 6.43 are compared. The fatigue properties of an alloy generally improve as the yield strength of the alloy increases.

From the results of the fatigue tests it was seen that 3CR12 exhibited poorer fatigue properties than the other alloys in the [illegible] tests. The Corten displayed better fatigue [illegible]

larger variations in the crack opening at this stage would however not shield the crack tip from the corrosive environment and a synergistic effect would be set up between the fatigue crack and the environment. This synergistic effect would result in the higher fatigue crack growth rates observed in region II.

When the corroded samples were examined under the electron microscope in the transverse direction, it could be seen that the thickness of the layer of corrosion product on the metal surface did not follow the order of corrosion rates (Figures 6.50 and 6.53 - 6.56).

The mild steel parent plate showed better corrosion-fatigue properties than the other two steels when tested in phosphoric acid. Corrosion in the weldment condition showed the most severe [illegible] of the welded samples showed the least [illegible] properties of [illegible]

6 [illegible]

The aim of this project was to compare the fatigue, corrosion and corrosion fatigue properties of 3CR12, corten and mild steel. Comparative experiments have been carried out and the following results have been achieved.

[illegible] Properties

[illegible] yield and the best mechanical properties compared to [illegible] and mild steel.

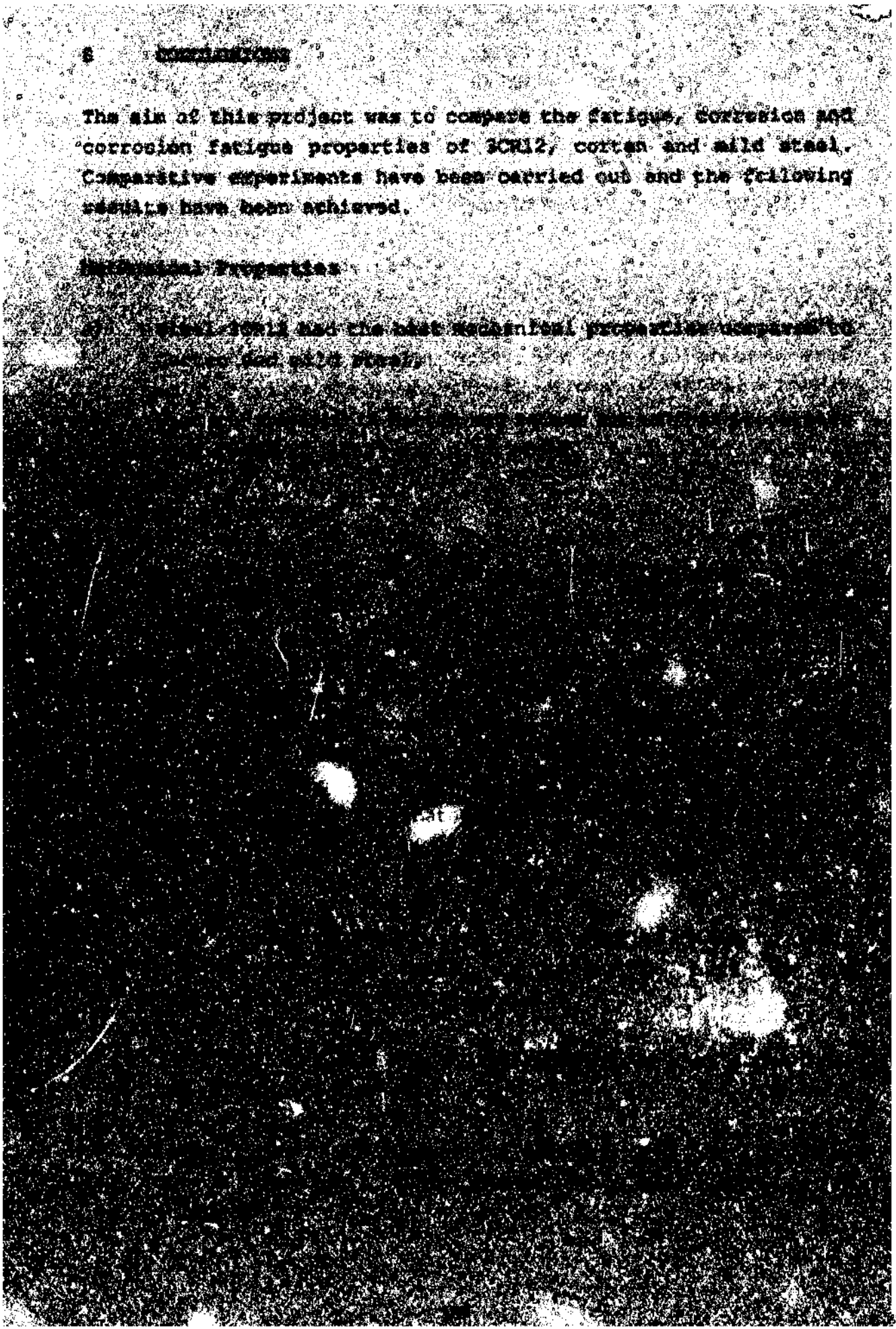

3CR12	$da/dN = 3.80 \times 10^{-9} (\Delta K)^{3.68}$
Corten steel	$da/dN = 8.49 \times 10^{-13} (\Delta K)^{3.99}$
Ni Steel	$da/dN = 1.04 \times 10^{-12} (\Delta K)^{3.89}$
3CR12-weld	$da/dN = 4.31 \times 10^{-11} (\Delta K)^{3.47}$
Corten-weld	$da/dN = 3.48 \times 10^{-10} (\Delta K)^{3.11}$
Ni Steel-weld	$da/dN = 1.93 \times 10^{-10} (\Delta K)^{3.02}$

Aluminium Rubber composites

a) [illegible] 2 weight fraction crack propagation rate [illegible] co-cured samples in the polychloric acid

1. Meyer, K. Introduction to physical ...

2. ... Bacteriol. 60, 9(1950). The ... DCHA to heat treatment. Cytobios for ...

12. Callaghan, DG. Performance of 3CR12 in building and construction. ibid.

13. Ambler, MN. A 3CR12 floating roof on a crude oil storage tank. ibid.

14. Barry, D. Abattoir application for 3CR12. ibid.

15. Graham, PW. Potential use of 3CR12 in railcar construction in US for corrosive dry bulk commodities. ibid.

16. Smith, PJ. Acid corrosion resisting steps in the treatment of [illegible]. ibid.

17. [illegible] Cracking of [illegible] in chloride, polluted [illegible] and [illegible] in corrosion resistant duplex stainless steel designated 3CR12. Materials Science and Technology. Vol.3. March 1987. pp 189 - 195.

25. Smallman, RE. Modern Physical Metallurgy, 4th Edition, 1985, pg 338-349.

26. Gooch, TG. Welding of 3CR12 corrosion resisting steel. Proceeding of the Inaugural International 3CR12 Conference, March 1984.

27. Wilson, JF. 3CR12 - An overview of mechanical and corrosion properties. Part II Corrosion properties. Proceedings of the Inaugural International 3CR12 Conference, March 1984.

[illegible] Journal of Materials Science, Letters [illegible] Effect of heat treatment on the [illegible] Grade 410 Martensitic Stainless Steel. Materials and Technology, January 1982, Vol. 111/82.

36. Jones, R. Applications of Fracture Mechanics for Selection of Metallic Structural Materials. American Society for Metals, 1982.

36. Paris, P. C., and Erdogan, F. Journal of Basic Engineering, Transaction of ASME, Volume 85, Dec 1963, p 528-534.

37. ASTM E647. Standard test method for constant- load-amplitude fatigue crack growth rates above 10 m/cycle. Section 3, Volume 03.01. 1985.

38. ASTM G35-73. Standard practice for determining the susceptibility of stainless steels and related nickel-chromium-iron alloys to stress corrosion cracking in polythionic acids. Section 3, Volume 03.02, 1985.